Spring 2023

GELATIN-BASED MICROPOROUS INJECTABLE HYDROGELS FOR IN SITU STEM CELL ENCAPSULATION

Seth David Edwards
University of New Hampshire, Durham

GELATIN-BASED MICROPOROUS INJECTABLE HYDROGELS FOR IN SITU STEM CELL ENCAPSULATION

By

SETH DAVID EDWARDS

B.S. Chemical Engineering, University of Rochester, 2018

DISSERTATION

Submitted to the University of New Hampshire

In Partial Fulfillment of

The Requirements for the Degree of

Doctor of Philosophy

in

Chemical Engineering

May, 2023

This dissertation has been examined and approved in partial fulfillment of the requirements for the degree of Doctor of Philosophy in Chemical Engineering by:

Kyung Jae Jeong, Ph.D.,
Thesis/Dissertation Director, Associate Professor,
Chemical Engineering, University of New Hampshire

Linqing Li, Ph.D., Assistant Professor,
Chemical Engineering, University of New Hampshire

Kang Wu, Ph.D., Associate Professor,
Chemical Engineering, University of New Hampshire

Young Jo Kim, Ph.D., Associate Professor,
Chemical Engineering, University of New Hampshire

John Tsavalas, Ph.D., Associate Professor,
Chemistry, University of New Hampshire

On April 25, 2023

Original approval signatures are on file with the University of New Hampshire Graduate School.

ACKNOWLEDGEMENTS

I would like to acknowledge my advisor, Dr. Kyung Jae Jeong, who has been a fantastic mentor and advisor over the course of my graduate studies. He has shared all of my failures and successes, and his contribution to this work and my development as a researcher is immeasurable.

I would also like to thank Dr. Shujie Hou, and Dr. Shiwha Park, previous laboratory members who helped to train and teach me about biomaterials research.

I want to thank the committee members, Dr. Young Jo Kim, Dr. Linqing Li, Dr. Kang Wu, and Dr. John Tsavalas who have committed their time and effort to review and provide feedback on this dissertation, and dissertation presentation.

I would like to acknowledge financial support of me, as well as the work presented in this dissertation, including the UNH Department of Chemical Engineering, who has supported me through a Teaching Assistantship, as well as National Institutes of Health Center of Integrated Biomedical and Bioengineering Research (CIBBR, P20 GM113131), National Science Foundation (OIA-1757371) and National Institute of Biomedical Imaging and Bioengineering (1R21EB032134-01).

I would like to thank the UNH University Instrumentation Center, in particular Nancy Cherim, Mark Townley, and John Wilderman who have taught and helped me with instrument use, as well as Dr. W. Kelley Thomas and Stephen Simpson from the Hubbard Center for Genome Studies, for their help with RNA sequencing, and Dr. Paul Tsang and his graduate student Donnelly Hutchings, for their help with PCR.

I would also like to thank Darcy Silver, who has been a continuous help with setup, repair, calibration, and maintenance of equipment, for the many hours that she has spent to help me.

Lastly, I would like to thank my family, in particular my parents Eric and Judy Edwards, and my girlfriend Monica Perrone, who have all been very supportive of me throughout the course of my graduate work.

TABLE OF CONTENTS

LIST OF FIGURES

ABSTRACT

In this dissertation, I developed and investigated gelatin-based microporous injectable hydrogels for the encapsulation of stem cells for multiple applications in cell delivery. Utilizing microgels composed from a mixture of gelatin and modified gelatin, I demonstrated the utility of a dual crosslinking mechanism, which enabled rapid gelation and tissue adhesion with improved cytocompatibility. Mesenchymal stem cells (MSCs) encapsulated in this hydrogel proliferated at a more rapid rate than in a nonporous counterpart, and showed increased immunomodulatory potential. Then, I investigated gelatin microporous hydrogel for the encapsulation of MSCs for bone tissue regeneration. Encapsulated cells more readily differentiated into osteoblasts (i.e. bone-forming cells) in the microporous environment observed by morphological changes and quantitative assays. This is believed to be due to enhanced cell spreading and cell-cell communication in the unique 3D environment provided to the cells by the microporous hydrogel. Transcriptomic analysis was performed by mRNA sequencing (RNA-seq) of MSCs encapsulated in the differing 3D microenvironments. Results indicated that the 3D environment influenced the expression of genes that are related to cell adhesions, cell-cell interactions, cytoskeletal organization, and matrix remodeling, in addition to MSC differentiation. Because neuronal development is highly dependent on cell-cell communication, I encapsulated an established neural stem cell line (ReNcell) in gelatin microporous hydrogel to investigate neuronal differentiation in comparison to a nonporous analog. Laminin was chemically conjugated to microgel surfaces, which controlled the organization of encapsulated cells in the hydrogel environment. Cell differentiation was examined by immunofluorescence staining, and JC-1 assay was utilized to examine mitochondrial membrane polarization. The microporous hydrogel

induced substantially greater cell spreading, morphological changes and cell-cell connections than nonporous hydrogel. The majority of the cells in the microporous hydrogel differentiated into neural lineages, evidenced by immunostaining by MAP2 and GFAP. In summary, this work demonstrates the utility of gelatin microporous injectable hydrogels for applications in in situ cell encapsulation and stem cell delivery for tissue regeneration.

Chapter 1

Introduction

1.1 Hydrogels for Tissue Engineering Applications

1.1.1 Introduction to Hydrogel

Biomaterials are materials that can interface with biological systems, and have been used for the treatment of many medical problems as in orthopedic implants, contact lenses, and sutures. The first generation biomaterials were made of bioinert and biocompatible materials such as metals, ceramics and plastics, merely serving as mechanical supports with minimal interactions with the surrounding tissues.[1] For more broad and impactful biomedical applications, functional biomaterials that control behavior of, and induce programed response from the cells are desired.[2,3] Hydrogel, a crosslinked network of hydrophilic polymers is an ideal biomaterial for these applications for the following reasons. 1) The high water content of hydrogel makes it suitable to interface with cells and tissue, 2) The physical/chemical properties of hydrogel can be tuned to match those of the target tissues through the control of polymer and crosslinker density and other processing variables, and 3) A variety of natural and synthetic polymers are available to produce hydrogels with low immunogenicity when implanted.[4] While there are many potential applications for hydrogels, the focus of this literature

review will be on the use of injectable hydrogel for applications in tissue engineering and regenerative medicine.

1.1.2 ECM-mimetic Biomaterials

Often, strategies in designing biomaterials are informed by biology. Mimicking the native extracellular matrix (ECM) is desirable for biomaterial scaffolds[5] to build human tissues with. The ECM consists of proteins, glycosaminoglycans, and soluble factors including growth factors and cytokines. Variations in composition and organization of the ECM create differing microenvironments to support the development and specialized function of organs, such as soft (brain), stiff (bone), or highly elastic (skin, heart) tissues.[6] In the body, the ECM and cells have a dynamic relationship. During development, complex cell signaling and interaction between cells and the surrounding ECM coordinate for healthy tissue development.[7] In addition to aiding during development and injury repair, the ECM provides mechanical integrity to tissues. In effect, the ECM is a functional biomaterial scaffold whose organization from molecular to macroscopic length scales coordinates with cells to create functioning tissues.[8] Biomaterials are often used to mimic these aspects of ECM, and the versatility of hydrogel enables it to mimic the composition and function of ECM of various tissues, making it an essential tool for tissue engineering.

1.1.3 Materials for Hydrogels

Hydrogels can be categorized based on the origin of the base polymers - natural or synthetic. Natural polymers such as collagen, alginate, chitosan, hyaluronic acid, and fibrin often have favorable properties for interfacing with cells and tissues, and have

high biocompatibility, meaning that these materials elicit only a mild immune response when implanted in the body.[9] ECM-derived proteins have natural moieties for cell adhesion, and sites for proteolytic cleavage, meaning they can be readily degraded by enzymes secreted from nearby cells. Additionally, degraded components, usually amino acids or short peptides are biocompatible. Commonly used natural polysaccharides, such as hyaluronic acid[10] and dextrin[11] are degradable by hydrolysis under physiological conditions, and alginate can be modified[12] to enable biodegradation. However, the use of natural materials has limitations due to heterogeneity of the starting materials, batch to batch variation, and potential presence of immunogenic impurities (e.g. viruses), which limit feasibility for manufacturing and clinical use.[4] These biopolymers can be produced by recombinant processes, but this strategy is cost prohibitive.[13,14]

Frequently used synthetic materials such as polyethylene glycol (PEG), polyacrylates, and polyamines are generally bioinert, and not readily degradable.[15] However, these materials are highly tunable, and cues to enable cell adhesion[16,17] and cell mediated degradation[18] can be easily incorporated into these materials. Chemistry of synthetic polymers can be precisely controlled to include essential biological information of ECM. For example, a key concept for design of a scaffold for tissue repair is that the scaffold degradation should match the creation of replacement tissue.[19] The concentration of cell degradable linkages can be tuned to match the desired degradation rate, which is more difficult to engineer for most naturally derived polymers.[20] The major limitations of synthetic materials are related to the relatively lower

biocompatibility in comparison to natural materials and the near impossibility of replicating the complexity and activity of natural tissues and ECM molecules.

In addition to the materials described here, many new materials are constantly being discovered or synthesized to create novel hydrogels which are continually finding applications in tissue engineering.

1.1.4 Hydrogel Crosslinking Mechanisms

Crosslinks cause hydrogel formation by creating a macromolecular network from the constituent polymers. Crosslinks can be broadly divided into physical interactions and covalent bonds. Physical interactions consist of ionic interactions, intermolecular forces such as hydrogen bonding and hydrophobic interactions, and supramolecular forces such as guest-host and ligand-receptor interactions.[21] These methods do not involve creation or breaking of chemical bonds, and as a result these crosslinking methods tend to be highly biocompatible, reversible and the resulting hydrogels are generally shear thinning.

Chemical crosslinks are formed through the creation of chemical bonds between hydrogel components, and tend to create a highly elastic matrix. Chemical crosslinking methods with high biocompatibility have been employed in tissue engineering, which include click chemistry, photopolymerization and enzymatic reactions. Unlike physical crosslinking, some damage to surrounding cells and tissues may be unavoidable, depending on the application at the time of crosslinking.[22]

Numerous starting materials, and many viable crosslinking strategies enable creation of tailored hydrogel systems for specific applications. Human tissues have a

very broad spread of mechanical properties, and hydrogel materials have been created to replicate the stiffest materials in the body, such as cartilage (Youngs modulus ~ 10 MPa)[23], in addition to the softest tissues in the body, such as brain (Young's modulus ~ 1 kPa)[24] (**Figure 1.1**).

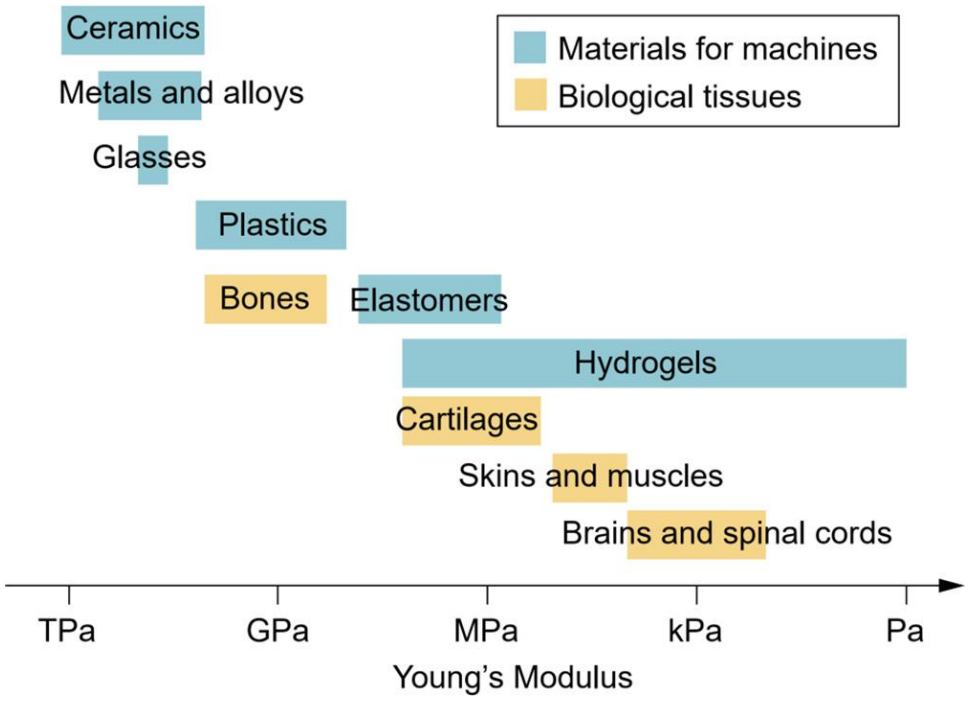

Figure 1.1. Hydrogels can be generated from a wide variety of materials, whose mechanical properties can be tuned to match properties of biological tissues. Adapted with permission from reference 8.

1.1.5 Injectable Hydrogels

Development of functional injectable hydrogels has become important due to the potential advantages over implantable materials. Injection through a needle is minimally invasive, in comparison to surgical implantation, which is more complicated, costly, and could have complications as a result of the surgery.[25] Traditional injectable hydrogels are made from aqueous polymer solutions, that crosslink after injection, in response to stimuli such as simultaneous injection of a crosslinker, temperature, ionic, or pH change, or activation of a crosslinker such as with light-triggered polymerization.[26] As a result, injectable formulations can fill a void or defect area, then form a hydrogel at the site of injection. Injectable hydrogels have been applied to applications such as delivery of cells[27] and drugs[28], as a scaffold to promote wound repair[29], and as a functional adhesive[30]. In addition, injectable hydrogels have found utility in the recent emergence of 3D bioprinting[31], which allows for precise control over biomaterial scaffold architecture. The major drawback of these materials is the required simplicity of design. Because the polymer solution must be injectable, processing methods that are available for implantable hydrogels to modify mechanical properties, porosity, or chemical functionality are not possible, such as incorporation of nanoparticles, addition and removal of porogens, or surface modifications.[32–34] Additionally, as injectable hydrogels are formed in the body, crosslinking methods are restricted to biocompatible mechanisms that can be done under physiological conditions[35–37]. Despite these limitations, injectable hydrogels have had promising results in animal studies, and research is ongoing to improve the function of these materials.

Contemporary research has developed avenues to introduce additional complexity to injectable hydrogels, to improve biological function. For example, an interpenetrating network[38], or nanoparticles[39] can improve mechanical properties. Incorporation of bioactive particles can enhance drug delivery[40], or to aid in crosslinking.[41] Stimuli-responsive behavior has been engineered for creating hydrogels aligned by magnetic field[42], for triggering crosslinking[43], or for drug delivery on demand; either in response to environmental changes, or via external stimulation, such as exposure to ultrasound.[44]

In particular, porosity is a highly important parameter for biomaterial implants, as integration into the host tissue is regulated by biomaterial porosity.[45] However, it is difficult to produce porous injectable hydrogels, because traditional methods of creating porous scaffolds, such as electrospinning, freeze drying, or gas foaming are either post-modifications of crosslinked scaffolds, or use harsh chemicals incompatible with the body. Some attempts to introduce porosity using similar methods have been successful[46], but as an alternative, microgel suspensions have gained considerable interest to create injectable hydrogels with macroscale porosity.

1.1.6 Microgels

Microgels, hydrogels with diameter on the micron scale, have been used for many years for applications in drug delivery,[47] but the strategy of using microgels to create microporous injectable hydrogels (MIHs) was first broadly introduced by Griffin et al. In 2015[48]. This group created hydrogel building blocks from microgels, which could be injected through a syringe as a suspension. Addition of crosslinking agent during injection created chemical bonds between adjacent microgels, creating a bulk hydrogel

scaffold, with an inherent interconnected pore network. These systems maintain the advantages of injectable hydrogels, primarily that they can be administered through minimally invasive methods, and can conform to wound or defect shape, but they are also highly porous. The use of microgels to form tissue engineering scaffolds is desirable because they can overcome some of the limitations of traditional injectable hydrogels, in that there is a tradeoff between mechanical properties, which govern the stability of the hydrogel, and interactions with cells; and porosity, which is required for tissue integration, transport of oxygen, nutrients, and waste, and facilitates cell migration, locomotion, and proliferation.[49] As a result of these distinct advantages, research on MIHs has become ubiquitous in biomaterials research.[50]. Microgels can be generated through the use of a batch emulsion, microfluidic channel, or from physical disruption of macro-scale hydrogels. Batch emulsion and physical disruption are considered to be more rapid methods of production, but microfluidic production allows for generation of monodisperse microgels, and thus the microgel diameter can be precisely tuned. Microgels have found applications in drug delivery, as a scaffold for encapsulated cells for regenerative medicine, and for biofabrication, in particular for 3D bioprinted scaffolds due to their inherent advantages over traditional injectable hydrogels.[50]

The utilization of hydrogels for drug delivery is well documented. Injectable hydrogels have been used for localized drug delivery, which can overcome some of the disadvantages of other delivery methods, namely that they can act as a depot for controlled and/or prolonged release, and local containment of the drug can help to prevent off target effects.[51] Similarly, microgels have been used as injectable drug

depots, with the advantage that microgels can be crosslinked to the required specification before injection. In addition, controlling crosslinking density and drug loaded in microgels enables individual control over release of multiple delivered drugs[52], and complex release dynamics such as staggered drug release[53,54].

MIH scaffolds have been researched for applications in wound healing and cell delivery. For these applications, the inherent porosity of MIH scaffolds enables increased nutrient diffusion, more rapid vascularization, and improved integration into the host tissue in comparison to traditional injectable hydrogels. Barriers to advancement of cell delivery for tissue repair include limited cell survival on injection, and limited cell function.[55] In providing an interconnected pore network, MIH scaffolds have increased potential to provide cues to improve therapeutic behavior of encapsulated cells, and the highly porous scaffold architecture can improve cell retention at the site of injection. MIH scaffolds have been demonstrated in vivo to improve wound healing, and retention of delivered cells.[56,57]

The use of microgel building blocks to generate 3D printed scaffolds is an area of current research, prompted by the introduction of jammed printing.[58] In essence, microgel suspensions can be extruded under application of shear stress, which enables fabricated scaffold assembly with a highly porous architecture. Recent research in this area has utilized nanoparticles as spacers to maintain the porous architecture of MIH scaffolds[59], and used heterogeneous microgel suspensions to control material properties[60] and porosity[61].

In 2018, our lab published work on generating an MIH from gelatin building blocks, led by a previous graduate student Shujie Hou.[62] Since this initial work, we have

focused on modifying this system through the addition of modified gelatin, and application to support cells that can directly benefit from an interconnected pore network. As a result of the potential utility of micron-sized building blocks to generate biomaterials, and based on recent reports of improvement in cell activity in in vivo studies, this area of research has high potential to improve future clinical outcomes of cell delivery.

1.2 Cell Delivery and Cell-Biomaterial Interactions

1.2.1 Cell Encapsulation and Delivery

Tissue engineering has been described as engineering materials, cells, and signaling molecules in order to fulfill a therapeutic purpose, such as repair or replacement of a tissue.[63] One promising strategy of regenerating damaged tissues is through the delivery of therapeutic cells. In concept, cells can be taken from adult stem cell populations, somatic cells, somatic cells that have been reprogrammed into an induced pluripotent state (induced Pluripotent Stem Cells (iPSCs)), or from allogeneic sources.[64] Stem cell populations are given high consideration because they can be extracted and expanded outside of the body, and either before or after delivery to the defect site, can differentiate into cells that will participate in the regrowth of tissue. Mesenchymal stem cells (MSCs), for example, have been shown to readily differentiate into cells of osteogenic (bone), adipogenic (fat), or chondrogenic (cartilage) lineage depending on the chemical and physical cues they are exposed to,[65] and have been explored for differentiation into cells of other lineages such as neural[66], muscle[67], and heart[68]. Clinical success in delivery of cells for tissue regeneration faces several major barriers, including high number of cells needed, and low survival, retention, and activity

of delivered cells.[69] Despite these limitations, the success of CAR-T therapy (which involves removing patient T cells, manipulation of the T cell receptor, then reintroducing the cells to the patient) has demonstrated the clinical potential of this approach.[70]

Biomaterials are being investigated for cell delivery to serve as a delivery vehicle, to improve retention, survival, and therapeutic efficacy of delivered cells.[71] For this application, injectable hydrogels are promising delivery vehicles, as cells can be mixed with the polymer solution, and after injection and crosslinking, encapsulated in the polymer network.[72] In order to promote desired therapeutic phenotypes of encapsulated cells, it is necessary to understand how materials can influence cell behavior.

1.2.2 Cells Respond to Cues in the ECM

Cell-material interactions are of utmost importance in biomaterials for regenerative medicine, and studying how cells respond to environmental cues allows for design of materials to meet cell needs, and to promote desired cell behaviors.[73] Cells can respond to both mechanical and chemical stimuli. It has been demonstrated that many aspects of the mechanical environment, including stiffness, viscoelasticity, topography, external mechanical stimuli such as cyclical strains, and direct cell-cell connections can all influence cell behaviors, such as proliferation, cell shape, migration, and lineage specification of stem cells.[74,75] Chemical stimuli range from growth factors and signaling molecules displayed on ECM, to response to environmental conditions (pH, oxygen, glucose). In the body, all of these signals, mechanical and chemical, coordinate to develop tissues from a small number of original cells, during wound healing, and for tissue maintenance, by directing cell function.

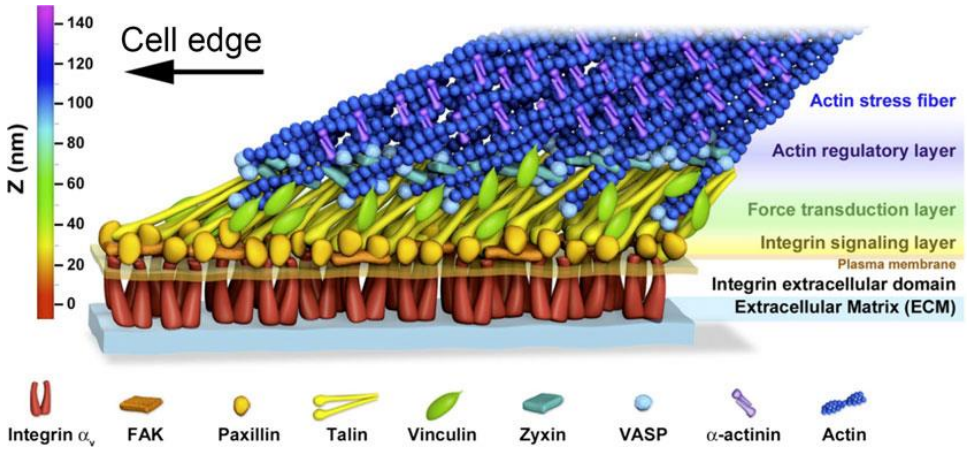

Figure 1.2: Mechanistic understanding of focal adhesion composition and structure. Adapted with permission from reference 79.

1.2.3 Cellular Reaction to Mechanical Forces from ECM

Cells can sense and respond to mechanical stimuli of their environment, and in living tissues this sensing regulates cell behavior such as tissue remodeling, cell adhesion, migration, proliferation, and stem cell differentiation. The primary mechanism for cells to interact mechanically with a surrounding substrate is through integrin-mediated adhesions. Integrins are transmembrane proteins that recognize and bind to ligands found in ECM, which on the cell interior are connected to the cytoskeleton. Integrins form as heterodimers, which due to protein variation can form 24 different proteins, with differing specificity for ligands found in the ECM.[76] For example, the often-used RGD (arginine-glycine-aspartic acid) amino acid sequence is known to be bound preferentially by α5β1 integrin[77], and laminin ligands by α3β1 integrin[78]. Adhesion complexes are created from a complex arrangement of intracellular proteins, including vinculin, talin, and focal adhesion kinase, among others (**Fig. 1.2**) which connect integrins to the cytoskeleton.[79] These adhesion complexes are involved in cell

locomotion, shape, and mechanotransduction, or the ability to convert mechanical input into chemical signals.[80] Through these adhesion complexes, cells can essentially sense the material properties (e.g. stiffness, stress relaxation, nanotopography, curvature) of the environment through traction-mediated forces, whereby cells impart stress through these adhesions, which will differ depending on the material properties. This sensing is involved in many signaling pathways related to cell function, and stem cell differentiation.[81]

Cells also sense and respond to forces exerted by other cells through direct cell-cell connections. Cadherins, transmembrane proteins that connect to the cytoskeleton, mediate cell-cell connections, to form adherins junctions, analogous to integrins and focal adhesions.[82] Similar to integrin binding, cadherin binding has been shown to contribute to cell mechanotransduction, and there is considerable evidence for crosstalk between cell-cell connections and focal adhesions.[83,84] Adherins junctions are prominent features in highly connected tissues, and importantly regulate tissue morphogenesis during development.[85]

1.2.4 Cellular Response to Chemical Cues in ECM

In addition to mechanical cues, cells respond to chemical cues in their environment. Growth factors and cytokines are cell-secreted messenger molecules that can affect cell phenotype, such as promote cell proliferation, or in the case of cytokines, modulate the inflammatory response of the tissue. The ECM has been shown to act as a reservoir for these cell signaling molecules. Several ECM components, including heparan sulfate, fibrinogen, and vitronectin, have been shown to bind to growth factors, which are released by the cells during tissue remodeling, and made available by

proteases.[86] In addition to mechanical design, chemical signals can be used in regenerative medicine to direct cell function.

1.2.5 Controlling Cell Behavior by Biomaterials

Biomaterials and regenerative medicine exploit these consequences of biology to influence cell behavior, including cell migration and organization, stem cell differentiation, and for amplifying material or cell function. By controlling material properties and organization, utilizing chemical signals, and controlling cell-cell communication and adhesion, cell function can be controlled and optimized, which is paramount for creating better biomaterial scaffolds, for regenerative medicine and development/disease modeling.

1.2.6 Controlling Cell Behavior with a Defined Mechanical Environment

Cellular response to mechanical environments has been extensively studied[87], and studies using biomaterials have been instrumental in probing cellular response to mechanical cues.

Stem cell differentiation has been shown to be particularly influenced by the mechanical environment and MSCs, an important adult stem cell population were found to preferentially differentiate into differing cell types depending on the substrate stiffness[88,89]. Cells grown on soft substrates favored differentiation into neuronal cells, and cells on stiff substrates into osteogenic lineages (**Fig. 1.3**). In addition to MSCs, other adult stem cell populations, such as neural progenitor cells (NPCs) and hematopoietic stem cells (HPSCs)[90] have been shown to respond to mechanical cues. In addition to stiffness, cells respond to material stress relaxation[91,92], a phenomenon of

viscoelastic materials such as hydrogels, and the ECM, whereby polymers relax under a constant stress, and matrix degradation rate. Furthermore, the binding rate constant of physically crosslinked hydrogels (highly viscoelastic) was found to influence cell spreading and stem cell differentiation.[93]

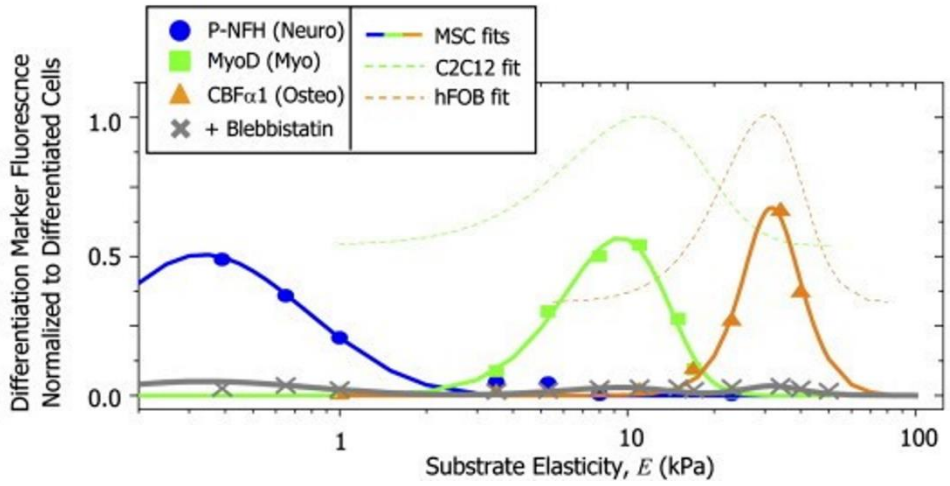

Figure 1.3: Mesenchymal stem cell fate is dependent on substrate elastic modulus. When MSCs were provided factors for differentiation into multiple lineages, lineage specification was dependent on substrate mechanical properties. Adapted with permission from reference 88.

1.2.7 Controlling Cell Behavior by Manipulating Cell Morphology

Fundamental studies on 2D substrates have illustrated that controlling cell shape can influence cell behavior such as apoptosis, cell proliferation, and stem cell differentiation.[94] Studies on the effect of cell shape on MSC differentiation seed cells on patterned surfaces, whereby cell morphology is controlled by the presence of cell-adhesive ligands templated in a defined area. When supplemented with medium containing factors to induce both adipogenic and osteogenic differentiation, it was found that MSCs preferentially differentiated into fat cells when cell area was small, and into bone forming cells when cell area was large, showing that cell spreading directly impacted lineage specification[95]. Cell shape itself, independent of cell area, has been shown to influence stem cell differentiation. For example, in one study MSCs in a pointed “star” geometry were more likely to undergo osteogenesis than cells in a rounded “flower” geometry despite the same area[96], and another study found similar results by comparing pointed and rounded cell geometries[97].

1.2.9 Control of Cell behavior Through Cell-Cell Interactions

Cell-cell signaling involves signaling through direct cell-cell connections, paracrine (between nearby cells) or endocrine (between distant cells) means. Direct cell-cell connections are important in development, as well as the function of mature tissues such as skin[98], vasculature[99], heart[100], and nervous system[101], so controlling and guiding the formation of these connections can be strategically employed to create functional synthetic tissues. In particular, poor vascularization of engineered tissues remains a key limitation.[102] Taking advantage of integrin-ECM interactions in the development of functional biomaterials is well-established. However, using biomaterials

to promote cadherin-based cell-cell interactions has been largely overlooked.[103] It has recently been demonstrated that cell-cell connections within biomaterials influence the lineage specification of MSC differentiation[104] as well as neuronal differentiation[105] of NPCs. cadherin ligands incorporated in biomaterial scaffolds[84,106], as well as on patterned surfaces[107] have been shown to augment MSC and NPC differentiation. Controlling scaffold porosity can passively impact cell-cell connections, which has been used to control MSC immunomodulatory function.[108–111]

In addition to direct cell-cell connections, controlling paracrine signaling, in particular of MSCs is of considerable interest, as the MSC secretome, consisting of growth factors, cytokines, and miRNA molecules, has shown anti-inflammatory and angiogenic capabilities, among other therapeutic benefits.[112] Furthermore, secretome composition has been shown to be highly dependent on the cell environmental conditions, such as material properties, cadherin signaling, hypoxic conditions and pro-inflammatory cytokine supplementation, which presents an opportunity to optimize the secretory profile depending on the application of interest.[113]

1.2.8 Controlling Cell Behavior with Biochemical Cues

The primary means of utilizing biomaterials to present biochemical signals to cells is by mimicking ECM sequestration and release of growth factors and chemokines, through either covalent[114] conjugation or affinity-based non-covalent attachment[115,116]. Heparin is well known for its affinity (mainly electrostatic interaction) with several growth factors such as TGF-β1 and bFGF, and as such functionalizing a biomaterial scaffold with heparin or heparin-mimicking chemical moeities is a common strategy for growth factor release.[117] In addition to drug release, these systems can be used to affect the

function of cells within the biomaterials. For example, IFN-γ was tethered to an injectable hydrogel to promote the immunomodulatory response of encapsulated MSCs[118], and in another study, TGF-β1 was chemically conjugated to a hydrogel to promote chondrogenic differentiation of MSCs[119].

1.3 Motivation for Research

In this work, I explored the use of MIHs for systems that benefit from the presence of the interconnected pore network. As cells are grown on the surface of microgels, and in the interstitial pore space between microgels, there is no barrier to cell spreading, and to making cell-cell connections. This is in stark contrast to traditional injectable hydrogels, where cells can be entrapped by the polymer mesh depending on the polymer concentration, delaying cell spreading, locomotion, and cell-cell contacts. Additionally, porosity of MIH facilitates nutrient transport, enables integration into the host tissue and induces cell migration into the hydrogel interior and vascularization, making them superior to traditional injectable hydrogels in many aspects. The work in this dissertation builds off of the platform previously developed in our lab[62] and its variations for examining the effect of this interconnected pore network on the phenotypic response of the encapsulated cells. In chapter 2, I first demonstrated the use of gelatin-based microporous injectable hydrogel systems for MSC delivery. In chapters 3-4, I applied this technology to MSC delivery for bone repair (chapter 3), and NPC delivery for CNS injury repair (chapter 4). Strategies for the future utilization of this technology are discussed in chapter 5.

References

(1) Huebsch, N.; Mooney, D. J. Inspiration and Application in the Evolution of Biomaterials. *Nature* **2009**, *462* (7272), 426. https://doi.org/10.1038/NATURE08601.

(2) Kim, H. S.; Kumbar, S. G.; Nukavarapu, S. P. Biomaterial-Directed Cell Behavior for Tissue Engineering. *Curr. Opin. Biomed. Eng.* **2021**, *17*. https://doi.org/10.1016/J.COBME.2020.100260.

(3) Balla, V. K.; Bodhak, S.; Datta, P.; Kundu, B.; Das, M.; Bandyopadhyay, A.; Bose, S. Biointegration of Three-Dimensional–Printed Biomaterials and Biomedical Devices. *Biointegration Med. Implant Mater.* **2020**, 433–482. https://doi.org/10.1016/B978-0-08-102680-9.00016-0.

(4) Lee, K. Y.; Mooney, D. J. Hydrogels for Tissue Engineering. *Chem. Rev.* **2001**, *101* (7), 1869–1879. https://doi.org/10.1021/cr000108x.

(5) Nair, L. S.; Laurencin, C. T. Biodegradable Polymers as Biomaterials. *Prog. Polym. Sci.* **2007**, *32* (8–9), 762–798. https://doi.org/10.1016/J.PROGPOLYMSCI.2007.05.017.

(6) Rozario, T.; DeSimone, D. W. The Extracellular Matrix in Development and Morphogenesis: A Dynamic View. *Dev. Biol.* **2010**, *341* (1), 126–140. https://doi.org/10.1016/J.YDBIO.2009.10.026.

(7) Vining, K. H.; Mooney, D. J. Mechanical Forces Direct Stem Cell Behaviour in Development and Regeneration. *Nat. Rev. Mol. Cell Biol.* **2017**, *18* (12), 728–742.

https://doi.org/10.1038/nrm.2017.108.

(8) Liu, X.; Liu, J.; Lin, S.; Zhao, X. Hydrogel Machines. *Mater. Today* **2020**, *36*, 102–124. https://doi.org/10.1016/J.MATTOD.2019.12.026.

(9) Catoira, M. C.; Fusaro, L.; Di Francesco, D.; Ramella, M.; Boccafoschi, F. Overview of Natural Hydrogels for Regenerative Medicine Applications. *J. Mater. Sci. Mater. Med.* **2019**, *30* (10), 1–10. https://doi.org/ 10.1007/s10856-019-6318-7.

(10) Patterson, J.; Siew, R.; Herring, S. W.; Lin, A. S. P.; Guldberg, R.; Stayton, P. S. Hyaluronic Acid Hydrogels with Controlled Degradation Properties for Oriented Bone Regeneration. *Biomaterials* **2010**, *31* (26), 6772–6781. https://doi.org/10.1016/J.BIOMATERIALS.2010.05.047.

(11) Van Dijk-Wolthuis, W. N. E.; Hoogeboom, J. A. M.; Van Steenbergen, M. J.; Tsang, S. K. Y.; Hennink, W. E. Degradation and Release Behavior of Dextran-Based Hydrogels. *Macromolecules* **1997**, *30* (16), 4639–4645. https://doi.org/10.1021/ma9704018.

(12) Jeon, O.; Alt, D. S.; Ahmed, S. M.; Alsberg, E. The Effect of Oxidation on the Degradation of Photocrosslinkable Alginate Hydrogels. *Biomaterials* **2012**, *33* (13), 3503–3514. https://doi.org/10.1016/J.BIOMATERIALS.2012.01.041.

(13) An, B.; Kaplan, D. L.; Brodsky, B. Engineered Recombinant Bacterial Collagen as an Alternative Collagen-Based Biomaterial for Tissue Engineering. *Front. Chem.* **2014**, *2*. https://doi.org/10.3389/FCHEM.2014.00040/BIBTEX.

(14) Farajollahi, M. M.; Hamzehlou, S.; Mehdipour, A.; Samadikuchaksaraei, A.

Recombinant Proteins: Hopes for Tissue Engineering. *Bioimpacts* **2012**, *2* (3), 123. https://doi.org/10.5681/BI.2012.010.

(15) Ulbricht, J.; Jordan, R.; Luxenhofer, R. On the Biodegradability of Polyethylene Glycol, Polypeptoids and Poly(2-Oxazoline)S. *Biomaterials* **2014**, *35* (17), 4848–4861. https://doi.org/10.1016/J.BIOMATERIALS.2014.02.029.

(16) Hern, D. L.; Hubbell, J. A. Incorporation of Adhesion Peptides into Nonadhesive Hydrogels Useful for Tissue Resurfacing. *J Biomed Mater Res* **1998**, *39*, 266–276. https://doi.org/10.1002/(SICI)1097-4636(199802)39:2.

(17) Schmedlen, R. H.; Masters, K. S.; West, J. L. Photocrosslinkable Polyvinyl Alcohol Hydrogels That Can Be Modified with Cell Adhesion Peptides for Use in Tissue Engineering. *Biomaterials* **2002**, *23* (22), 4325–4332. https://doi.org/10.1016/S0142-9612(02)00177-1.

(18) Lutolf, M. P.; Lauer-Fields, J. L.; Schmoekel, H. G.; Metters, A. T.; Weber, F. E.; Fields, G. B.; Hubbell, J. A. Synthetic Matrix Metalloproteinase-Sensitive Hydrogels for the Conduction of Tissue Regeneration: Engineering Cell-Invasion Characteristics. *Proc. Natl. Acad. Sci. U. S. A.* **2003**, *100* (9), 5413–5418. https://doi.org/10.1073/PNAS.0737381100.

(19) Umuhoza, D.; Yang, F.; Long, D.; Hao, Z.; Dai, J.; Zhao, A. Strategies for Tuning the Biodegradation of Silk Fibroin-Based Materials for Tissue Engineering Applications. *ACS Biomater. Sci. Eng.* **2020**, *6* (3), 1290–1310. https://doi.org/10.1021/ACSBIOMATERIALS.9B01781.

(20) Monzack, E. L.; Rodriguez, K. J.; McCoy, C. M.; Gu, X.; Masters, K. S. Natural

Materials in Tissue Engineering Applications. *Biomater. Tissue Eng. Appl. A Rev. Past Futur. Trends* **2011**, 209–241. https://doi.org/10.1007/978-3-7091-0385-2_8.

(21) Hu, W.; Wang, Z.; Xiao, Y.; Zhang, S.; Wang, J. Advances in Crosslinking Strategies of Biomedical Hydrogels. *Biomater. Sci.* **2019**, *7* (3), 843–855. https://doi.org/10.1039/C8BM01246F.

(22) Echalier, C.; Valot, L.; Martinez, J.; Mehdi, A.; Subra, G. Chemical Cross-Linking Methods for Cell Encapsulation in Hydrogels. *Mater. Today Commun.* **2019**, *20*, 100536. https://doi.org/10.1016/J.MTCOMM.2019.05.012.

(23) Means, A. K.; Shrode, C. S.; Whitney, L. V.; Ehrhardt, D. A.; Grunlan, M. A. Double Network Hydrogels That Mimic the Modulus, Strength, and Lubricity of Cartilage. *Biomacromolecules* **2019**, *20* (5), 2034–2042. https://doi.org/10.1021/acs.biomac.9b00237.

(24) Hu, Y.; Jia, Y.; Wang, S.; Ma, Y.; Huang, G.; Ding, T.; Feng, D.; Genin, G. M.; Wei, Z.; Xu, F. An ECM-Mimicking, Injectable, Viscoelastic Hydrogel for Treatment of Brain Lesions. *Adv. Healthc. Mater.* **2023**, *12* (1), 2201594. https://doi.org/10.1002/ADHM.202201594.

(25) Dimatteo, R.; Darling, N. J.; Segura, T. In Situ Forming Injectable Hydrogels for Drug Delivery and Wound Repair. *Adv. Drug Deliv. Rev.* **2018**, *127*, 167–184. https://doi.org/10.1016/J.ADDR.2018.03.007.

(26) Almawash, S.; Osman, S. K.; Mustafa, G.; El Hamd, M. A. Current and Future Prospective of Injectable Hydrogels—Design Challenges and Limitations. *Pharmaceuticals* **2022**, *15* (3). https://doi.org/10.3390/PH15030371.

(27) Sisso, A. M.; Boit, M. O.; DeForest, C. A. Self-Healing Injectable Gelatin Hydrogels for Localized Therapeutic Cell Delivery. *J. Biomed. Mater. Res. Part A* **2020**, *108* (5), 1112–1121. https://doi.org/10.1002/JBM.A.36886.

(28) Thambi, T.; Li, Y.; Lee, D. S. Injectable Hydrogels for Sustained Release of Therapeutic Agents. *J. Control. Release* **2017**, *267*, 57–66. https://doi.org/10.1016/J.JCONREL.2017.08.006.

(29) Hoque, J.; Prakash, R. G.; Paramanandham, K.; Shome, B. R.; Haldar, J. Biocompatible Injectable Hydrogel with Potent Wound Healing and Antibacterial Properties. *Mol. Pharm.* **2017**, *14* (4), 1218–1230. https://doi.org/10.1021/ACS.MOLPHARMACEUT.6B01104.

(30) Wei, K.; Senturk, B.; Matter, M. T.; Wu, X.; Herrmann, I. K.; Rottmar, M.; Toncelli, C. Mussel-Inspired Injectable Hydrogel Adhesive Formed under Mild Conditions Features Near-Native Tissue Properties. *ACS Appl. Mater. Interfaces* **2019**, *11* (51), 47707–47719. https://doi.org/10.1021/ACSAMI.9B16465.

(31) C Morgan, F. L.; Moroni, L.; Baker, M. B.; C Morgan, F. L.; Moroni, L.; Baker, M. B. Dynamic Bioinks to Advance Bioprinting. *Adv. Healthc. Mater.* **2020**, *9* (15), 1901798. https://doi.org/10.1002/ADHM.201901798.

(32) Tang, Y.; Lin, S.; Yin, S.; Jiang, F.; Zhou, M.; Yang, G.; Sun, N.; Zhang, W.; Jiang, X. In Situ Gas Foaming Based on Magnesium Particle Degradation: A Novel Approach to Fabricate Injectable Macroporous Hydrogels. *Biomaterials* **2020**, *232*, 119727. https://doi.org/10.1016/J.BIOMATERIALS.2019.119727.

(33) Riau, A. K.; Mondal, D.; Setiawan, M.; Palaniappan, A.; Yam, G. H. F.; Liedberg,

B.; Venkatraman, S. S.; Mehta, J. S. Functionalization of the Polymeric Surface with Bioceramic Nanoparticles via a Novel, Nonthermal Dip Coating Method. *ACS Appl. Mater. Interfaces* **2016**, *8* (51), 35565–35577. https://doi.org/10.1021/ACSAMI.6B12371.

(34) Ding, D.; Zhu, Z.; Li, R.; Li, X.; Wu, W.; Jiang, X.; Liu, B. Nanospheres-Incorporated Implantable Hydrogel as a Trans-Tissue Drug Delivery System. *ACS Nano* **2011**, *5* (4), 2520–2534. https://doi.org/10.1021/NN102138U.

(35) Gkioni, K.; Leeuwenburgh, S. C. G.; Douglas, T. E. L.; Mikos, A. G.; Jansen, J. A. Mineralization of Hydrogels for Bone Regeneration. *https://home.liebertpub.com/teb* **2010**, *16* (6), 577–585. https://doi.org/10.1089/TEN.TEB.2010.0462.

(36) Chen, Q.; Chen, H.; Zhu, L.; Zheng, J. Fundamentals of Double Network Hydrogels. *J. Mater. Chem. B* **2015**, *3* (18), 3654–3676. https://doi.org/10.1039/C5TB00123D.

(37) Kim, J.; Yaszemski, M. J.; Lu, L. Three-Dimensional Porous Biodegradable Polymeric Scaffolds Fabricated with Biodegradable Hydrogel Porogens. *Tissue Eng. - Part C Methods* **2009**, *15* (4), 583–594. https://doi.org/10.1089/TEN.TEC.2008.0642.

(38) Zhao, Y.; Li, M.; Liu, B.; Xiang, J.; Cui, Z.; Qu, X.; Qiu, D.; Tian, Y.; Yang, Z. Ultra-Tough Injectable Cytocompatible Hydrogel for 3D Cell Culture and Cartilage Repair. *J. Mater. Chem. B* **2018**, *6* (9), 1351–1358. https://doi.org/10.1039/C7TB03177G.

(39) Boyer, C.; Figueiredo, L.; Pace, R.; Lesoeur, J.; Rouillon, T.; Visage, C. Le; Tassin, J. F.; Weiss, P.; Guicheux, J.; Rethore, G. Laponite Nanoparticle-Associated Silated Hydroxypropylmethyl Cellulose as an Injectable Reinforced Interpenetrating Network Hydrogel for Cartilage Tissue Engineering. *Acta Biomater.* **2018**, *65*, 112–122. https://doi.org/10.1016/J.ACTBIO.2017.11.027.

(40) Lokhande, G.; Carrow, J. K.; Thakur, T.; Xavier, J. R.; Parani, M.; Bayless, K. J.; Gaharwar, A. K. Nanoengineered Injectable Hydrogels for Wound Healing Application. *Acta Biomater.* **2018**, *70*, 35–47. https://doi.org/10.1016/J.ACTBIO.2018.01.045.

(41) Pérez-Rafael, S.; Ivanova, K.; Stefanov, I.; Puiggalí, J.; del Valle, L. J.; Todorova, K.; Dimitrov, P.; Hinojosa-Caballero, D.; Tzanov, T. Nanoparticle-Driven Self-Assembling Injectable Hydrogels Provide a Multi-Factorial Approach for Chronic Wound Treatment. *Acta Biomater.* **2021**, *134*, 131–143. https://doi.org/10.1016/J.ACTBIO.2021.07.020.

(42) Tran, K. A.; Jin, Y.; Bouyer, J.; DeOre, B. J.; Suprewicz, Ł.; Figel, A.; Walens, H.; Fischer, I.; Galie, P. A. Magnetic Alignment of Injectable Hydrogel Scaffolds for Spinal Cord Injury Repair. *Biomater. Sci.* **2022**, *10* (9), 2237–2247. https://doi.org/10.1039/D1BM01590G.

(43) Qu, J.; Zhao, X.; Liang, Y.; Zhang, T.; Ma, P. X.; Guo, B. Antibacterial Adhesive Injectable Hydrogels with Rapid Self-Healing, Extensibility and Compressibility as Wound Dressing for Joints Skin Wound Healing. *Biomaterials* **2018**, *183*, 185–199. https://doi.org/10.1016/J.BIOMATERIALS.2018.08.044.

(44) Huebsch, N.; Kearney, C. J.; Zhao, X.; Kim, J.; Cezar, C. A.; Suo, Z.; Mooney, D. J. Ultrasound-Triggered Disruption and Self-Healing of Reversibly Cross-Linked Hydrogels for Drug Delivery and Enhanced Chemotherapy. *Proc. Natl. Acad. Sci. U. S. A.* **2014**, *111* (27), 9762–9767. https://doi.org/10.1073/PNAS.1405469111.

(45) Hernandez, J. L.; Woodrow, K. A. Medical Applications of Porous Biomaterials: Features of Porosity and Tissue-Specific Implications for Biocompatibility. *Adv. Healthc. Mater.* **2022**, *11* (9), 2102087. https://doi.org/10.1002/ADHM.202102087.

(46) Griveau, L.; Lafont, M.; le Goff, H.; Drouglazet, C.; Robbiani, B.; Berthier, A.; Sigaudo-Roussel, D.; Latif, N.; Visage, C. Le; Gache, V.; Debret, R.; Weiss, P.; Sohier, J. Design and Characterization of an in Vivo Injectable Hydrogel with Effervescently Generated Porosity for Regenerative Medicine Applications. *Acta Biomater.* **2022**, *140*, 324–337. https://doi.org/10.1016/J.ACTBIO.2021.11.036.

(47) Oh, J. K.; Drumright, R.; Siegwart, D. J.; Matyjaszewski, K. The Development of Microgels/Nanogels for Drug Delivery Applications. *Prog. Polym. Sci.* **2008**, *33* (4), 448–477. https://doi.org/10.1016/J.PROGPOLYMSCI.2008.01.002.

(48) Griffin, D. R.; Weaver, W. M.; Scumpia, P. O.; Di Carlo, D.; Segura, T. Accelerated Wound Healing by Injectable Microporous Gel Scaffolds Assembled from Annealed Building Blocks. *Nat. Mater. 2014 147* **2015**, *14* (7), 737–744. https://doi.org/10.1038/nmat4294.

(49) Loh, Q. L.; Choong, C. Three-Dimensional Scaffolds for Tissue Engineering Applications: Role of Porosity and Pore Size. *Tissue Eng. - Part B Rev.* **2013**, *19* (6), 485–502. https://doi.org/10.1089/TEN.TEB.2012.0437.

(50) Daly, A. C.; Riley, L.; Segura, T.; Burdick, J. A. Hydrogel Microparticles for Biomedical Applications. *Nat. Rev. Mater. 2019 51* **2019**, *5* (1), 20–43. https://doi.org/10.1038/s41578-019-0148-6.

(51) Li, J.; Mooney, D. J. Designing Hydrogels for Controlled Drug Delivery. *Nat. Rev. Mater. 2016 112* **2016**, *1* (12), 1–17. https://doi.org/10.1038/natrevmats.2016.71.

(52) Nguyen, A. H.; McKinney, J.; Miller, T.; Bongiorno, T.; McDevitt, T. C. Gelatin Methacrylate Microspheres for Controlled Growth Factor Release. *Acta Biomater.* **2015**, *13*, 101–110. https://doi.org/10.1016/J.ACTBIO.2014.11.028.

(53) Jaklenec, A.; Hinckfuss, A.; Bilgen, B.; Ciombor, D. M.; Aaron, R.; Mathiowitz, E. Sequential Release of Bioactive IGF-I and TGF-Beta 1 from PLGA Microsphere-Based Scaffolds. *Biomaterials* **2008**, *29* (10), 1518–1525. https://doi.org/10.1016/J.BIOMATERIALS.2007.12.004.

(54) Wang, Y.; Cooke, M. J.; Sachewsky, N.; Morshead, C. M.; Shoichet, M. S. Bioengineered Sequential Growth Factor Delivery Stimulates Brain Tissue Regeneration after Stroke. *J. Control. Release* **2013**, *172* (1), 1–11. https://doi.org/10.1016/J.JCONREL.2013.07.032.

(55) Bertsch, P.; Diba, M.; Mooney, D. J.; Leeuwenburgh, S. C. G. Self-Healing Injectable Hydrogels for Tissue Regeneration. *Chem. Rev.* **2023**, *123* (2), 834–873. https://doi.org/10.1021/ACS.CHEMREV.2C00179.

(56) Koh, J.; Griffin, D. R.; Archang, M. M.; Feng, A. C.; Horn, T.; Margolis, M.; Zalazar, D.; Segura, T.; Scumpia, P. O.; Di Carlo, D. Enhanced In Vivo Delivery of Stem Cells Using Microporous Annealed Particle Scaffolds. *Small* **2019**, *15* (39),

1903147. https://doi.org/10.1002/SMLL.201903147.

(57) Nih, L. R.; Sideris, E.; Carmichael, S. T.; Segura, T. Injection of Microporous Annealing Particle (MAP) Hydrogels in the Stroke Cavity Reduces Gliosis and Inflammation and Promotes NPC Migration to the Lesion. *Adv. Mater.* **2017**, *29* (32). https://doi.org/10.1002/ADMA.201606471.

(58) Highley, C. B.; Hoon Song, K.; Daly, A. C.; Burdick, J. A.; Highley, C. B.; Song, K. H.; Daly, A. C.; Burdick, J. A. Jammed Microgel Inks for 3D Printing Applications. *Adv. Sci.* **2019**, *6* (1), 1801076. https://doi.org/10.1002/ADVS.201801076.

(59) Ataie, Z.; Kheirabadi, S.; Zhang, J. W.; Kedzierski, A.; Petrosky, C.; Jiang, R.; Vollberg, C.; Sheikhi, A. Nanoengineered Granular Hydrogel Bioinks with Preserved Interconnected Microporosity for Extrusion Bioprinting. *Small* **2022**, *18* (37), 2202390. https://doi.org/10.1002/SMLL.202202390.

(60) Muir, V. G.; Qazi, T. H.; Weintraub, S.; Torres Maldonado, B. O.; Arratia, P. E.; Burdick, J. A. Sticking Together: Injectable Granular Hydrogels with Increased Functionality via Dynamic Covalent Inter-Particle Crosslinking. *Small* **2022**, *18* (36), 2201115. https://doi.org/10.1002/SMLL.202201115.

(61) Seymour, A. J.; Shin, S.; Heilshorn, S. C. 3D Printing of Microgel Scaffolds with Tunable Void Fraction to Promote Cell Infiltration. *Adv. Healthc. Mater.* **2021**, *10* (18), 2100644. https://doi.org/10.1002/ADHM.202100644.

(62) Hou, S.; Lake, R.; Park, S.; Edwards, S.; Jones, C.; Jeong, K. J. Injectable Macroporous Hydrogel Formed by Enzymatic Cross-Linking of Gelatin Microgels. *ACS Appl. Bio Mater.* **2018**, *1* (5), 1430–1439.

https://doi.org/10.1021/ACSABM.8B00380.

(63) Ikada, Y. Challenges in Tissue Engineering. *J. R. Soc. Interface* **2006**, *3* (10), 589–601. https://doi.org/10.1098/RSIF.2006.0124.

(64) Soto-Gutierrez, A.; Yagi, H.; Uygun, B. E.; Navarro-Alvarez, N.; Uygun, K.; Kobayashi, N.; Yang, Y. G.; Yarmush, M. L. Cell Delivery: From Cell Transplantation to Organ Engineering. *Cell Transplant.* **2010**, *19* (6), 655. https://doi.org/10.3727/096368910X508753.

(65) Hwang, N. S.; Zhang, C.; Hwang, Y. S.; Varghese, S. Mesenchymal Stem Cell Differentiation and Roles in Regenerative Medicine. *Wiley Interdiscip. Rev. Syst. Biol. Med.* **2009**, *1* (1), 97–106. https://doi.org/10.1002/WSBM.26.

(66) George, S.; Hamblin, M. R.; Abrahamse, H. Differentiation of Mesenchymal Stem Cells to Neuroglia: In the Context of Cell Signalling. *Stem Cell Rev. Reports* **2019**, *15* (6), 814–826. https://doi.org/10.1007/S12015-019-09917-Z.

(67) Yu, D.; Cai, Z.; Li, D.; Zhang, Y.; He, M.; Yang, Y.; Liu, D.; Xie, W.; Li, Y.; Xiao, W. Myogenic Differentiation of Stem Cells for Skeletal Muscle Regeneration. *Stem Cells Int.* **2021**, *2021*. https://doi.org/10.1155/2021/8884283.

(68) Guo, X.; Bai, Y.; Zhang, L.; Zhang, B.; Zagidullin, N.; Carvalho, K.; Du, Z.; Cai, B. Cardiomyocyte Differentiation of Mesenchymal Stem Cells from Bone Marrow: New Regulators and Its Implications. *Stem Cell Res. Ther. 2018 91* **2018**, *9* (1), 1–12. https://doi.org/10.1186/S13287-018-0773-9.

(69) Amer, M. H.; Rose, F. R. A. J.; Shakesheff, K. M.; Modo, M.; White, L. J.

Translational Considerations in Injectable Cell-Based Therapeutics for Neurological Applications: Concepts, Progress and Challenges. *npj Regen. Med. 2017 21* **2017**, *2* (1), 1–13. https://doi.org/10.1038/s41536-017-0028-x.

(70) Milone, M. C.; Xu, J.; Chen, S. J.; Collins, M. K. A.; Zhou, J.; Powell, D. J.; Melenhorst, J. J. Engineering-Enhanced CAR T Cells for Improved Cancer Therapy. *Nat. Cancer 2021 28* **2021**, *2* (8), 780–793. https://doi.org/10.1038/s43018-021-00241-5.

(71) Mandal, A.; Clegg, J. R.; Anselmo, A. C.; Mitragotri, S. Hydrogels in the Clinic. *Bioeng. Transl. Med.* **2020**, *5* (2). https://doi.org/10.1002/BTM2.10158.

(72) Toh, W. S.; Loh, X. J. Advances in Hydrogel Delivery Systems for Tissue Regeneration. *Mater. Sci. Eng. C. Mater. Biol. Appl.* **2014**, *45*, 690–697. https://doi.org/10.1016/J.MSEC.2014.04.026.

(73) Wade, R. J.; Burdick, J. A. Engineering ECM Signals into Biomaterials. *Mater. Today* **2012**, *15* (10), 454–459. https://doi.org/10.1016/S1369-7021(12)70197-9.

(74) Ahearne, M. Introduction to Cell–Hydrogel Mechanosensing. *Interface Focus* **2014**, *4* (2). https://doi.org/10.1098/RSFS.2013.0038.

(75) Moreo, P.; García-Aznar, J. M.; Doblaré, M. Modeling Mechanosensing and Its Effect on the Migration and Proliferation of Adherent Cells. *Acta Biomater.* **2008**, *4* (3), 613–621. https://doi.org/10.1016/J.ACTBIO.2007.10.014.

(76) Stanton, A. E.; Tong, X.; Yang, F. Extracellular Matrix Type Modulates Mechanotransduction of Stem Cells. *Acta Biomater.* **2019**, *96*, 310–320.

https://doi.org/10.1016/J.ACTBIO.2019.06.048.

(77) Kapp, T. G.; Rechenmacher, F.; Neubauer, S.; Maltsev, O. V.; Cavalcanti-Adam, E. A.; Zarka, R.; Reuning, U.; Notni, J.; Wester, H. J.; Mas-Moruno, C.; Spatz, J.; Geiger, B.; Kessler, H. A Comprehensive Evaluation of the Activity and Selectivity Profile of Ligands for RGD-Binding Integrins. *Sci. Reports 2017 71* **2017**, *7* (1), 1–13. https://doi.org/10.1038/srep39805.

(78) DiPersio, C. M.; Hodivala-Dilke, K. M.; Jaenisch, R.; Kreidberg, J. A.; Hynes, R. O. A3β1 Integrin Is Required for Normal Development of the Epidermal Basement Membrane. *J. Cell Biol.* **1997**, *137* (3), 729. https://doi.org/10.1083/JCB.137.3.729.

(79) Kanchanawong, P.; Shtengel, G.; Pasapera, A. M.; Ramko, E. B.; Davidson, M. W.; Hess, H. F.; Waterman, C. M. Nanoscale Architecture of Integrin-Based Cell Adhesions. *Nat. 2010 4687323* **2010**, *468* (7323), 580–584. https://doi.org/10.1038/nature09621.

(80) Burridge, K. Focal Adhesions: A Personal Perspective on a Half Century of Progress. *FEBS J.* **2017**, *284* (20), 3355–3361. https://doi.org/10.1111/FEBS.14195.

(81) Dupont, S.; Morsut, L.; Aragona, M.; Enzo, E.; Giulitti, S.; Cordenonsi, M.; Zanconato, F.; Le Digabel, J.; Forcato, M.; Bicciato, S.; Elvassore, N.; Piccolo, S. Role of YAP/TAZ in Mechanotransduction. *Nat. 2011 4747350* **2011**, *474* (7350), 179–183. https://doi.org/10.1038/nature10137.

(82) Chen, C. S.; Tan, J.; Tien, J. Mechanotransduction at Cell-Matrix and Cell-Cell

Contacts. *https://doi.org/10.1146/annurev.bioeng.6.040803.140040* **2004**, *6*, 275–302. https://doi.org/10.1146/ANNUREV.BIOENG.6.040803.140040.

(83) Zhang, Z.; Sha, B.; Zhao, L.; Zhang, H.; Feng, J.; Zhang, C.; Sun, L.; Luo, M.; Gao, B.; Guo, H.; Wang, Z.; Xu, F.; Lu, T. J.; Genin, G. M.; Lin, M. Programmable Integrin and N-Cadherin Adhesive Interactions Modulate Mechanosensing of Mesenchymal Stem Cells by Cofilin Phosphorylation. *Nat. Commun. 2022 131* **2022**, *13* (1), 1–14. https://doi.org/10.1038/s41467-022-34424-0.

(84) Ke, W.; Ma, L.; Wang, B.; Song, Y.; Luo, R.; Li, G.; Liao, Z.; Shi, Y.; Wang, K.; Feng, X.; Li, S.; Hua, W.; Yang, C. N-Cadherin Mimetic Hydrogel Enhances MSC Chondrogenesis through Cell Metabolism. *Acta Biomater.* **2022**, *150*, 83–95. https://doi.org/10.1016/J.ACTBIO.2022.07.050.

(85) Niessen, C. M.; Leckband, D.; Yap, A. S. Tissue Organization by Cadherin Adhesion Molecules: Dynamic Molecular and Cellular Mechanisms of Morphogenetic Regulation. *Physiol. Rev.* **2011**, *91* (2), 691. https://doi.org/10.1152/PHYSREV.00004.2010.

(86) Briquez, P. S.; Hubbell, J. A.; Martino, M. M. Extracellular Matrix-Inspired Growth Factor Delivery Systems for Skin Wound Healing. *Adv. Wound Care* **2015**, *4* (8), 479. https://doi.org/10.1089/WOUND.2014.0603.

(87) Naqvi, S. M.; McNamara, L. M. Stem Cell Mechanobiology and the Role of Biomaterials in Governing Mechanotransduction and Matrix Production for Tissue Regeneration. *Front. Bioeng. Biotechnol.* **2020**, *8*, 1375. https://doi.org/10.3389/FBIOE.2020.597661.

(88) Engler, A. J.; Sen, S.; Sweeney, H. L.; Discher, D. E. Matrix Elasticity Directs Stem Cell Lineage Specification. *Cell* **2006**, *126* (4), 677–689. https://doi.org/10.1016/J.CELL.2006.06.044.

(89) Discher, D. E.; Janmey, P.; Wang, Y. L. Tissue Cells Feel and Respond to the Stiffness of Their Substrate. *Science (80-.).* **2005**, *310* (5751), 1139–1143. https://doi.org/10.1126/SCIENCE.1116995.

(90) Choi, J. S.; Harley, B. A. C. The Combined Influence of Substrate Elasticity and Ligand Density on the Viability and Biophysical Properties of Hematopoietic Stem and Progenitor Cells. *Biomaterials* **2012**, *33* (18), 4460–4468. https://doi.org/10.1016/J.BIOMATERIALS.2012.03.010.

(91) Chaudhuri, O.; Gu, L.; Klumpers, D.; Darnell, M.; Bencherif, S. A.; Weaver, J. C.; Huebsch, N.; Lee, H. P.; Lippens, E.; Duda, G. N.; Mooney, D. J. Hydrogels with Tunable Stress Relaxation Regulate Stem Cell Fate and Activity. *Nat. Mater. 2015 153* **2015**, *15* (3), 326–334. https://doi.org/10.1038/nmat4489.

(92) Chaudhuri, O.; Gu, L.; Darnell, M.; Klumpers, D.; Bencherif, S. A.; Weaver, J. C.; Huebsch, N.; Mooney, D. J. Substrate Stress Relaxation Regulates Cell Spreading. *Nat. Commun.* **2015**, *6*. https://doi.org/10.1038/ncomms7365.

(93) Yang, B.; Wei, K.; Loebel, C.; Zhang, K.; Feng, Q.; Li, R.; Wong, S. H. D.; Xu, X.; Lau, C.; Chen, X.; Zhao, P.; Yin, C.; Burdick, J. A.; Wang, Y.; Bian, L. Enhanced Mechanosensing of Cells in Synthetic 3D Matrix with Controlled Biophysical Dynamics. *Nat. Commun. 2021 121* **2021**, *12* (1), 1–13. https://doi.org/10.1038/s41467-021-23120-0.

(94) Chen, C. S.; Mrksich, M.; Huang, S.; Whitesides, G. M.; Ingber, D. E. Geometric Control of Cell Life and Death. *Science (80-.).* **1997**, *276* (5317), 1425–1428. https://doi.org/10.1126/SCIENCE.276.5317.1425.

(95) McBeath, R.; Pirone, D. M.; Nelson, C. M.; Bhadriraju, K.; Chen, C. S. Cell Shape, Cytoskeletal Tension, and RhoA Regulate Stem Cell Lineage Commitment. *Dev. Cell* **2004**, *6* (4), 483–495. https://doi.org/10.1016/S1534-5807(04)00075-9.

(96) Kilian, K. A.; Bugarija, B.; Lahn, B. T.; Mrksich, M. Geometric Cues for Directing the Differentiation of Mesenchymal Stem Cells. *Proc. Natl. Acad. Sci. U. S. A.* **2010**, *107* (11), 4872–4877. https://doi.org/10.1073/PNAS.0903269107.

(97) Wu, M. C.; Yu, H. W.; Chen, Y. Q.; Ou, M. H.; Serrano, R.; Huang, G. L.; Wang, Y. K.; Lin, K. hui; Fan, Y. J.; Wu, C. C.; del Álamo, J. C.; Chiou, A.; Chien, S.; Kuo, J. C. Early Committed Polarization of Intracellular Tension in Response to Cell Shape Determines the Osteogenic Differentiation of Mesenchymal Stromal Cells. *Acta Biomater.* **2022**. https://doi.org/10.1016/J.ACTBIO.2022.10.052.

(98) Furukawa, F.; Fujii, K.; Horiguchi, Y.; Matsuyoshi, N.; Fujita, M.; Toda, K.-I.; Imamura, S.; Wakita, H.; Shirahama, S.; Takigawa, M. Roles of E-and P-Cadherin in the Human Skin. *Microsc. Res. Tech* **1997**, *38*, 343–352. https://doi.org/10.1002/(SICI)1097-0029(19970815)38:4.

(99) Lagendijk, A. K.; Hogan, B. M. VE-Cadherin in Vascular Development: A Coordinator of Cell Signaling and Tissue Morphogenesis. *Curr. Top. Dev. Biol.* **2015**, *112*, 325–352. https://doi.org/10.1016/BS.CTDB.2014.11.024.

(100) Howard, C. M.; Baudino, T. A. Dynamic Cell–Cell and Cell–ECM Interactions in

the Heart. *J. Mol. Cell. Cardiol.* **2014**, *70*, 19–26. https://doi.org/10.1016/J.YJMCC.2013.10.006.

(101) Pereda, A. E. Electrical Synapses and Their Functional Interactions with Chemical Synapses. *Nat. Rev. Neurosci. 2014 154* **2014**, *15* (4), 250–263. https://doi.org/10.1038/nrn3708.

(102) Novosel, E. C.; Kleinhans, C.; Kluger, P. J. Vascularization Is the Key Challenge in Tissue Engineering. *Adv. Drug Deliv. Rev.* **2011**, *63* (4–5), 300–311. https://doi.org/10.1016/J.ADDR.2011.03.004.

(103) Passanha, F. R.; Geuens, T.; LaPointe, V. L. S. Sticking Together: Harnessing Cadherin Biology for Tissue Engineering. *Acta Biomater.* **2021**, *134*, 107–115. https://doi.org/10.1016/J.ACTBIO.2021.07.070.

(104) Le Saux, G.; Wu, M. C.; Toledo, E.; Chen, Y. Q.; Fan, Y. J.; Kuo, J. C.; Schvartzman, M. Cell-Cell Adhesion-Driven Contact Guidance and Its Effect on Human Mesenchymal Stem Cell Differentiation. *ACS Appl. Mater. Interfaces* **2020**, *12* (20), 22399–22409. https://doi.org/10.1021/ACSAMI.9B20939.

(105) Jiao, Q.; Li, X.; An, J.; Zhang, Z.; Chen, X.; Tan, J.; Zhang, P.; Lu, H.; Liu, Y. Cell-Cell Connection Enhances Proliferation and Neuronal Differentiation of Rat Embryonic Neural Stem/Progenitor Cells. *Front. Cell. Neurosci.* **2017**, *11*. https://doi.org/10.3389/FNCEL.2017.00200.

(106) Kwon, M. Y.; Vega, S. L.; Gramlich, W. M.; Kim, M.; Mauck, R. L.; Burdick, J. A. Dose and Timing of N-Cadherin Mimetic Peptides Regulate MSC Chondrogenesis within Hydrogels. *Adv. Healthc. Mater.* **2018**, *7* (9).

https://doi.org/10.1002/ADHM.201701199.

(107) Cherry, J. F.; Bennett, N. K.; Schachner, M.; Moghe, P. V. Engineered N-Cadherin and L1 Biomimetic Substrates Concertedly Promote Neuronal Differentiation, Neurite Extension and Neuroprotection of Human Neural Stem Cells. *Acta Biomater.* **2014**, *10* (10), 4113–4126. https://doi.org/10.1016/J.ACTBIO.2014.06.001.

(108) Qazi, T. H.; Mooney, D. J.; Duda, G. N.; Geissler, S. Niche-Mimicking Interactions in Peptide-Functionalized 3D Hydrogels Amplify Mesenchymal Stromal Cell Paracrine Effects. *Biomaterials* **2020**, *230*. https://doi.org/10.1016/J.BIOMATERIALS.2019.119639.

(109) Qazi, T. H.; Mooney, D. J.; Duda, G. N.; Geissler, S. Biomaterials That Promote Cell-Cell Interactions Enhance the Paracrine Function of MSCs. *Biomaterials* **2017**, *140*, 103–114. https://doi.org/10.1016/J.BIOMATERIALS.2017.06.019.

(110) Caldwell, A. S.; Rao, V. V.; Golden, A. C.; Anseth, K. S. Porous Bio-Click Microgel Scaffolds Control HMSC Interactions and Promote Their Secretory Properties. *Biomaterials* **2020**, *232*. https://doi.org/10.1016/J.BIOMATERIALS.2019.119725.

(111) Rao, V. V.; Wechsler, M. E.; Cravens, E.; Wojda, S. J.; Caldwell, A. S.; Kirkpatrick, B. E.; Donahue, S. W.; Anseth, K. S. Granular PEG Hydrogels Mediate Osteoporotic MSC Clustering via N-Cadherin Influencing the pro-Resorptive Bias of Their Secretory Profile. *Acta Biomater.* **2022**, *145*, 77–87. https://doi.org/10.1016/J.ACTBIO.2022.04.023.

(112) Sears, V.; Ghosh, G. Harnessing Mesenchymal Stem Cell Secretome: Effect of

Extracellular Matrices on Proangiogenic Signaling. *Biotechnol. Bioeng.* **2020**, *117* (4), 1159–1171. https://doi.org/10.1002/BIT.27272.

(113) Wechsler, M. E.; Rao, V. V.; Borelli, A. N.; Anseth, K. S. Engineering the MSC Secretome: A Hydrogel Focused Approach. *Adv. Healthc. Mater.* **2021**, *10* (7). https://doi.org/10.1002/ADHM.202001948.

(114) Mccall, J. D.; Luoma, J. E.; Anseth, K. S. Covalently Tethered Transforming Growth Factor Beta in PEG Hydrogels Promotes Chondrogenic Differentiation of Encapsulated Human Mesenchymal Stem Cells. *Drug Deliv. Transl. Res.* **2012**, *2* (5), 305–312. https://doi.org/10.1007/S13346-012-0090-2.

(115) Martino, M. M.; Briquez, P. S.; Güç, E.; Tortelli, F.; Kilarski, W. W.; Metzger, S.; Rice, J. J.; Kuhn, G. A.; MuÏller, R.; Swartz, M. A.; Hubbell, J. A. Growth Factors Engineered for Super-Affinity to the Extracellular Matrix Enhance Tissue Healing. *Science* **2014**, *343* (6173), 885–888. https://doi.org/10.1126/SCIENCE.1247663.

(116) Martino, M. M.; Briquez, P. S.; Ranga, A.; Lutolf, M. P.; Hubbell, J. A. Heparin-Binding Domain of Fibrin(Ogen) Binds Growth Factors and Promotes Tissue Repair When Incorporated within a Synthetic Matrix. *Proc. Natl. Acad. Sci. U. S. A.* **2013**, *110* (12), 4563–4568. https://doi.org/10.1073/PNAS.1221602110.

(117) Paluck, S. J.; Nguyen, T. H.; Maynard, H. D. Heparin-Mimicking Polymers: Synthesis and Biological Applications. *Biomacromolecules* **2016**, *17* (11), 3417–3440. https://doi.org/10.1021/ACS.BIOMAC.6B01147.

(118) García, J. R.; Quirós, M.; Han, W. M.; O'Leary, M. N.; Cox, G. N.; Nusrat, A.; García, A. J. IFN-γ-Tethered Hydrogels Enhance Mesenchymal Stem Cell-Based

Immunomodulation and Promote Tissue Repair. *Biomaterials* **2019**, *220*. https://doi.org/10.1016/J.BIOMATERIALS.2019.119403.

(119) Sridhar, B. V.; Doyle, N. R.; Randolph, M. A.; Anseth, K. S. Covalently Tethered TGF-B1 with Encapsulated Chondrocytes in a PEG Hydrogel System Enhances Extracellular Matrix Production. *J. Biomed. Mater. Res. A* **2014**, *102* (12), 4464–4472. https://doi.org/10.1002/JBM.A.35115.

Chapter 2

Fast-Curing Injectable Microporous Hydrogel for in Situ Cell Encapsulation

2.1 Introduction

Injectable hydrogels are of high interest for use in regenerative medicine due to their high-water content and their ability to conform to the shape of surrounding tissue.[1] They have been used as a temporary matrix for tissue regeneration,[2,3] or as a delivery vehicle for therapeutic substances such as cells,[4–6] growth factors,[7–9] or small molecule drugs.[10–12] However, most injectable hydrogels do not possess large enough pores to allow for host cell migration into the hydrogel interior, as the hydrogel mesh size is on the order of nanometers. When applied for *in situ* cell encapsulation, encapsulated cells are trapped by the polymer chains delaying cell spreading and proliferation. Lowering the polymer concentration of the injectable hydrogel (lower than 5% w/v) will increase the gel mesh size, and can improve its interaction with cells,[13–15] but the mechanical stability of such gels can be significantly compromised.

One strategy to create pores in an injectable hydrogel is through injection and subsequent annealing of microgels.[16–23] Pores are formed by the interstitial space between adjacent microgels which allows for infiltration of host cells, and rapid

spreading and proliferation of encapsulated cells. Such microporous hydrogels have applications in accelerated wound healing,[24] bone regeneration,[25] and *in situ* cell encapsulation for tissue engineering.[26–30] An optimal cell delivery vehicle should be capable of supporting a high concentration of cells, and facilitate interactions with the host tissue. Due to the high internal growth area, and demonstrated improved retention of delivered cells *in vivo*,[26] assembled microparticle scaffolds are a promising approach for delivery of therapeutic cells.

Previously, we reported an injectable microporous hydrogel composed of gelatin microgels enzymatically crosslinked by microbial transglutaminase (mTG).[31] This novel formulation did not require any chemical modifications to the starting reagents, and the resulting microporous hydrogel allowed the migration of surrounding cells to the hydrogel interior both *in vitro* and *ex vivo*, demonstrating its potential use in wound healing. This injectable formulation was also capable of *in situ* cell encapsulation, which resulted in rapid spreading and proliferation of encapsulated human dermal fibroblasts (hDFs) compared to the nonporous counterpart (**Fig. 2.2**). However, the enzymatic crosslinking by mTG requires a long curing time (~ 30 min), which limits its suitability for clinical applications.

Presented herein is a rapidly curing microporous hydrogel composed of composite microgels that are made of gelatin and gelatin methacryloyl (GelMA). A microporous hydrogel can be formed within 2.5 minutes by dual-crosslinking mechanisms – photopolymerization of GelMA and enzymatic crosslinking of unmodified gelatin by mTG (**Fig. 2.1**). Photopolymerization of GelMA allows for rapid formation of bulk gel from microgel building blocks, while enzymatic crosslinking by mTG further

stabilizes the hydrogel by forming additional covalent bonds between glutamine and lysine residues of gelatin and allows for tissue adhesion of the resulting hydrogel.[32] We demonstrate that this system enables the encapsulation human primary cells, such as hDFs and human mesenchymal stem cells (hMSCs), with high viability and cell spreading. In addition, priming hMSCs encapsulated in this system using IFN-γ enhanced the cellular secretion of anti-inflammatory molecules, which points to the potential use of this system for inflammatory diseases.

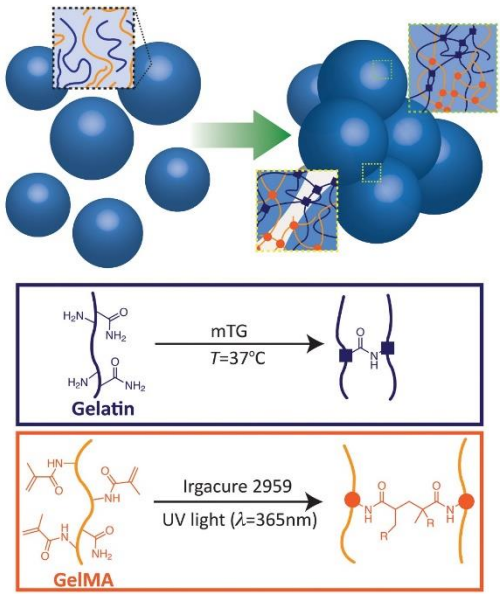

Figure 2.1. Schematic of the dual-crosslinking mechanisms of gelatin/GelMA microgels used to form a bulk hydrogel. A dual crosslinking approach is employed to rapidly cure microgels.

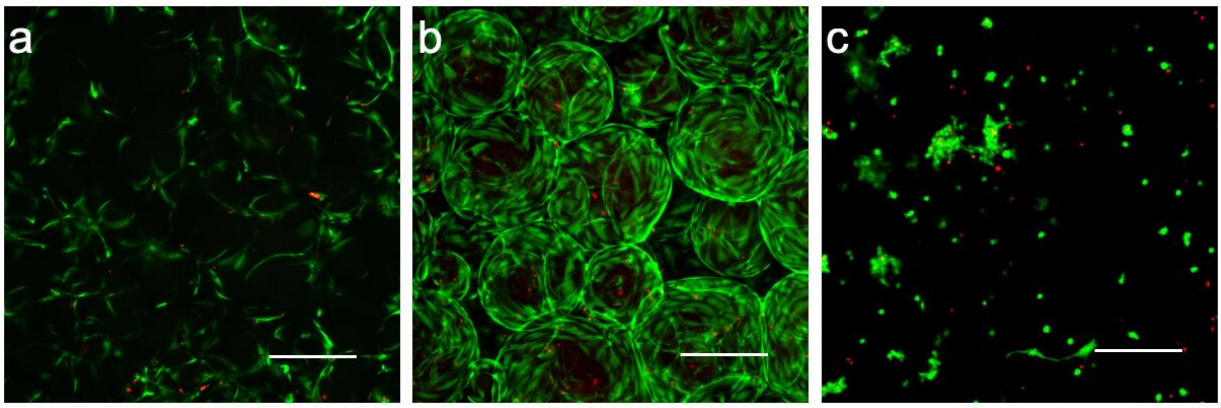

Figure 2.2. 2D projections of confocal microscope images of human dermal fibroblasts (hDFs) encapsulated in (a, b) microporous gelatin hydrogels and (c) nonporous gelatin hydrogel. The images were taken on (a) day 1 and (b, c) day 4 post encapsulation. Green and red fluorescence stains viable and dead cells, respectively. Scale bar = 200 μm.

2.2 Materials and Methods

2.2.1 Materials

All materials were purchased from Sigma-Aldrich (St. Louis, MO) unless specified. mTG was purchased from Ajinomoto (Fort Lee, NJ). Sterile phosphate buffer saline (PBS, pH 7.4), Dulbecco's Modified Eagle's Medium (DMEM), fetal bovine serum (FBS), and 10,000 U/ml penicillin/streptomycin (pen/strep) were purchased from Gibco (Carlsbad, CA). Human dermal fibroblasts (hDFs) were purchased from Lonza (Portsmouth, NH). Live/Dead Assay, Lactate Dehydrogenase (LDH) assay, IDO ELISA kit, and ActinRed 555 were purchased from Thermo Fisher Scientific (Waltham, MA). Fresh pig eyeballs were obtained from Visiontech (Sunnyvale, TX). Bone marrow derived hMSCs and media were purchased from Cell Applications (San Diego, CA). IL-6 and PGE2 ELISA kits were purchased from Abcam (Cambridge, MA).

2.2.2 Synthesis of Gelatin/GelMA Composite Microgels

The gelatin/GelMA composite microgels were prepared using a method similar to one previously described.[31] Due to the photoactive nature of GelMA, all procedures involving GelMA were performed in the dark. A 2:1 mixture (by weight) of gelatin (type A, from bovine and porcine bones, bloom 300 g) and gelatin methacryloyl (bloom 300 g, 80% degree of substitution) was dissolved in 20 mL of deionized water at 50−55 °C to make a total 10% (w/v) aqueous solution. This solution was added dropwise to 200 mL of olive oil at 50−55 °C and stirred for 1 hour. The temperature of the mixture was lowered to reach room temperature for 30 min with stirring. Then the mixture was placed in an ice−water bath for an additional 30 min with stirring to solidify the microgels by inducing physical crosslinking. To precipitate the microgels, 100 mL of pre-cooled acetone (4 °C) were added to the mixture with stirring for 30 min in the ice−water bath. The microgels were separated from the olive oil and acetone by vacuum filtration and further washed with two 60 mL aliquots of precooled (4 °C) acetone. The microgels were immediately frozen at -80 °C, lyophilized, and kept dry until used.

2.2.3 Characterization of Microgels

Microgels were visualized by scanning electron microscopy (SEM) (Tescan Lyra3 GMU FIB SEM, Brno, Czech Republic) and optical microscopy (EVOS XL, Life Technologies, Carlsbad, CA). Prior to the SEM imaging, lyophilized microgels were coated with gold/palladium to avoid charging. For quantification of hydrated microgel size distribution, 20 µL of a dilute microgel suspension in PBS was observed using an optical microscope. Size distribution of microgels was obtained from SEM and optical microscope images using ImageJ.

2.2.4 Bulk Hydrogel Formation

Microporous hydrogels were made by mixing gelatin/GelMA composite microgels (10% w/v) with photoinitiator (PI) (Irgacure 2959) in PBS (0.5% or 0.05% w/v). Ascorbic acid was added to a final concentration of 0.005% (w/v) to minimize cytotoxicity during the UV irradiation. This mixture was mixed with 20% (w/v) mTG in PBS in a 4:1 ratio. The final concentration of gelatin/GelMA polymer and mTG was 8.3% and 3.3%, respectively. UV light (365nm, ~35 mW/cm^2) was applied for 2.5 mins to induce photoinitiated crosslinking. Nonporous hydrogels were made using the same methods except that a gelatin/GelMA solution was used instead of gelatin/GelMA microgels.

2.2.5 Characterization of Hydrogels

After the hydrogels were formed, their detailed structures were visualized with SEM. Prior to SEM imaging, the hydrogels were dehydrated through an ethanol series (30%, 50%, 60%, 70%, 80% and 90% once each, and then 100% twice) before being dried by critical point drying and coated with gold/palladium.

The viscoelastic properties of the hydrogels were characterized by rheometry (TA Instruments AR 550, New Castle, DE). A gelatin/GelMA microgel suspension was made in PBS containing PI and ascorbic acid as previously described. Crosslinking was initiated by mixing of mTG, and/or introduction of UV source. The gelation kinetics were observed at 37 °C, with an oscillatory stress of 1 Pa at 10 rad/s. Once gelation was completed, a frequency sweep was performed, increasing angular frequency from 0.1 to 100 rad/s with an oscillatory stress of 1 Pa at 37 °C. Then, temperature sweep was performed. Temperature was gradually increased from 5 to 45 °C with an oscillatory stress of 1 Pa at 10 rad/s.

The enzymatic degradation of microporous gelatin/GelMA hydrogels and gelatin/GelMA microgels was examined by incubating in collagenase type II solution (concentration = 0.5 U/mL) at 37 °C. At different time points (0h, 4h, 24 h), the hydrogels and microgels were collected, lyophilized, and weighed to calculate the fraction of remaining solids content.

2.2.6 Tissue Adhesion of the Hydrogels

Porcine corneas were used to examine the tissue adhesion capability of the hydrogels. Corneas were collected from freshly obtained pig eyeballs using surgical scissors. A hole was created in the middle of the cornea using a biopsy punch (diameter = 8 mm) and was filled by injecting microgel solution prepared as previously described. After 2.5 min of crosslinking under different conditions, the tissue/hydrogel construct was immersed in a 45 °C warm water bath, to test for gelation and tissue adhesion.

2.2.7 Cell Encapsulation and Characterization

hDFs and hMSCs were cultured in T75 flasks using DMEM, supplemented with FBS and pen/strep or MSC growth medium, respectively. Cells of passage 3 were used for all experiments.

Prior to cell encapsulation, the gelatin/GelMA microgels were sterilized by incubation in 70% ethanol overnight, at 4 °C, then lyophilized before use. Gelatin, GelMA, mTG, Irgacure 2959, and ascorbic acid solutions were sterilized by syringe/vacuum filtration. For encapsulation, cells were mixed with microgel suspension or gelatin/GelMA solution in media, containing mTG, PI, and ascorbic acid, followed by 2.5 mins of UV irradiation. Hydrogels were then incubated at 37 °C for 1 hour. The encapsulated cells were cultured in the media described above.

The three-dimensional distribution of hDFs and hMSCs in hydrogel was visualized by confocal microscopy (Nikon A1R HD, Tokyo, Japan) on days 1 and 7 post-encapsulation using a live/dead cell viability kit, which stains living cells green (by calcein-AM) and dead cells red (by ethidium homodimer). To visualize the details of cell spreading and morphology inside the hydrogel, hDF samples were fixed in 4% paraformaldehyde (in PBS) overnight and stained with ActinRed 555. Z-stacked images were then obtained using the confocal microscope, and 2D projections were generated from Z-stacks using ImageJ. Sphericity, viability and proliferation were calculated using the plug-ins provided by ImageJ.

LDH assay was performed to assess cytotoxic effects related to the encapsulation process. hDFs seeded on well plates were used for maximum LDH controls, and hydrogels formed without encapsulated cells were used as negative controls. The culture media was removed on day 1 and 7 for analysis.

hMSC-laden hydrogels were exposed to growth medium with or without IFN-γ (50 ng/mL) after cell encapsulation. After 72 hours, the medium was removed and frozen at -20 °C until use. The media was tested for secreted factors IL-6, IDO, and PGE2, using ELISA kits.

2.2.8 Statistical Analysis

All data is represented as means, and all error bars represent standard deviations. All experiments were run with at least n = 3 samples. Statistical significance was determined using a student's t-test when comparing two groups, or Tukey's HSD post hoc test for experiments comparing more than two groups. $P < 0.05$ was considered statistically significant.

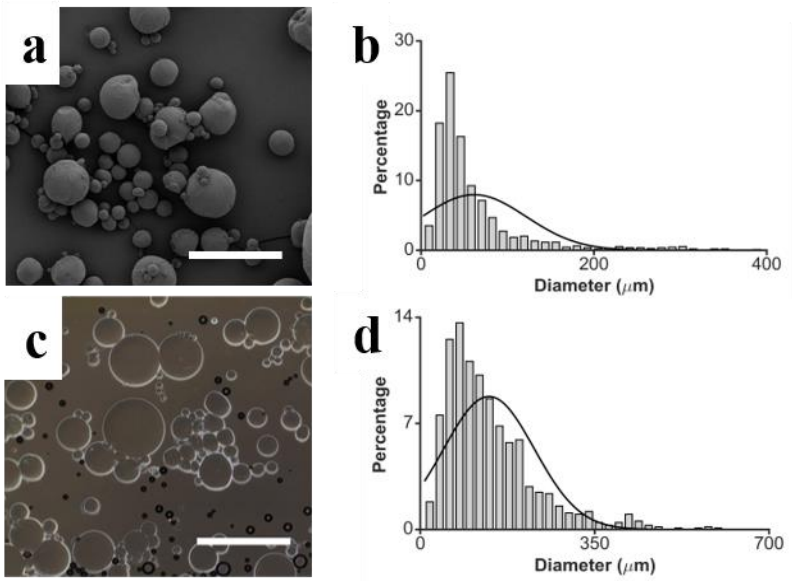

Figure 2.3. Composite microgel characterization. (a) SEM image of dry gelatin/GelMA microspheres. Scale bar = 200 μm (b) Size distribution of dry microspheres. The average diameter = 61 ± 60 μm. (c) Optical micrograph of gelatin/GelMA microgels in PBS. Scale bar = 200 μm. (d) Size distribution of swelled microgels. The average diameter = 139 ± 90 μm.

2.3 Results and Discussion

2.3.1 Microgel characterization

Gelatin/GelMA microgels were produced using a 10% (w/v) aqueous mixture of unmodified gelatin and GelMA (80% substitution) at a 2:1 ratio by weight, to achieve both enzymatic crosslinking by mTG and photocrosslinking by UV irradiation. A water-in-oil emulsion was created using this solution, which generated physically crosslinked polydisperse microspheres (**Fig. 2.3**). The freeze-dried microgels were spherical in shape (Fig. 2.3a) with an average diameter of 61 (± 60) μm (Fig. 2.3b). When equilibrated in an aqueous environment (Fig. 2.3c), the average diameter increased to 139 (± 90) μm due to swelling (Fig. 2.3d). Based on this, the space between assembled

microgels is on the order of tens of microns in size, which allows adequate space for encapsulation of human cells. Microgel polydispersity is a result of batch manufacture of microgels, and could be controlled through use of sieves. Photo-curable microgels from a mixture of unmodified gelatin and GelMA have advantages over GelMA-only microgels, as the mixture can be cured also by enzymatic crosslinking, and thermal stability of microgels can be fine-tuned by adjusting the gelatin/GelMA ratio. For example, previously described microgels that are made by GelMA only (80% substitution) are unstable at room temperature and the curing has to be done using chilled solutions,[17] which is not an ideal condition for *in situ* cell encapsulation. High-substitution GelMA microgels can be partially UV cured to improve stability,[33] but this solution creates a tradeoff between stability and hydrogel gelation that is not necessary when using composite microgels. Composite microgels are stable in an aqueous solution at room temperature (**Fig. 2.4**), allowing for cell encapsulation under ambient conditions. Physically crosslinked microgels dissociate rapidly at 37 °C and thus require rapid curing.

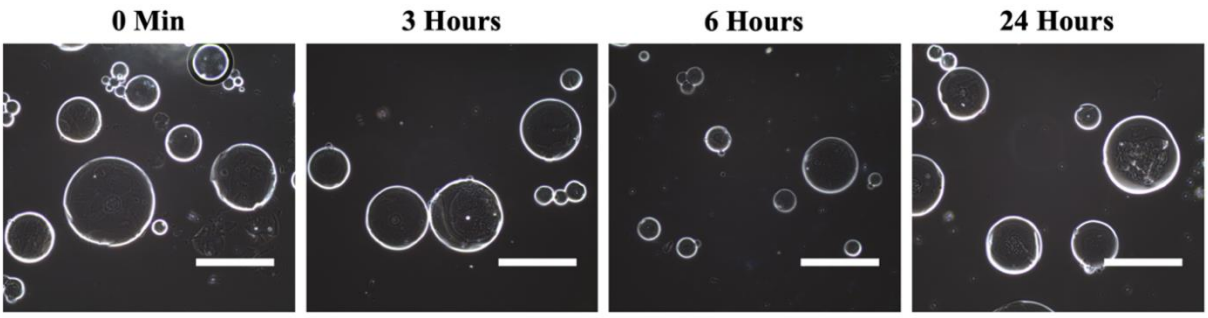

Figure 2.4. Microgels are stable when immersed in PBS at room temperature. Images taken with a light microscope show that microgels retain their shape in solution for at least 24 hours at 20 °C. Scale bar = 400 µm.

2.3.2 Rapid crosslinking

The gelatin/GelMA microgels are cured to form a bulk hydrogel by photopolymerization in the presence of photoinitiator (PI) and the addition of mTG. Rapid curing of the gelatin/GelMA microgels and the stability of the resulting bulk hydrogel were tested by immersing the hydrogels in a warm water bath (45 °C) after 2.5 min of crosslinking at room temperature (**Fig. 2.5a-d**). Immersion in a warm water bath removes the physical network formed by gelatin chains, so a bulk hydrogel would remain intact only if held together through covalent crosslinks. Experiments were performed using either high PI concentration (0.5%) or low PI concentration (0.05%). PI-induced radicals during photopolymerization are known to be cytotoxic,[34,35] thus minimizing the PI concentration is important for applications in biological systems.

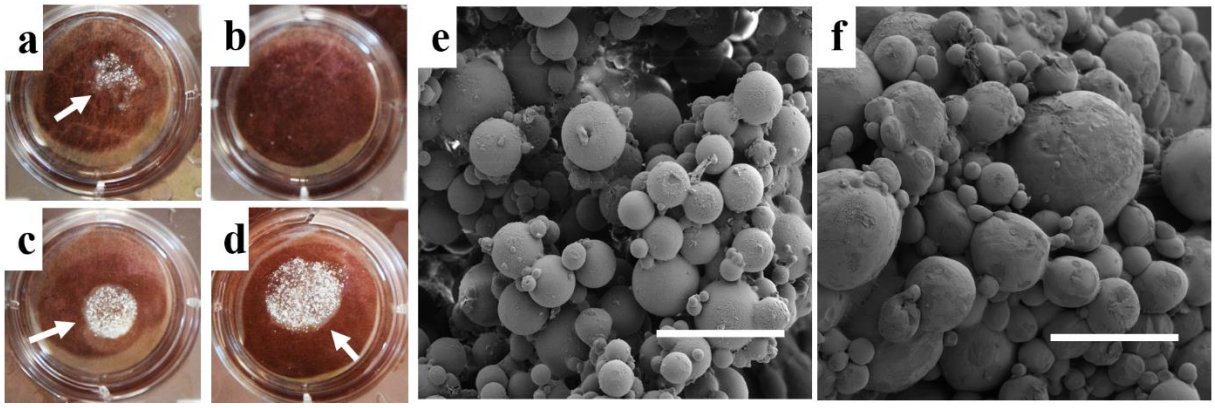

Figure 2.5. Dual-crosslinking approach promotes rapid gelation. Stability of the microgel assembly after curing the microgels only with UV irradiation using (a) 0.5% PI and (b) 0.05% PI, or mTG + UV irradiation using (c) 0.5% PI and (d) 0.05% PI. Arrows indicate the bulk hydrogels. (e-f) SEM images of microgels crosslinked by mTG and UV irradiation using (e) 0.5% PI and (f) 0.05% PI. Scale bar = 200 μm.

Microgels cured only by mTG dissociated completely after immersion in the warm water bath, indicating that the mTG-based crosslinking was not fast enough to cure the microgels in 2.5 min. When the same microgels were cured under 2.5 min of UV irradiation, a stable bulk hydrogel was formed (Fig. 2.5a) in the presence of high PI concentration (0.5%), due to the rapid formation of covalent crosslinks within and between microgels by photopolymerization among GelMA chains. However, the microgel assembly completely dissociated when cured in the presence of low PI concentration (Fig. 2.5b) because photopolymerization alone was insufficient to cure the microgels. For both PI concentrations, a more stable hydrogel was formed when microgels were cured by both mTG and UV irradiation (Fig. 2.5c, d). The additive effects of UV photopolymerization and mTG facilitates rapid curing of the gelatin/GelMA microgels even with a low PI concentration. When viewed by SEM (Fig. 2.5e, f),

hydrogels were clearly made of microspheres, with pores created by the interstitial space.

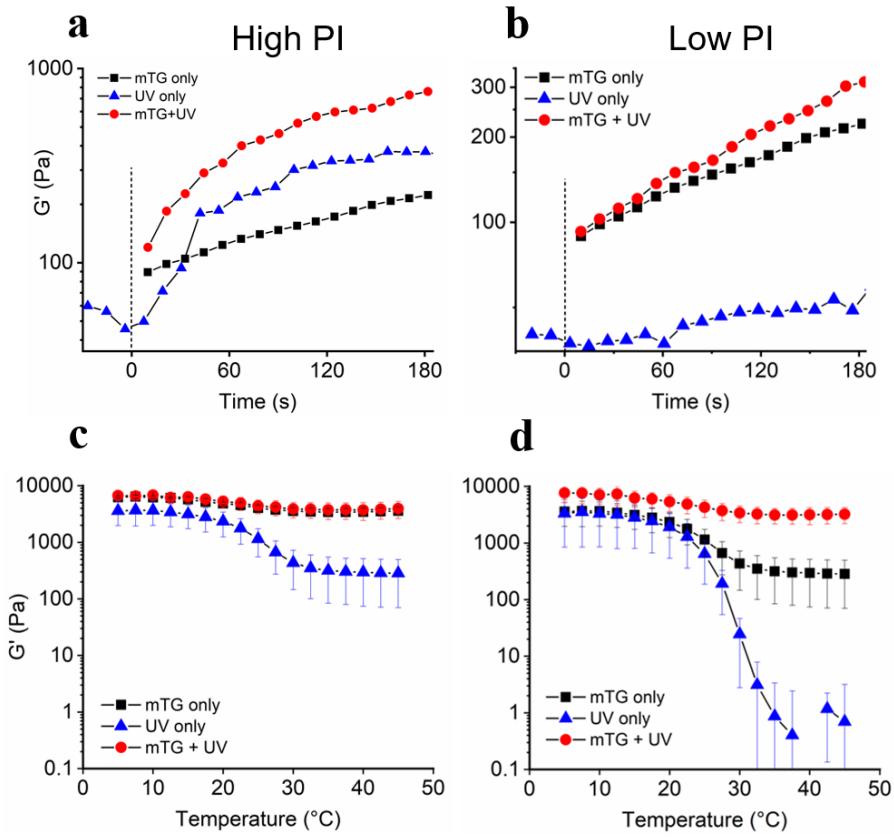

Figure 2.6. Rheological analysis of microporous hydrogel crosslinking. (a, b) Gelation kinetics measured by time sweep of storage moduli (G') for (a) high PI concentration (0.5%) and (b) low PI concentration (0.05%). The dotted lines indicate the time at which UV irradiation began (for 2.5 min). Note that for mTG-only and mTG + UV crosslinking, the crosslinking began as soon as mTG was mixed with microgels, and the moduli before mixing could not be measured. (c, d) Temperature sweep of hydrogels after curing using high PI concentration (c) and low PI concentration (d). For the simplicity of the data presentation, only the storage moduli (G') are presented in this figure. The plots of loss moduli, and frequency sweep can be found in Figure 2.7. The shown curves are representative of 3 independent experiments.

2.3.3 Rheology

Gelation kinetics and viscoelastic properties of the hydrogels were quantified by rheology (**Fig. 2.6, Fig. 2.7**). UV irradiation for 2.5 min with a high PI concentration (0.5%) rapidly increased the storage modulus (G') (Fig. 2.6a), compared to the mTG-only crosslinking until removal of the UV source. The combination of both curing methods (mTG + UV) resulted in a rapid initial increase of G' due to photocrosslinking, and a continual increase of G' due to the action of mTG. When a low PI concentration (0.05%) was used (Fig. 2.6b), UV irradiation alone did not result in a significant increase in G', which is consistent with the macroscopic observation (Fig. 2.5b). When both curing methods were combined (mTG + UV), the microgels were cured at a more rapid rate than by mTG alone, demonstrating that the efficiency of photocrosslinking is improved when used in conjunction with mTG. Temperature sweep after the completion of curing provides further information about the nature of crosslinks within hydrogels.[36] For both PI concentrations, G' decreased for all curing methods as temperature increased, which is characteristic of physically crosslinked gelatin hydrogels (Fig. 2.6c, d). For the case of mTG + UV, G' settled at 3500~4000 Pa above 30 °C, which verifies the presence of covalent crosslinks within the hydrogels which do not dissociate at or above physiological temperature. When the microgels were cured by UV irradiation only, G' settled at much lower values. A higher PI concentration resulted in higher G' at 45 °C (284 +/- 214 Pa vs 0.70 +/- 2.5 Pa for the low PI concentration), indicating increased crosslinking as the PI concentration increased.

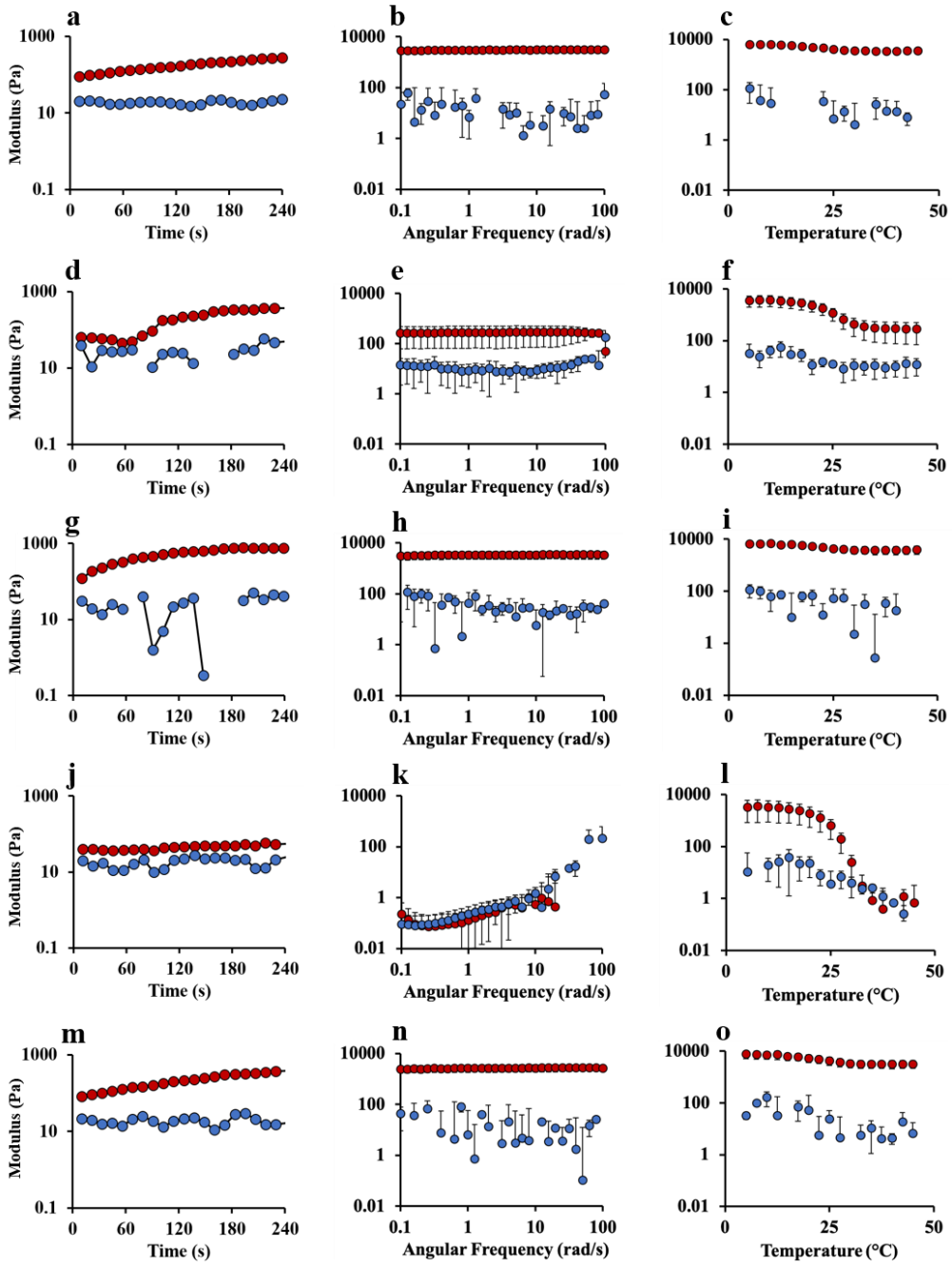

Figure 2.7. Comprehensive results of rheological testing. Representative time, average frequency and temperature sweep for microporous hydrogel using: (a-c) mTG only, (d-f) 0.5% PI, UV only, initiated at 60 seconds, (g-i) 0.5% PI, UV + mTG, UV crosslinking initiated at 0 seconds, (j-l) 0.05% PI, UV only, initiated at 30 seconds, and (m-o) 0.05% PI, UV + mTG, UV crosslinking initiated at 0 seconds. Red represents storage modulus, and blue represents loss modulus. Means and standard deviations are of three independent experiments.

2.3.4 Tissue adhesion

In addition to rapid curing, adhesion of the resulting hydrogel to the applied tissue serves to improve clinical viability of the injectable formulation,[37–39] by improving the hydrogel retention at the intended target site.[40] Previously, we demonstrated that the microporous hydrogel made by assembly of gelatin microgels adhered to porcine corneal tissue within 1 hour by the action of mTG.[31] mTG has been used as a tissue adhesive and is considered biocompatible.[41,42] Porcine cornea was used as a model tissue due to having rich collagen content and ready availability. mTG-catalyzed tissue adhesion was examined when used in conjunction with photopolymerization (**Fig. 2.8**). The microgels were injected into an 8 mm hole in a porcine cornea and allowed to crosslink by UV irradiation alone or by both mTG crosslinking and UV irradiation (mTG + UV). After curing, the cornea-hydrogel construct was immersed and shaken in a warm water bath (45 °C).

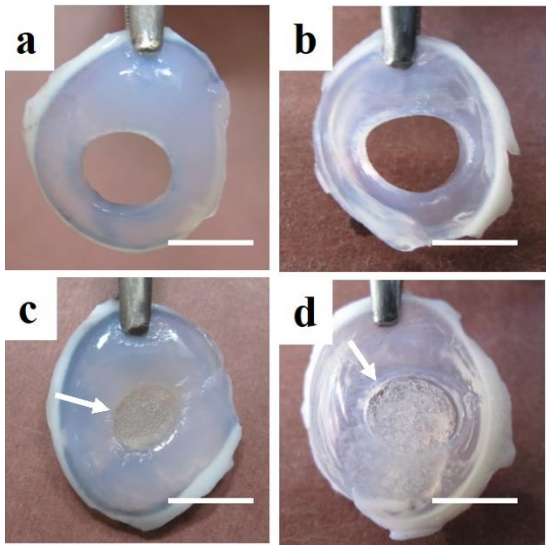

Figure 2.8. Tissue adhesion test. Microgels were injected into 8 mm holes made in porcine cornea and crosslinked for 2.5 min by UV irradiation only using (a) 0.5% PI, and (b) 0.05% PI, or by mTG + UV irradiation using (c) 0.5% PI and (d) 0.05% PI. Scale bar = 10 mm. Hydrogels are denoted by arrows.

For the high PI concentration, UV irradiation created a stable hydrogel, but it readily detached from the tissue when immersed in the warm water bath (Fig. 2.8a). When the low PI concentration was used, the UV irradiation alone did not form a bulk hydrogel, precluding tissue adhesion (Fig. 2.8b). When mTG was added in addition to UV irradiation, not only did a stable hydrogel form (Fig. 2.6 c, d), but the resulting hydrogel also adhered to the cornea tissue with both PI concentrations (Fig. 2.8 c, d). These results clearly show that the dual-crosslinking achieves rapid curing of the gelatin/GelMA microgels and enables stable adhesion of the hydrogel to tissue even at low PI concentration (0.05%). Our results also show that photopolymerization alone does not allow the tissue adhesion of the microgel-based hydrogel even at a high PI concentration (0.5%).

Two independent factors contribute to stable adhesion of a hydrogel to a wet tissue surface – interfacial adhesion (i.e. crosslinking between the hydrogel and tissue) and cohesion (i.e. mechanical strength of the hydrogel). We attribute the rapid and stable tissue adhesion of the microgel-based hydrogel to the simultaneous enhancement of both interfacial adhesion (by mTG) and cohesion (by UV) enabled by the dual-crosslinking approach.

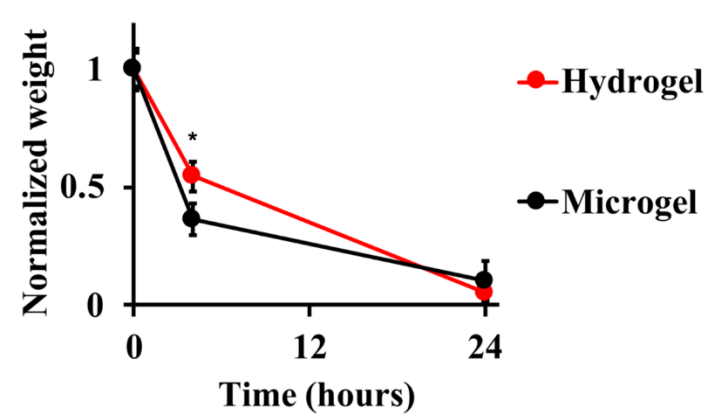

Figure 2.9. Degradation of gelatin/GelMA microgels and hydrogel. The error bars represent standard deviations (n = 4). (*) Denotes statistical significance between means ($p < 0.05$).

2.3.5 Enzymatic Degradation

Enzymatic degradation of gelatin/GelMA microgels and the annealed hydrogel was measured using collagenase type II (**Fig. 2.9**) as previously described.[43] Both microgels and the bulk hydrogel degraded completely within 24 hours, demonstrating the biodegradability of this formulation. This result is consistent with the fact that gelatin and GelMA have been shown to be degraded both *in vitro* and *in vivo* by various enzymes.[31,44]

2.3.6 Encapsulation of Human Dermal Fibroblasts

In situ cell encapsulation in a hydrogel is an important technology for the delivery of viable cells for wound healing and regenerative medicine.[26,45,46] The feasibility of using the microgel-based injectable hydrogel for cell delivery was investigated using human dermal fibroblasts (hDFs) (**Fig. 2.10**, **2.11, 2.12**). Unlike most injectable hydrogel

systems in which cells are homogeneously distributed within the hydrogel, cells are encapsulated in the interstitial space between microgels.

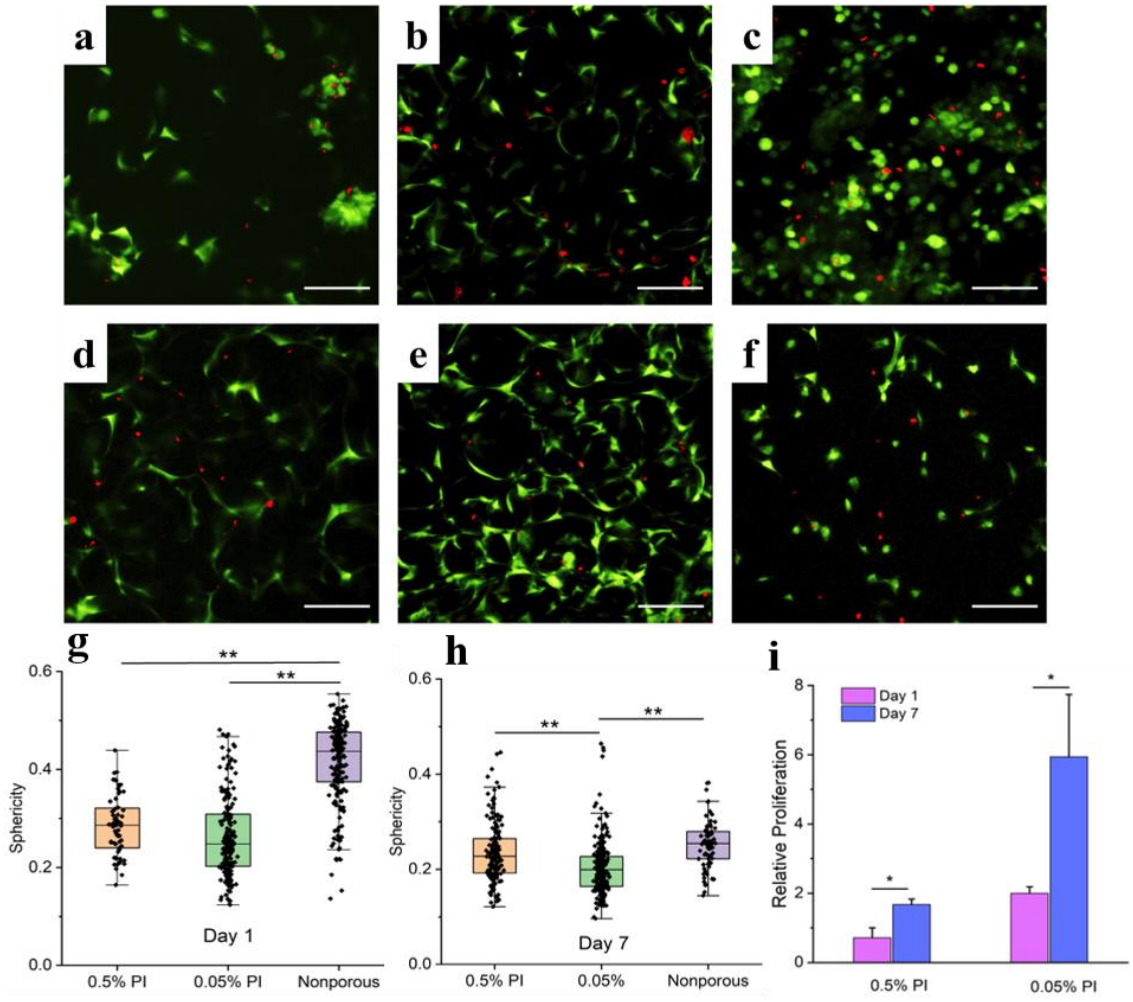

Figure 2.10. Cell encapsulation in the interstitial space between annealed microgels. (a-f) 2D projections of confocal microscope images of live/dead assay. (a-c) Day 1 and (d-f) day 7 post-encapsulation. The microgels were cured with mTG and UV irradiation using (a, d) 0.5% or (b, e) 0.05% PI concentration. Nonporous hydrogel was formed with mTG and UV irradiation using 0.05% PI concentration. Scale bar = 100 µm, green = living, red = dead. (g-h) Sphericity of encapsulated cells (g) day 1 and (h) day 7 post encapsulation. (i) Cell proliferation in the microporous hydrogels relative to the nonporous control (n=3). (*) = $p < 0.05$ and (**) = $p < 0.001$

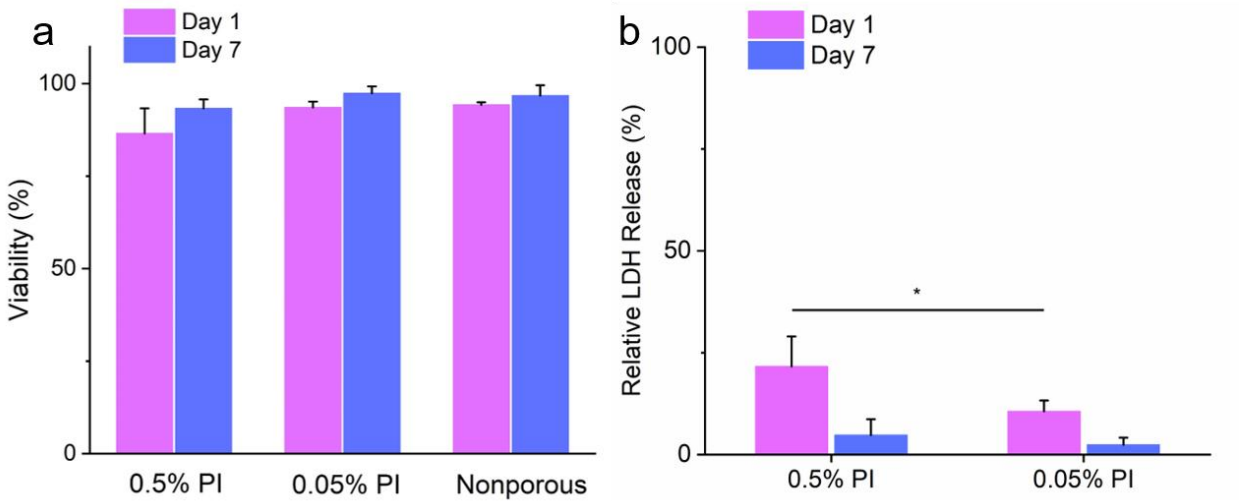

Figure 2.11. Viability and relative LDH release of encapsulated cells. (a) Viability was measured through analysis of confocal microscopy images taken on day 1 and 7 post encapsulation. There was no significant difference between groups (n = 3). (b) Relative LDH release was measured through comparison to maximum LDH 2D culture controls, and acellular hydrogel negative controls. Low PI LDH release was statistically lower than the High PI condition on day 1 post encapsulation (n = 4).

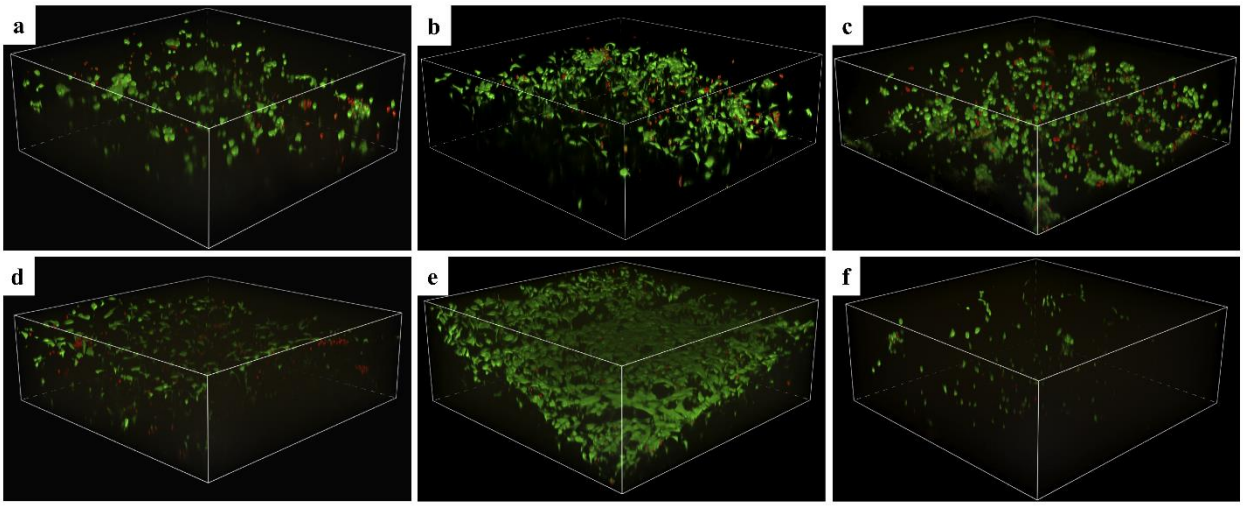

Figure 2.12. 3-Dimensional representations of live/dead images, on (a-c) days 1 and (d-f) 7 post encapsulation. Shown are hDFs encapsulated in the (a, d) microporous hydrogels made using 0.5% PI, (b, e) microporous hydrogels made with 0.05% PI, and (c, f) nonporous hydrogels made with 0.05% PI (Green = living, red = dead)

Cell-encapsulating constructs were formed by curing the microgels by both mTG and UV irradiation using either 0.5% PI or 0.05% PI. For a comparison, cells were also encapsulated in a nonporous hydrogel, which was formed by crosslinking a homogeneous solution of gelatin and GelMA using mTG and UV irradiation (with 0.05% PI). At all time points (day 1 and day 7 post encapsulation), cell viability was high for all groups (Fig. 2.10a-f, Fig. 2.11a), although the porous hydrogel with 0.5% PI resulted in the lowest viability on day 1 ($p > 0.05$). Strikingly, the cells encapsulated in the microporous hydrogels exhibited fully spread morphologies as early as day 1 post encapsulation (Fig. 2.10a-b, g). Rapid spreading of encapsulated cells, which is attributed to the large available void space within the porous hydrogels, is distinct from most nonporous hydrogels in which the encapsulated cells are trapped by the polymer chains and cannot spread immediately (Fig. 2.10c). Although it is not the focus of this

report, the current injectable formulation, which induces rapid spreading of the encapsulated cells, will be useful when the differentiation into a specific lineage is facilitated by cell spreading (e.g. osteogenic).[47]

The advantage of encapsulating cells in the pores of the microgel-assembly was further proven by the live/dead assay performed on day 7 post encapsulation (Fig. 2.10 d-f). As on day 1, the cells were well-spread around the microgels within the interstitial space, resulting in decreased sphericities compared to day 1 (Fig. 2.10h). The cells encapsulated in the nonporous hydrogel still exhibited higher sphericity likely due to prevention of spreading by the polymer mesh. The detailed structures of actin cytoskeleton on day 7 confirmed these results (**Fig. 2.13**).

The benefit of lowering the PI concentration is highlighted by the assessment of cell proliferation. At both time points, the samples with 0.05% PI concentration resulted in higher proliferation than the samples with 0.5% PI concentration (Fig. 2.10i), presumably due to decreased exposure of cells to free radicals during encapsulation. This result is supported by the significant increase in cytotoxicity on day 1 for the 0.5% PI group measured by lactate dehydrogenase (LDH) release (Fig. 2.11b). By day 7, LDH release was substantially lower for both groups, indicating that the lower proliferation of the 0.5% PI group resulted from the initial cytotoxicity during the photopolymerization. For both PI concentrations, proliferation on day 7 was higher than the cells encapsulated in the nonporous hydrogels, which is consistent with the recent report that MSCs encapsulated in a microporous hydrogel exhibited significantly higher proliferation than the cells encapsulated in nonporous hydrogel in vivo.[26]

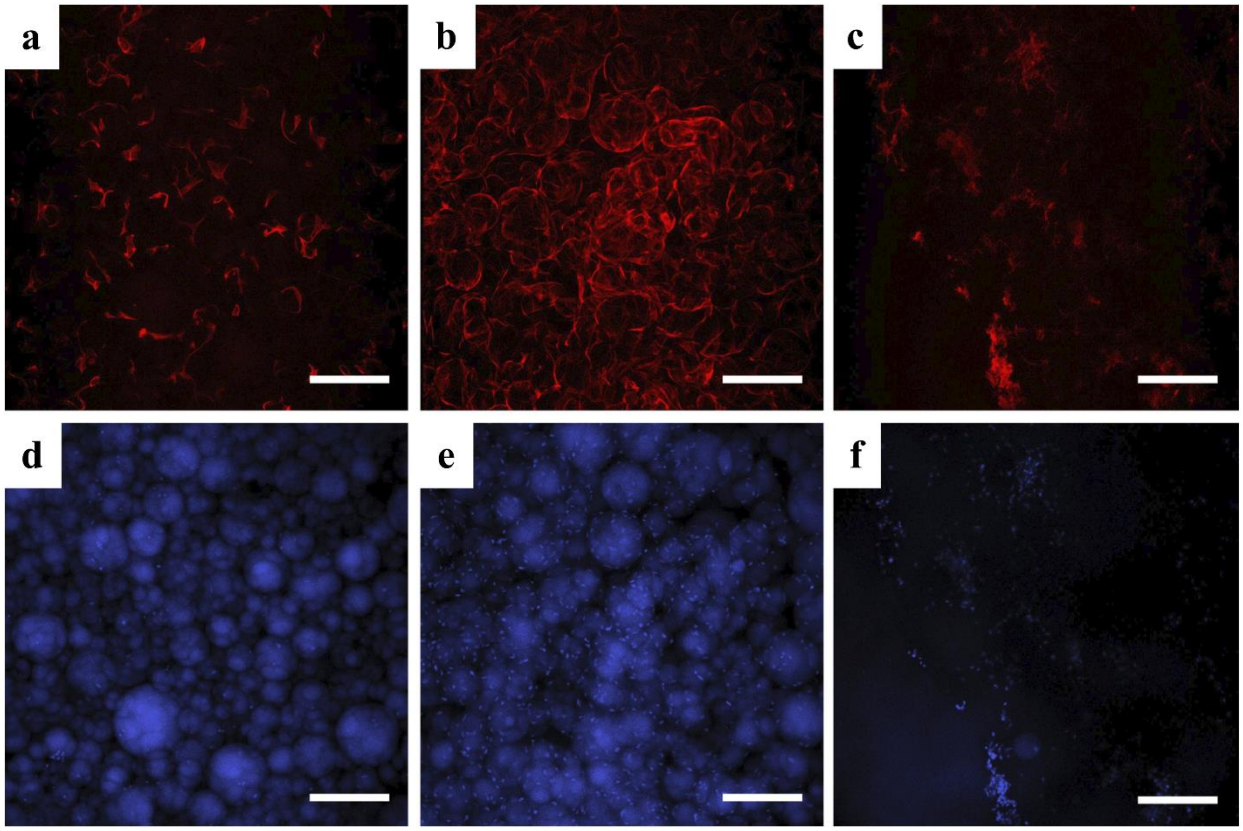

Figure 2.13. Cell encapsulation in microporous hydrogel and reduction of photoinitiator concentration improve cell spreading. (a-c) Actin cytoskeleton (a-c) and (d-f) cell nuclei of the encapsulated cells on day 7. (a, d) Microporous hydrogel with 0.5% or (b, e) 0.05% PI. (c, f) nonporous hydrogel with 0.05% PI. Red fluorescence is actin cytoskeleton, and blue fluorescence is cell nuclei. There was significant non-specific blue staining of the microgels, but the cell nuclei could still be visualized. Scale bar = 200 µm.

2.3.7 Encapsulation of hMSCs

Next, hMSC encapsulation was performed to demonstrate high hMSC viability in this fast-curing microporous hydrogel and its potential use in MSC-based therapies, such as immunomodulation (**Fig. 2.14**). MSC delivery has been explored to reduce autoimmune responses to organ transplants or biomaterial implants,[48,49] and treat

chronic inflammatory diseases,[50] whereby MSCs are primed by proinflammatory signals, such as IFN-γ before delivery to improve their immunosuppressive properties.[51] A major limiting factor of MSC-based therapy is the limited residence time of MSCs at the site of injection, and thus encapsulation in biomaterials is being explored to address this limitation.[52,53] The hydrogel platform described here is advantageous for this application due to having high internal growth area and the ability to promote cell growth.

Similar to the encapsulated hDFs, hMSCs rapidly spread around the microgels as early as day 1 (**Fig 2.14**, **Fig. 2.15**), and showed improved cell spreading and proliferation over 7 days in comparison to the nonporous counterpart (Fig. 2.14a-d).

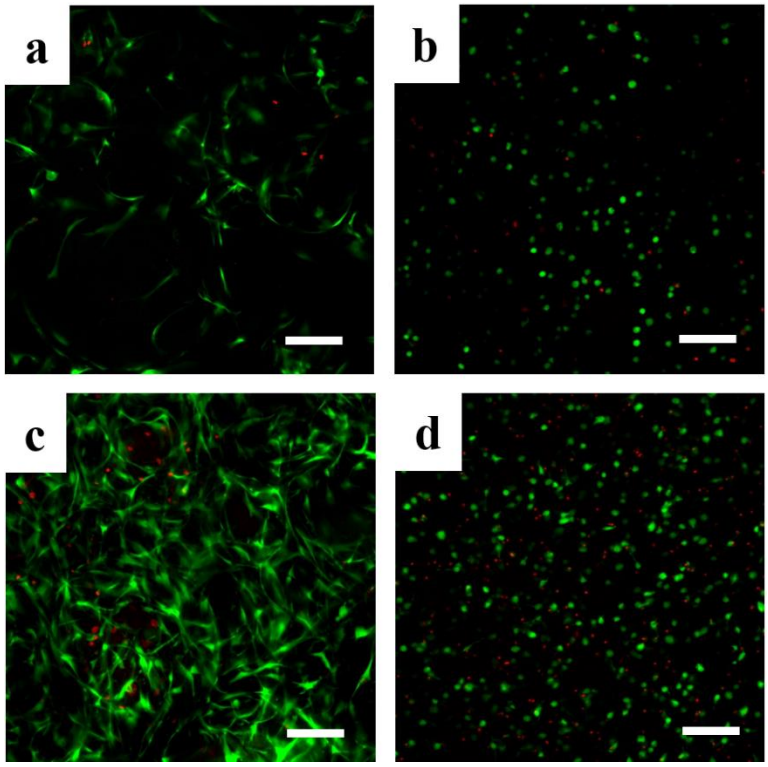

Figure 2.14. Gelatin/GelMA composite microgels enhance mesenchymal stem cell (MSC) growth. (a-d) 2D projections of confocal microscopy images for cells encapsulated in the (a, c) microporous and (b, d) nonporous hydrogels, on days 1 and 7 respectively. Scale bar: 100 μm.

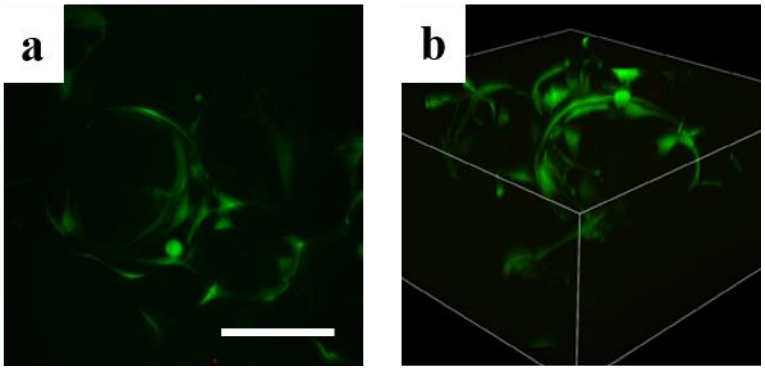

Figure 2.15. High magnification (a) 2D projection and (b) 3D view of cells adhered and spreading around a microgel on day 1 post-encapsulation. Scale bar = 100 μm.

When hMSCs were primed with IFN-γ (50 ng/mL) for 72 hours immediately after encapsulation, the secretion of factors involved in MSC-mediated immunosuppression (IL-6, PGE2 and IDO)[54] significantly increased compared to the non-primed samples (Fig. 2.16). These results clearly show that this injectable microporous hydrogel can be used to deliver hMSCs with high viability and alleviate local inflammation by the release of anti-inflammatory factors when the hMSCs are primed by IFN-γ. In the future, the microgels can be further modified with IFN-γ so that the encapsulated hMSCs can be primed without exogenous IFN-γ.

2.4. Conclusion

Overall, the injectable hydrogel formulation described here has several major advantages compared to previously reported injectable hydrogels: (1) enhanced thermal stability of microgels allows for more favorable conditions during cell encapsulation; (2) rapid gelation (2.5 min) under UV irradiation even at a low PI concentration (0.05%) was achieved due to the synergistic actions of UV photopolymerization and mTG-based

enzymatic crosslinking; (3) the use of low PI concentration results in high viability and proliferation of the encapsulated cells; (4) due to the action of mTG in conjunction with UV photopolymerization, the hydrogel can adhere to the target tissue stably within 2.5 min; (5) the presence of pores allows rapid adhesion, spreading, and proliferation of the encapsulated cells. We demonstrated the applicability of this platform for priming MSCs for immunomodulation, and we anticipate that this formulation will find many applications related to cell delivery-based therapeutics.

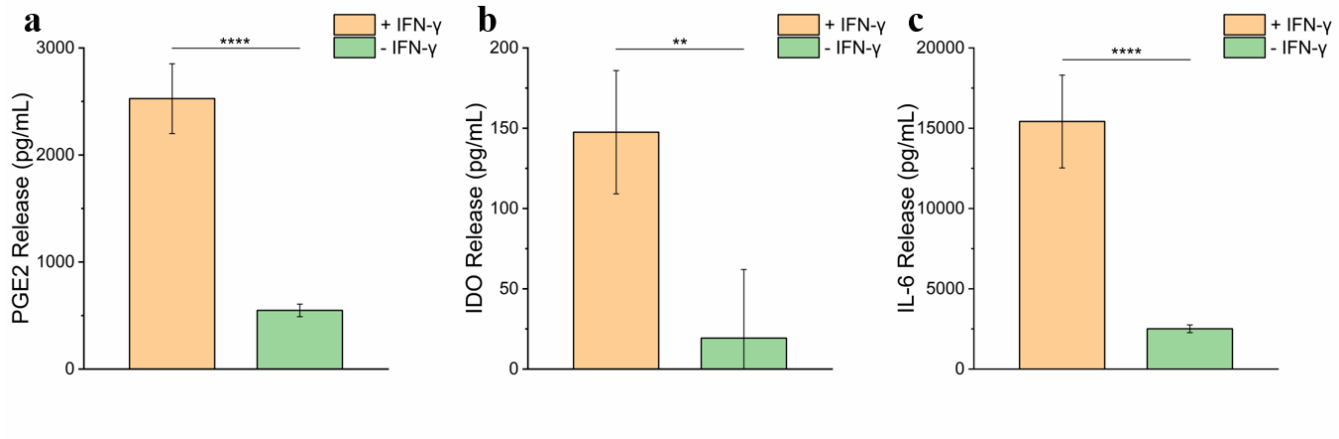

Figure 2.16. Analysis of factors secreted by encapsulated hMSCs in the microporous and nonporous hydrogels. Culture media concentration of secreted factors prostaglandin E2 (a), indoleamine-2,3-dioxygenase (b), and interleukin-6 (c) from hydrogel-cell constructs after 72 hours of culture in either IFN-γ-containing media or media only. (*) $p < 0.05$, (**) $p < 0.01$, (***) $p < 0.001$ (****) $p < 0.0001$.

References

(1) Li, Y.; Rodrigues, J.; Tomás, H. Injectable and Biodegradable Hydrogels: Gelation, Biodegradation and Biomedical Applications. *Chem. Soc. Rev*. **2012**, 2193–2221. https://doi.org/10.1039/c1cs15203c.

(2) Liu, M.; Zeng, X.; Ma, C.; Yi, H.; Ali, Z.; Mou, X.; Li, S.; Deng, Y.; He, N. Injectable Hydrogels for Cartilage and Bone Tissue Engineering. *Bone Res.* **2017**. https://doi.org/10.1038/boneres.2017.14.

(3) Ren, K.; He, C.; Xiao, C.; Li, G.; Chen, X. Injectable Glycopolypeptide Hydrogels as Biomimetic Scaffolds Forcartilage Tissue Engineering. *Biomaterials* **2015**, *51*, 238–249. https://doi.org/10.1016/j.biomaterials.2015.02.026.

(4) Popa, E. G.; Caridade, S. G.; Mano, J. F.; Reis, R. L.; Gomes, M. E. Chondrogenic Potential of Injectablеκ-Carrageenan Hydrogel with Encapsulated Adipose Stem Cells for Cartilage Tissue-Engineering Applications. *J. Tissue Eng. Regen. Med.* **2015**, *9* (5), 550–563. https://doi.org/10.1002/term.1683.

(5) Jooybar, E.; Abdekhodaie, M. J.; Alvi, M.; Mousavi, A.; Karperien, M.; Dijkstra, P. J. An Injectable Platelet Lysate-Hyaluronic Acid Hydrogel Supports Cellular Activities and Induces Chondrogenesis of Encapsulated Mesenchymal Stem Cells. *Acta Biomater.* **2019**, *83*, 233–244. https://doi.org/10.1016/j.actbio.2018.10.031.

(6) Cai, L.; Dewi, R. E.; Heilshorn, S. C. Injectable Hydrogels with In Situ Double Network Formation Enhance Retention of Transplanted Stem Cells. *Adv. Funct. Mater.* **2015**, *25* (9), 1344–1351. https://doi.org/10.1002/adfm.201403631.

(7) Anjum, F.; Lienemann, P. S.; Metzger, S.; Biernaskie, J.; Kallos, M. S.; Ehrbar, M. Enzyme Responsive GAG-Based Natural-Synthetic Hybrid Hydrogel for Tunable Growth Factor Delivery and Stem Cell Differentiation. *Biomaterials* **2016**, *87*, 104–117. https://doi.org/10.1016/j.biomaterials.2016.01.050.

(8) Lindsey, S.; Piatt, J. H.; Worthington, P.; Sönmez, C.; Satheye, S.; Schneider, J. P.; Pochan, D. J.; Langhans, S. A. Beta Hairpin Peptide Hydrogels as an Injectable Solid Vehicle for Neurotrophic Growth Factor Delivery. *Biomacromolecules* **2015**, *16* (9), 2672–2683. https://doi.org/10.1021/acs.biomac.5b00541.

(9) Park, H.; Temenoff, J. S.; Tabata, Y.; Caplan, A. I.; Mikos, A. G. Injectable Biodegradable Hydrogel Composites for Rabbit Marrow Mesenchymal Stem Cell and Growth Factor Delivery for Cartilage Tissue Engineering. *Biomaterials* **2007**, *28* (21), 3217–3227. https://doi.org/10.1016/j.biomaterials.2007.03.030.

(10) Sun, J. E. P.; Stewart, B.; Litan, A.; Lee, S. J.; Schneider, J. P.; Langhans, S. A.; Pochan, D. J. Sustained Release of Active Chemotherapeutics from Injectable-Solid β-Hairpin Peptide Hydrogel. *Biomater. Sci.* **2016**, *4* (5), 839–848. https://doi.org/10.1039/c5bm00538h.

(11) Norouzi, M.; Nazari, B.; Miller, D. W. Injectable Hydrogel-Based Drug Delivery Systems for Local Cancer Therapy. *Drug Discovery Today*. Elsevier Ltd November 1, 2016, pp 1835–1849. https://doi.org/10.1016/j.drudis.2016.07.006.

(12) Joshi, N.; Yan, J.; Levy, S.; Bhagchandani, S.; Slaughter, K. V.; Sherman, N. E.; Amirault, J.; Wang, Y.; Riegel, L.; He, X.; Rui, T. S.; Valic, M.; Vemula, P. K.;

Miranda, O. R.; Levy, O.; Gravallese, E. M.; Aliprantis, A. O.; Ermann, J.; Karp, J. M. Towards an Arthritis Flare-Responsive Drug Delivery System. *Nat. Commun.* **2018**, *9* (1). https://doi.org/10.1038/s41467-018-03691-1.

(13) Li, L.; Lu, C.; Wang, L.; Chen, M.; White, J.; Hao, X.; McLean, K. M.; Chen, H.; Hughes, T. C. Gelatin-Based Photocurable Hydrogels for Corneal Wound Repair. *ACS Appl. Mater. Interfaces* **2018**, *10* (16), 13283–13292. https://doi.org/10.1021/acsami.7b17054.

(14) Phelps, E. A.; Enemchukwu, N. O.; Fiore, V. F.; Sy, J. C.; Murthy, N.; Sulchek, T. A.; Barker, T. H.; García, A. J. Maleimide Cross-Linked Bioactive PEG Hydrogel Exhibits Improved Reaction Kinetics and Cross-Linking for Cell Encapsulation and in Situ Delivery. *Adv. Mater.* **2012**, *24* (1), 64–70. https://doi.org/10.1002/adma.201103574.

(15) Chen, M. B.; Srigunapalan, S.; Wheeler, A. R.; Simmons, C. A. A 3D Microfluidic Platform Incorporating Methacrylated Gelatin Hydrogels to Study Physiological Cardiovascular Cell-Cell Interactions. *Lab Chip* **2013**, *13* (13), 2591–2598. https://doi.org/10.1039/c3lc00051f.

(16) Griffin, D. R.; Weaver, W. M.; Scumpia, P. O.; Di Carlo, D.; Segura, T. Accelerated Wound Healing by Injectable Microporous Gel Scaffolds Assembled from Annealed Building Blocks. *Nat. Mater.* **2015**, *14* (7), 737–744. https://doi.org/10.1038/nmat4294.

(17) Sheikhi, A.; de Rutte, J.; Haghniaz, R.; Akouissi, O.; Sohrabi, A.; Di Carlo, D.; Khademhosseini, A. Microfluidic-Enabled Bottom-up Hydrogels from Annealable

Naturally-Derived Protein Microbeads. *Biomaterials* **2019**, *192*, 560–568. https://doi.org/10.1016/j.biomaterials.2018.10.040.

(18) Sideris, E.; Griffin, D. R.; Ding, Y.; Li, S.; Weaver, W. M.; Di Carlo, D.; Hsiai, T.; Segura, T. Particle Hydrogels Based on Hyaluronic Acid Building Blocks. *ACS Biomater. Sci. Eng.* **2016**, *2* (11), 2034–2041. https://doi.org/10.1021/acsbiomaterials.6b00444.

(19) Darling, N. J.; Sideris, E.; Hamada, N.; Carmichael, S. T.; Segura, T. Injectable and Spatially Patterned Microporous Annealed Particle (MAP) Hydrogels for Tissue Repair Applications. *Adv. Sci.* **2018**, *5* (11), 1801046. https://doi.org/10.1002/advs.201801046.

(20) Daly, A. C.; Riley, L.; Segura, T.; Burdick, J. A. Hydrogel Microparticles for Biomedical Applications. *Nat. Rev. Mater.* **2019**.

(21) Mealy, J. E.; Chung, J. J.; Jeong, H. H.; Issadore, D.; Lee, D.; Atluri, P.; Burdick, J. A. Injectable Granular Hydrogels with Multifunctional Properties for Biomedical Applications. *Adv. Mater.* **2018**, *30* (20). https://doi.org/10.1002/adma.201705912.

(22) Arun Kumar, R.; Sivashanmugam, A.; Deepthi, S.; Iseki, S.; Chennazhi, K. P.; Nair, S. V.; Jayakumar, R. Injectable Chitin-Poly(ε-Caprolactone)/Nanohydroxyapatite Composite Microgels Prepared by Simple Regeneration Technique for Bone Tissue Engineering. *ACS Appl. Mater. Interfaces* **2015**, *7* (18), 9399–9409. https://doi.org/10.1021/acsami.5b02685.

(23) Xin, S.; Chimene, D.; Garza, J. E.; Gaharwar, A. K.; Alge, D. L. Clickable PEG

Hydrogel Microspheres as Building Blocks for 3D Bioprinting. *Biomater. Sci.* **2019**, *7* (3), 1179–1187. https://doi.org/10.1039/c8bm01286e.

(24) Qu, J.; Zhao, X.; Liang, Y.; Zhang, T.; Ma, P. X.; Guo, B. Antibacterial Adhesive Injectable Hydrogels with Rapid Self-Healing, Extensibility and Compressibility as Wound Dressing for Joints Skin Wound Healing. *Biomaterials* **2018**, *183*, 185–199. https://doi.org/10.1016/j.biomaterials.2018.08.044.

(25) Huang, W.; Li, X.; Shi, X.; Lai, C. Microsphere Based Scaffolds for Bone Regenerative Applications. *Biomaterials Science*. Royal Society of Chemistry 2014, pp 1145–1153. https://doi.org/10.1039/c4bm00161c.

(26) Koh, J.; Griffin, D. R.; Archang, M. M.; Feng, A.; Horn, T.; Margolis, M.; Zalazar, D.; Segura, T.; Scumpia, P. O.; Carlo, D. Enhanced In Vivo Delivery of Stem Cells Using Microporous Annealed Particle Scaffolds. *Small* **2019**, *15* (39), 1903147. https://doi.org/10.1002/smll.201903147.

(27) Duan, B.; Shou, K.; Su, X.; Niu, Y.; Zheng, G.; Huang, Y.; Yu, A.; Zhang, Y.; Xia, H.; Zhang, L. Hierarchical Microspheres Constructed from Chitin Nanofibers Penetrated Hydroxyapatite Crystals for Bone Regeneration. *Biomacromolecules* **2017**, *18* (7), 2080–2089. https://doi.org/10.1021/acs.biomac.7b00408.

(28) Jiang, W.; Li, M.; Chen, Z.; Leong, K. W. Cell-Laden Microfluidic Microgels for Tissue Regeneration. *Lab Chip*. **2016**, *16,* 4482–4506. https://doi.org/10.1039/c6lc01193d.

(29) Xin, S.; Wyman, O. M.; Alge, D. L. Assembly of PEG Microgels into Porous Cell-

Instructive 3D Scaffolds via Thiol-Ene Click Chemistry. *Adv. Healthc. Mater.* **2018**, *7* (11). https://doi.org/10.1002/adhm.201800160.

(30) Choi, Y. H.; Kim, S. H.; Kim, I. S.; Kim, K. M.; Kwon, S. K.; Hwang, N. S. Gelatin-Based Micro-Hydrogel Carrying Genetically Engineered Human Endothelial Cells for Neovascularization. *Acta Biomater.* **2019**. https://doi.org/10.1016/j.actbio.2019.01.057.

(31) Hou, S.; Lake, R.; Park, S.; Edwards, S.; Jones, C.; Jeong, K. J. Injectable Macroporous Hydrogel Formed by Enzymatic Cross-Linking of Gelatin Microgels. *ACS Appl. Bio Mater.* **2018**, *1* (5). https://doi.org/10.1021/acsabm.8b00380.

(32) Besser, R. R.; Bowles, A. C.; Alassaf, A.; Carbonero, D.; Claure, I.; Jones, E.; Reda, J.; Wubker, L.; Batchelor, W.; Ziebarth, N.; Silvera, R.; Khan, A.; MacIel, R.; Saporta, M.; Agarwal, A. Enzymatically Crosslinked Gelatin-Laminin Hydrogels for Applications in Neuromuscular Tissue Engineering. *Biomater. Sci.* **2020**, *8* (2), 591–606. https://doi.org/10.1039/c9bm01430f.

(33) Zoratto, N.; Di Lisa, D.; de Rutte, J.; Sakib, M. N.; Alves e Silva, A. R.; Tamayol, A.; Di Carlo, D.; Khademhosseini, A.; Sheikhi, A. In Situ Forming Microporous Gelatin Methacryloyl Hydrogel Scaffolds from Thermostable Microgels for Tissue Engineering. *Bioeng. Transl. Med.* **2020**, *5* (3). https://doi.org/10.1002/BTM2.10180.

(34) Shearier, E. R.; Bowen, P. K.; He, W.; Drelich, A.; Drelich, J.; Goldman, J.; Zhao, F. In Vitro Cytotoxicity, Adhesion, and Proliferation of Human Vascular Cells Exposed to Zinc. *ACS Biomater. Sci. Eng.* **2016**, *2* (4), 634–642.

https://doi.org/10.1021/acsbiomaterials.6b00035.

(35) Wang, M. O.; Etheridge, J. M.; Thompson, J. A.; Vorwald, C. E.; Dean, D.; Fisher, J. P. Evaluation of the in Vitro Cytotoxicity of Cross-Linked Biomaterials. *Biomacromolecules* **2013**, *14* (5), 1321–1329. https://doi.org/10.1021/bm301962f.

(36) Van, A. I.; Bulcke, D.; Bogdanov, B.; De Rooze, N.; Schacht, E. H.; Cornelissen, M.; Berghmans, H. Structural and Rheological Properties of Methacrylamide Modified Gelatin Hydrogels. *Biomacromolecules* **2000**. https://doi.org/10.1021/bm990017d.

(37) Nicodemus, G. D.; Bryant, S. J. Cell Encapsulation in Biodegradable Hydrogels for Tissue Engineering Applications. *Tissue Eng. Part B Rev.* **2008,** *14* (2), 149-165. https://doi.org/10.1089/ten.teb.2007.0332.

(38) Wang, D. A.; Varghese, S.; Sharma, B.; Strehin, I.; Fermanian, S.; Gorham, J.; Fairbrother, D. H.; Cascio, B.; Elisseeff, J. H. Multifunctional Chondroitin Sulphate for Cartilage Tissue-Biomaterial Integration. *Nat. Mater.* **2007**, *6* (5), 385–392. https://doi.org/10.1038/nmat1890.

(39) Seliktar, D. Designing Cell-Compatible Hydrogels for Biomedical Applications. *Science* **2012**, 1124–1128. https://doi.org/10.1126/science.1214804.

(40) Feng, Q.; Wei, K.; Lin, S.; Xu, Z.; Sun, Y.; Shi, P.; Li, G.; Bian, L. Mechanically Resilient, Injectable, and Bioadhesive Supramolecular Gelatin Hydrogels Crosslinked by Weak Host-Guest Interactions Assist Cell Infiltration and in Situ Tissue Regeneration. *Biomaterials* **2016**, *101*, 217–228.

https://doi.org/10.1016/j.biomaterials.2016.05.043.

(41) McDermott, M. K.; Chen, T.; Williams, C. M.; Markley, K. M.; Payne, G. F. Mechanical Properties of Biomimetic Tissue Adhesive Based on the Microbial Transglutaminase-Catalyzed Crosslinking of Gelatin. *Biomacromolecules* **2004**, *5* (4), 1270–1279. https://doi.org/10.1021/bm034529a.

(42) Dinh, T. N.; Hou, S.; Park, S.; Shalek, B. A.; Jeong, K. J. Gelatin Hydrogel Combined with Polydopamine Coating To Enhance Tissue Integration of Medical Implants. *ACS Biomater. Sci. Eng.* **2018**. https://doi.org/10.1021/acsbiomaterials.8b00886.

(43) Shin, S. R.; Aghaei-Ghareh-Bolagh, B.; Dang, T. T.; Topkaya, S. N.; Gao, X.; Yang, S. Y.; Jung, S. M.; Oh, J. H.; Dokmeci, M. R.; Tang, X. S.; Khademhosseini, A. Cell-Laden Microengineered and Mechanically Tunable Hybrid Hydrogels of Gelatin and Graphene Oxide. *Adv. Mater.* **2013**, *25* (44), 6385–6391. https://doi.org/10.1002/adma.201301082.

(44) Zhu, M.; Wang, Y.; Ferracci, G.; Zheng, J.; Cho, N. J.; Lee, B. H. Gelatin Methacryloyl and Its Hydrogels with an Exceptional Degree of Controllability and Batch-to-Batch Consistency. *Sci. Rep.* **2019**, *9* (1). https://doi.org/10.1038/s41598-019-42186-x.

(45) Dimatteo, R.; Darling, N. J.; Segura, T. In Situ Forming Injectable Hydrogels for Drug Delivery and Wound Repair. *Adv. Drug Deliv. Rev.* **2018**, 167–184. https://doi.org/10.1016/j.addr.2018.03.007.

(46) Truong, V. X.; Ablett, M. P.; Richardson, S. M.; Hoyland, J. A.; Dove, A. P. Simultaneous Orthogonal Dual-Click Approach to Tough, in-Situ -Forming Hydrogels for Cell Encapsulation. *J. Am. Chem. Soc.* **2015**, *137* (4), 1618–1622. https://doi.org/10.1021/ja511681s.

(47) Chaudhuri, O.; Gu, L.; Klumpers, D.; Darnell, M.; Bencherif, S. A.; Weaver, J. C.; Huebsch, N.; Lee, H. P.; Lippens, E.; Duda, G. N.; Mooney, D. J. Hydrogels with Tunable Stress Relaxation Regulate Stem Cell Fate and Activity. *Nat. Mater.* **2016**, *15* (3), 326–334. https://doi.org/10.1038/nmat4489.

(48) Swartzlander, M. D.; Blakney, A. K.; Amer, L. D.; Hankenson, K. D.; Kyriakides, T. R.; Bryant, S. J. Immunomodulation by Mesenchymal Stem Cells Combats the Foreign Body Response to Cell-Laden Synthetic Hydrogels. *Biomaterials* **2015**, *41*, 79–88. https://doi.org/10.1016/j.biomaterials.2014.11.020.

(49) Renner, P.; Eggenhofer, E.; Rosenauer, A.; Popp, F. C.; Steinmann, J. F.; Slowik, P.; Geissler, E. K.; Piso, P.; Schlitt, H. J.; Dahlke, M. H. Mesenchymal Stem Cells Require a Sufficient, Ongoing Immune Response to Exert Their Immunosuppressive Function. *Transplant. Proc.* **2009**, *41* (6), 2607–2611. https://doi.org/10.1016/j.transproceed.2009.06.119.

(50) Chen, S.; Shi, J.; Zhang, M.; Chen, Y.; Wang, X.; Zhang, L.; Tian, Z.; Yan, Y.; Li, Q.; Zhong, W.; Xing, M.; Zhang, L.; Zhang, L. Mesenchymal Stem Cell-Laden Anti-Inflammatory Hydrogel Enhances Diabetic Wound Healing. *Sci. Rep.* **2015**, *5*. https://doi.org/10.1038/srep18104.

(51) Kim, D. S.; Jang, I. K.; Lee, M. W.; Ko, Y. J.; Lee, D. H.; Lee, J. W.; Sung, K. W.;

Koo, H. H.; Yoo, K. H. Enhanced Immunosuppressive Properties of Human Mesenchymal Stem Cells Primed by Interferon-γ. *EBioMedicine* **2018**, *28*, 261–273. https://doi.org/10.1016/j.ebiom.2018.01.002.

(52) Mao, A. S.; Özkale, B.; Shah, N. J.; Vining, K. H.; Descombes, T.; Zhang, L.; Tringides, C. M.; Wong, S. W.; Shin, J. W.; Scadden, D. T.; Weitz, D. A.; Mooney, D. J. Programmable Microencapsulation for Enhanced Mesenchymal Stem Cell Persistence and Immunomodulation. *Proc. Natl. Acad. Sci. U. S. A.* **2019**, *116* (31), 15392–15397. https://doi.org/10.1073/pnas.1819415116.

(53) García, J. R.; Quirós, M.; Han, W. M.; O'Leary, M. N.; Cox, G. N.; Nusrat, A.; García, A. J. IFN-γ-Tethered Hydrogels Enhance Mesenchymal Stem Cell-Based Immunomodulation and Promote Tissue Repair. *Biomaterials* **2019**, *220*, 119403. https://doi.org/10.1016/j.biomaterials.2019.119403.

(54) Ghannam, S.; Bouffi, C.; Djouad, F.; Jorgensen, C.; Noël, D. Immunosuppression by Mesenchymal Stem Cells: Mechanisms and Clinical Applications. *Stem Cell Res. Ther*. **2010**. https://doi.org/10.1186/scrt2.

Chapter 3

Injectable Microporous Gelatin Hydrogel for Encapsulation and Differentiation of Mesenchymal Stem Cells for Bone Repair

3.1 Introduction

Existing treatments for bone defects are insufficient to meet the current need. Autograft and allograft - the current gold standard - have complications related to the scarcity of donor tissue, surgical complications, and insufficient integration of allogeneic tissue[1,2]. Injection of therapeutic cells is a promising approach to improve tissue regeneration, because it is minimally invasive, and the cells can be derived from the patient, diminishing the risk of a foreign body response. Mesenchymal stem cell (MSC) delivery has been considered as a potential treatment for bone defects because MSCs are known to promote wound healing and they readily differentiate into osteoblasts[3,4]. Despite some positive outcomes, MSC delivery for bone repair faces limitations due to several significant barriers to translation, including low cell viability and retention at the site of injection, leading to disappointing therapeutic efficacy after injection.

Injectable biomaterials have been shown to improve cell retention and survival at the injection site, improving the practicality of stem cell delivery[5]. To promote MSC osteogenic differentiation for bone repair, the materials of the injectable hydrogel should provide proper physical/mechanical cues to the delivered cells as well as the biochemical cues. Fundamental studies, mainly in 2D systems, have demonstrated that MSC differentiation is influenced by various physical properties of the environment, such as stiffness[6], micro/nano-topography[7], and mechanical stimulation. In general, stiff substrates are known to promote osteogenic differentiation of MSCs[8]. It has recently been shown that substrate stress-relaxation[9] and matrix degradability[10] also play important roles in regulating MSC differentiation in 3D.

One important factor for regulating MSC differentiation, which has not been fully explored is cell-cell interactions. Physical contacts between cells regulate the Notch signaling pathway, which has previously been shown to positively influence osteogenic differentiation[11,12], although conflicting results have also been reported[13]. Cadherin mediated cell-cell adhesions are involved with cell mechanotransduction, have crosstalk with focal adhesion-mediated signalling[14], and have been shown to influence MSC osteogenesis[15]. Additionally, cells cultured in aggregate rely more on cell-cell connections rather than cell-matrix interactions to drive phenotypic changes such as stem cell differentiation[16]. Injectable biomaterials that promote such cell-cell interactions are highly desirable.

However, most injectable hydrogels are non-porous (with the typical mesh size being in nanometer scales), and delivery of MSCs in stiff injectable hydrogels inhibits cell spreading[17], migration[18,19], and cell-cell communication[20,21], all of which play

important roles in regulating osteogenic differentiation of MSCs. To overcome this barrier, we examined the use of an injectable hydrogel made of an assembly of gelatin microgels, which form an interconnected pore network through the interstitial space. When mixed with the cells and crosslinked, the hydrogel provides a three dimensional, stiff environment that promotes cell spreading, migration, and cell-cell contact through the pore network. Injectable microporous scaffolds have been previously used for cell delivery[22,23], wound healing[24], drug release, and 3D printing[25], but their unique ability to naturally facilitate cell spreading and cell-cell contacts, and the resulting changes in cellular phenotypes have not been well studied. Facilitating cell-cell connections has implications in regulating other important cell phenomena, including endothelial cell organization[26], and neural progenitor cell differentiation[27].

Previously we used a gelatin microgel-based microporous platform as an injectable scaffold for wound healing, which improved migration of cells from excised cornea to the hydrogel interior in an ex-vivo study[28]. The use of gelatin allows for stiff hydrogel formation, while providing natural sites for cell adhesion and remodeling. Here we examine the use of this system to facilitate MSC osteogenic differentiation, and demonstrate that this system improved both MSC growth and osteogenic differentiation in comparison to a nonporous analog (**Fig. 3.1**). In addition, genome-wide differences in gene expression were investigated using RNA Sequencing (RNA-Seq).

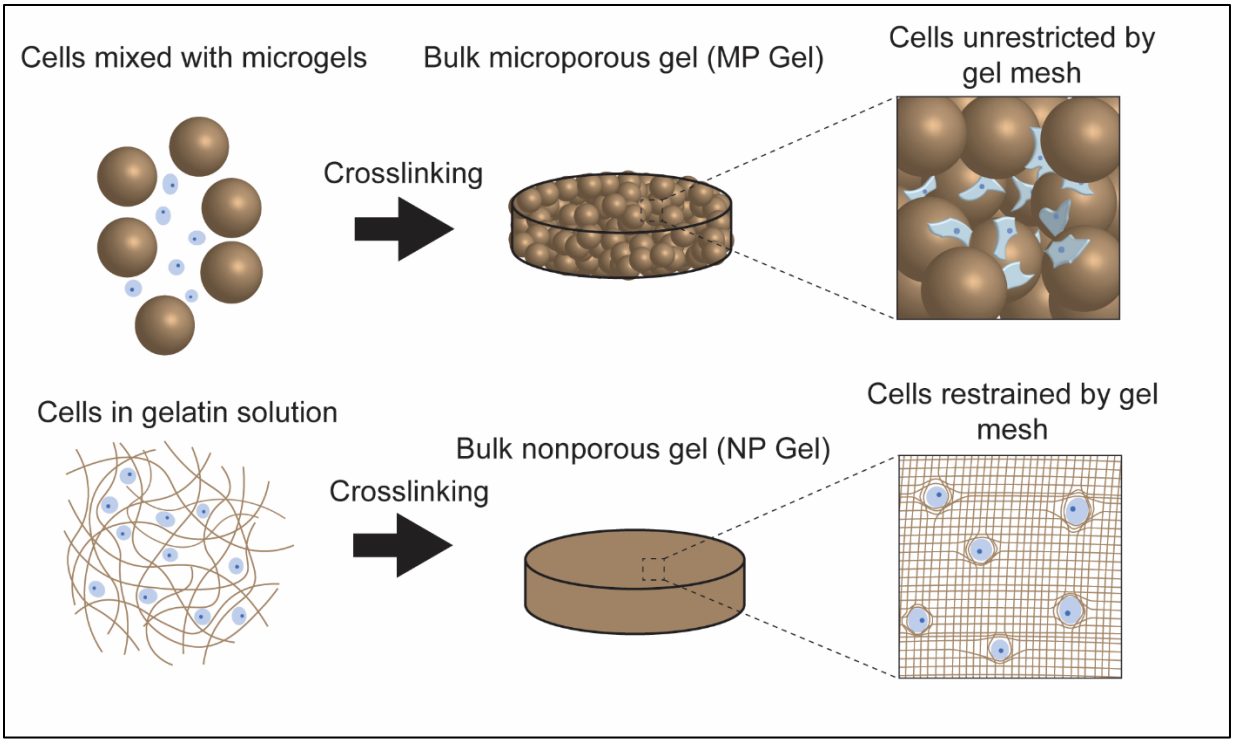

Figure 3.1: Schematic of experimental approach. Encapsulation of cells in microporous hydrogel provides an interconnected pore network regardless of scaffold stiffness. Cells encapsulated in stiff hydrogels are prevented from spreading by the surrounding dense polymer mesh. The differing 3D environment has implications related to cell behavior.

3.2 Materials and Methods

3.2.1 Materials

Bone marrow human mesenchymal stem cells (MSCs) were purchased from ATCC. Minimum Essential Medium α (MEM-α), fetal bovine serum (FBS), penicillin/streptomycin (pen/strep), Lactate Dehydrogenase (LDH) assay, AlamarBlue assay, actin red 555 and 4',6-Diamidino-2-Phenylindole Dihydrochloride (DAPI), Quant-iT dsDNA assay, Point Scientific Calcium Assay and Live/Dead assay were purchased from Thermo Fisher Scientific. 300 Bloom gelatin type A was obtained from Sigma Aldrich. Osteogenic differentiation medium (ODM) was purchased from Promocell. Alkaline phosphatase (ALP) staining kit, and ALP assay were obtained from Abcam.

3.2.2 Microgel Production

Gelatin microgel production has been previously reported[28]. In brief, 20 mL 10% w/v gelatin in DI H_2O was added to 200 mL olive oil at 55 °C and stirred for 1 hour. To create physically crosslinked microgels, the temperature was dropped through addition to an ice bath for 30 minutes while stirring. 100 mL precooled acetone was added to dehydrate the microgels and aid in filtration, mixing for 30 minutes. Microgels were separated by vacuum filtration, washed with additional acetone, then sterilized in 70% ethanol, and freeze dried, before being used in cell experiments. The produced gelatin microgels have an average diameter of 253 μm in diameter after swelling[28].

3.2.3 Cell encapsulation

MSCs were cultured on T-75 flasks prior to cell encapsulation in MSC growth medium (MEM-α, 10 % FBS, 1% pen/strep). For cell encapsulation experiments, 20 mg

of microgel was mixed with 150 µl MEM-α in a 48 well plate well, for rehydration. Then, 50 µl of cell suspension and 50 µl filter-sterilized mTG solution was mixed with the swelled microgels to a final concentration of 8% gelatin, $1x10^6$ cells/ml, and 4% mTG. The hydrogels were incubated at 37 °C for 1 hour for crosslinking. For nonporous hydrogels, 150 µl of 13.3% gelatin solution in MEM-α was mixed with 50 µl of cell suspension and 50 µl mTG solution, before incubation at 37 °C for 1 hour. After crosslinking, cell-encapsulated hydrogels were moved to 24 well plates, and fed daily with 1.5 ml of media. For cell growth experiments, MSC growth medium was used, and for differentiation experiments, ODM was used after 24 hours of incubation in growth medium. Cells of passage 3 were used for all experiments.

3.2.4 Proliferation/Cytotoxicity Experiments

Cell-encapsulated hydrogels were tested for LDH activity 24 hours after encapsulation to assess the cytotoxicity as a result of the encapsulation process. Cells seed on TCPS were used as the negative control, and for the positive control after treatment with lysis buffer. Cell proliferation was measured using alamarBlue assay at 24 hours and 7 days after encapsulation, where cells seeded on TCPS were used as a positive control.

3.2.5 Live/Dead Assay

Live/Dead assay was performed on cell-encapsulated hydrogels at 1, 7, and 14 days after encapsulation, for hydrogels incubated with either growth medium or ODM to monitor cell growth and morphological changes as a result of differentiation. Hydrogels were incubated with HBSS containing calcein-AM and ethidium homodimer to visualize

living and dead cells respectively, for 1 hour before imaging (Nikon A1R HD). 3D sections of cell encapsulated hydrogels were imaged, and images were processed and converted to Z projections using ImageJ.

3.2.6 Actin Cytoskeleton Imaging

Cells encapsulated in MP gels and NP gels were fixed in 4% paraformaldehyde for 1 hour after 3 and 14 days of culture in growth medium. Cells were permeabilized in 1% Triton X-100 for 1 hour, stained with DAPI and actin red 555 overnight at 4 °C. Constructs were washed in PBS for 1 hour before confocal imaging. Images were analyzed using ImageJ.

3.2.7 SEM/EDS

Cell-encapsulated hydrogels were fixed with 2.5% glutaraldehyde solution in PBS, then moved to ethanol by serial dilution, and critical point dried. Hydrogels were mounted and sputter coated with Au/Pd before SEM/EDS.

3.2.8 Alkaline Phosphatase Staining and Quantitative Assay

Alkaline phosphatase staining kit (Abcam) was used according to the manufacturer protocol. Cell encapsulated constructs after 14 days of incubation in ODM were fixed with the provided fixative, then stained for 30 minutes, before washing 4x with PBS for 1 hour to remove the discoloration of the hydrogel. High magnification images were taken using the DS-Ri2 camera attachment for the confocal microscope.

ALP assay (Abcam) was used to determine ALP activity in cell-encapsulated constructs after 14 days of incubation of ODM, normalized to measured dsDNA content.

Cell-encapsulated constructs were homogenized, and incubated in RIPA lysis buffer before processing.

3.2.9 Calcium Assay

Cell encapsulated hydrogels were homogenized using a rotor homogenizer, and 50 µl 12 N HCl was added to cell encapsulated constructs for 72 hours at 4 °C to dissolve deposited calcium. A Pointe Scientific Calcium assay was used to measure calcium concentration. Samples were diluted in PBS to fall in the linear range of the assay before measuring. As pH was seen to influence the assay results, all samples were diluted until sample pH was neutral.

3.2.10 RNA Sequencing

RNA extraction was carried out using the RNeasy Plus Mini kit from Qiagen according to the manufacturer's protocol. Cell encapsulated constructs were homogenized with a rotor homogenizer before extracting the RNA. Due to the lower RNA yield for NP samples, a higher sample number was used. Isolated RNA was frozen at –80 °C until use. Extracted RNA was supplied to the UNH Hubbard Center for Genome Studies for mRNA isolation, library preparation, and sequencing. Sequencing was performed on Illumina NovaSeq 6000. Paired end reads were trimmed using trimmomatic[29], aligned to the human genome using STAR[30], and raw reads were counted using HT-seq[31]. Data normalization and analysis was done in R using the Deseq2 package. PCA was performed using a regularized log dataset using tools from the Deseq2 package[32].

3.2.11 Statistical Analysis

Quantitative data other than RNA-Seq data are represented as means, and error bars represent standard deviations. A student's t-test was used to determine statistical significance, where $p < 0.05$ was considered statistically significant. RNA-seq data is shared as median (line) and the interquartile range to mitigate the effect of statistical outliers.

3.3 Results and Discussion

3.3.1 Cell viability, proliferation and morphological changes

The potential for the injectable microgel-based microporous hydrogels (MP gels) to support cell encapsulation was explored through live/dead and alamarBlue proliferation assays, (**Fig. 3.2**) and LDH cytotoxicity assays (**Fig. 3.3**). Cells encapsulated in MP gel demonstrated high viability with robust cell spreading as early as 1 day post encapsulation (Figure 3.2a), while cells in the nonporous hydrogel (NP gel) remained highly spherical due to the entrapment by the surrounding polymers (Fig. 3.2 d). The cells in the NP gel can fully spread only by matrix degradation or stress relaxation of the surrounding polymers. Live/dead assay on day 7 and 14 showed continuation of these trends (Fig. 3.2 b, c, e, f), and cells encapsulated in both conditions began to spread more compared with day 1 (Fig. 3.2e,f). Cell proliferation in the MP gel was markedly higher than the NP gel (Fig. 3.2g). Cytotoxicity during the encapsulation process by the enzymatic crosslinking of gelatin was low for both MP and NP gels (**Fig. 3.3**). When the cells were cultured in osteogenic differentiation media, MSCs in the MP gel adopted a distinct morphology (Fig. 3.2h) compared to the cells cultured in the growth media (Fig. 3.2c). In contrast, morphological changes of the cells encapsulated in the NP gel were indiscernible (Fig. 3.2i, Fig. 3.2f). MP gel also induced

early formation of actin stress fibers of the encapsulated cells (**Fig. 3.4**). The formation of actin stress fibers is known to enable mechanotransduction-mediated osteogenesis, suggesting MP gel may enhance MSC osteogenic differentiation[34].

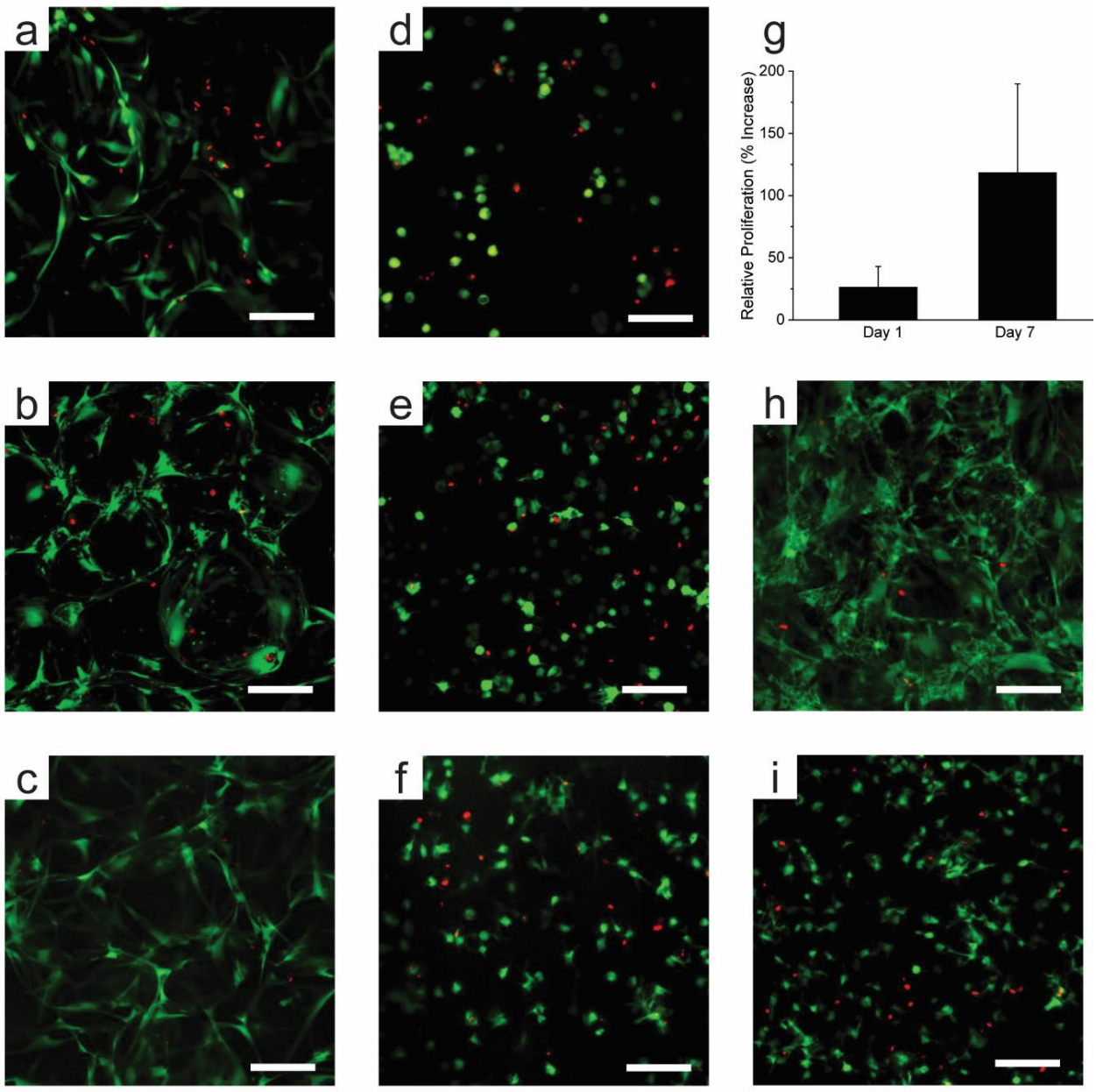

Figure 3.2: Mesenchymal stem cell (MSC) growth in differing 3D culture conditions. Representative Z projections of living (green) and dead (red) staining of MSCs encapsulated in microporous (a, b, c) and nonporous (d, e, f) hydrogel in growth medium for 1 (a, d), 7 (b, e), and 14 (c, f) days. MSC proliferation was quantified by alamarBlue assay (g). MSCs encapsulated in microporous (h) and nonporous (i) hydrogels after 14 days of incubation in osteogenic differentiation medium. Scale bar = 50 µm.

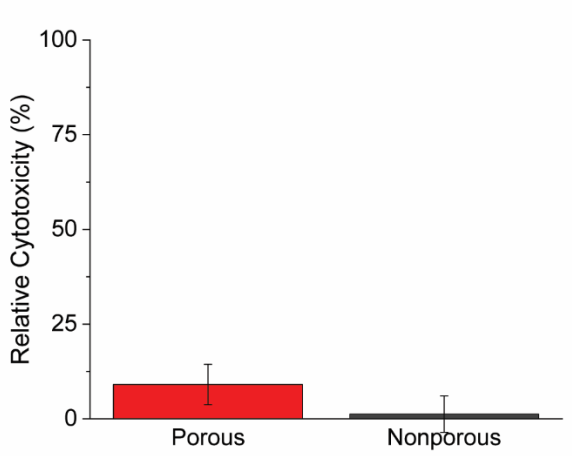

Figure 3.3. Cytotoxicity of the encapsulation procedure. LDH assay of cells 24 hours after encapsulation in either the porous, or nonporous condition.

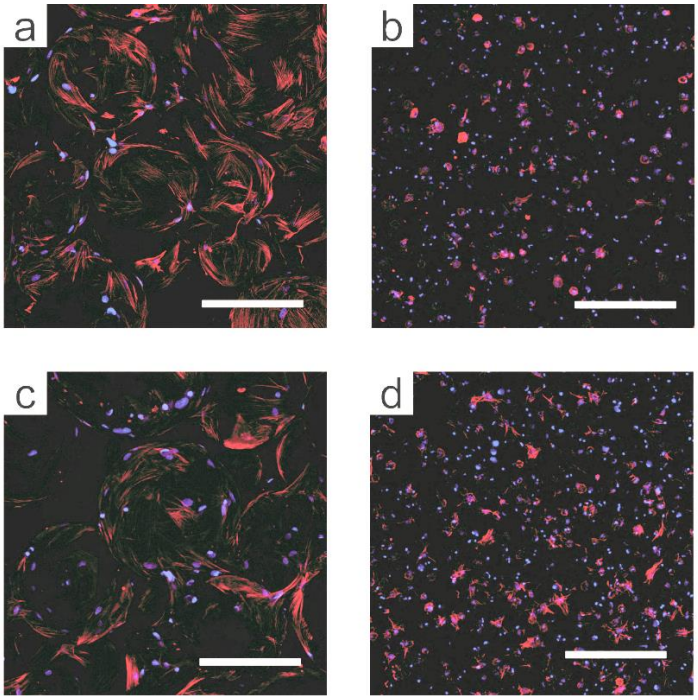

Figure 3.4. Cytoskeletal organization of encapsulated cells. Z-projection images of cell nuclei (blue) and actin cytoskeleton (red) after 1 (a, b) and 7 (c, d) days of culture, after encapsulation in the microporous (a, c) or nonporous (b, d) environment. Scale = 200 µm.

3.3.2 Osteogenic differentiation examined by SEM and EDS

Morphological changes as a result of osteogenic differentiation, and associated calcium mineral deposition, were observed under SEM and EDS (**Fig. 3.5**). The cells encapsulated in NP gel were not examined, as the cells are buried within the hydrogel, making it difficult to image using SEM. In agreement with the confocal imaging (Fig. 3.2), cells appear to adopt a more pointed, spindle-like morphology when incubated in osteogenic medium, which has been previously associated with MSC osteogenesis[35,36]. In contrast, cells grown in growth medium maintain a smooth, fibroblast-like morphology. Calcium and phosphate deposition was examined by EDS. The increase in calcium and phosphate in hydrogels incubated in osteogenic differentiation media is attributable to bone mineral deposition, which is characteristic of osteogenic differentiation. Unlabeled peaks at 2.12 and 2.84 keV correspond to Au and Pd, respectively, which were used for conductive coating.

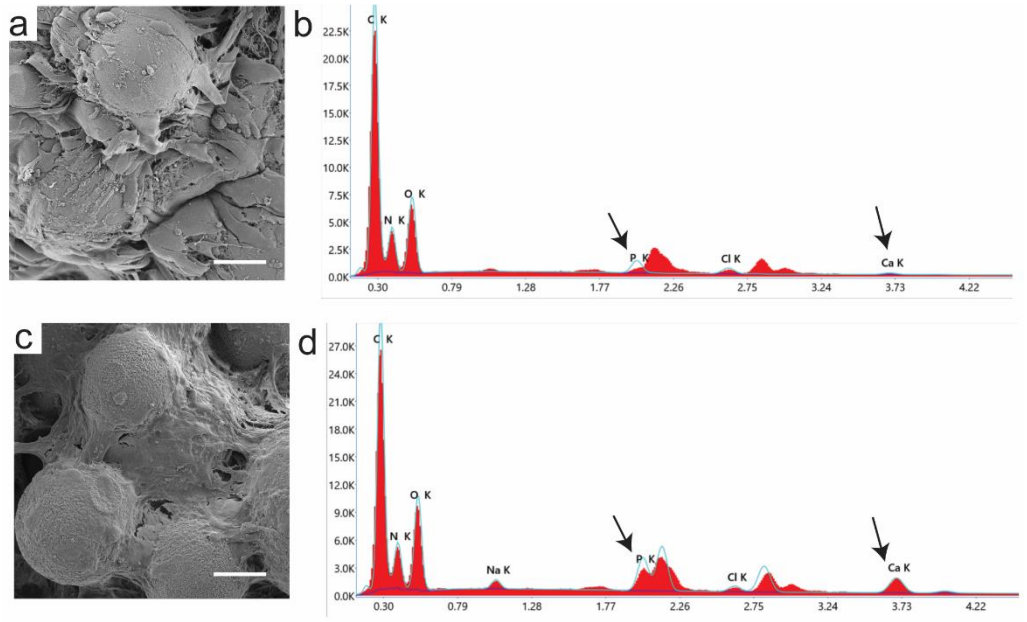

Figure 3.5. Cell morphology in microporous hydrogels and initial evidence of mineral deposition. SEM and EDS chemical composition report for cells grown for 14 days in (a, b) growth medium or (c, d) osteogenic differentiation medium. Arrows denote peaks of interest for mineralization. Scale = 50 µm.

3.3.3 Biochemical characterization of osteogenic differentiation

Osteogenic differentiation of MSCs encapsulated in MP gel and NP gel was further examined by alkaline phosphatase (ALP) and calcium assays after 14 days of incubation in osteogenic differentiation medium (**Fig. 3.6**).

ALP staining shows a contrast between cells encapsulated in MP gels (Fig. 3.6a) and NP gels (Fig. 3.6b), where cells encapsulated in MP gel appear to have increased ALP activities. ALP is an enzyme involved with the mineralization of bone tissue, and is a marker of early MSC osteogenic differentiation. This microscopic observation is consistent with the quantitative results. On average, ALP activity increased by a factor

of 4 on a per cell basis (Fig. 3.6c), and calcium deposition increased by a factor of 10 (Fig. 3.6d) for cells encapsulated in MP gel in comparison to NP gel. Calcium deposition is indicative of mature osteoblasts, demonstrating that encapsulation in MP gel improved mineral deposition over the culture period.

Considering that the same material was used as the 3D matrix for both MP and NP with comparable stiffness, these results highlight the importance of differing 3D micro-environments for the control of osteogenesis by MSCs. More specifically, MP gels allow rapid morphological changes of the encapsulated cells and direct cell-cell physical contacts through the interconnected micropore network, which may have promoted osteogenesis and calcium mineral deposition.

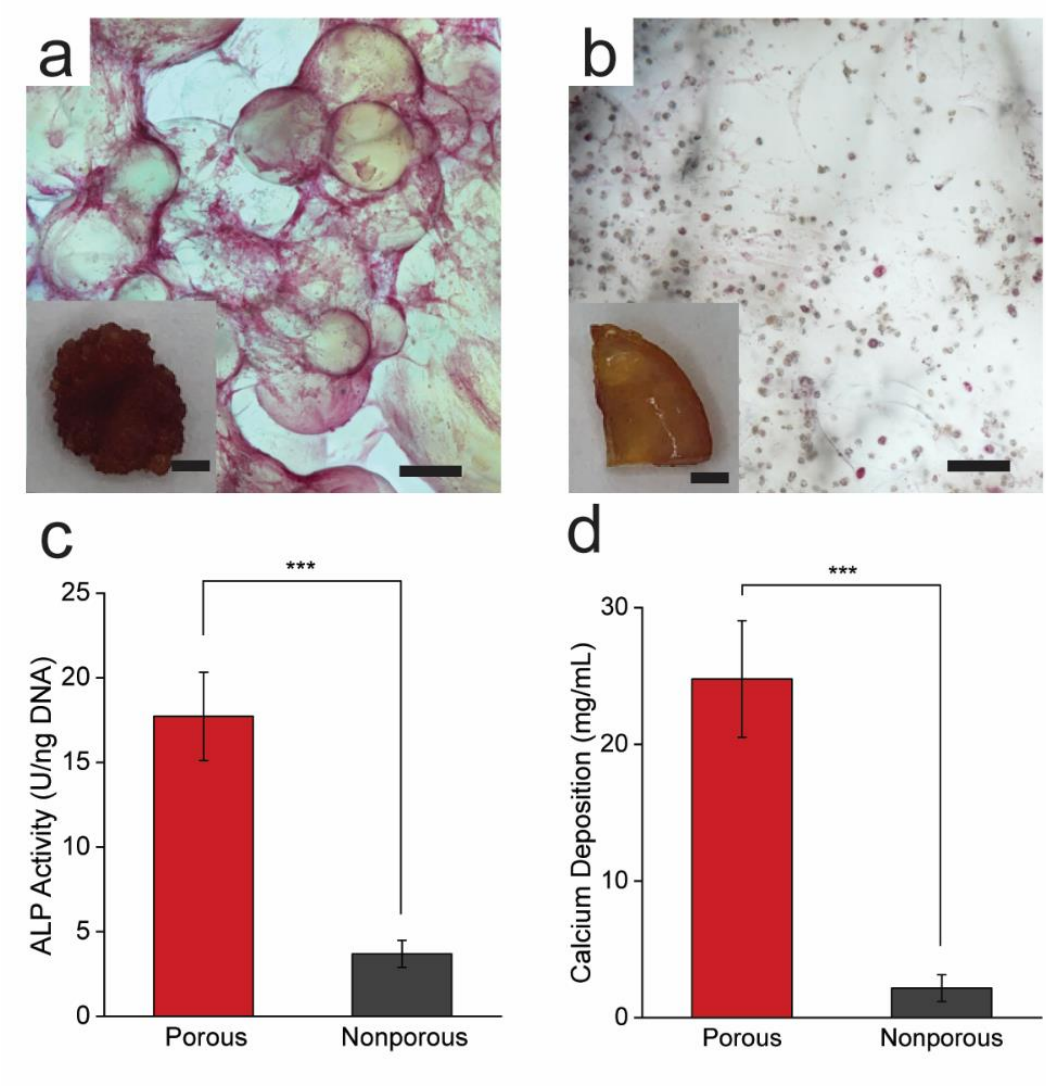

Figure 3.6. Microporous hydrogel enhances mesenchymal stem cell osteogenic differentiation. After 14 days of incubation in osteogenic differentiation medium: Alkaline phosphatase staining of cells encapsulated in (a) microporous and (b) nonporous hydrogels. (c) Alkaline phosphatase activity normalized to DNA content, and (d) calcium mineral deposition in equal volumes of cell-encapsulated hydrogels. Scale bar = 200 µm, inset scale bar = 1 mm.

3.3.4 Transcriptomic analysis by RNA-seq

RNA-Seq was used to examine the changes of gene expressions of MSC encapsulation in the different 3D environments. RNA from MSCs encapsulated in MP and NP hydrogels was extracted at 3 days (MP3, NP3), and 14 days (MP14, NP14) after encapsulation to assess early and late differentiation (**Fig. 3.7**, **Fig. 3.8**). PCA analysis (Fig. 3.7a) shows a clear trend based on sample condition and time, indicating that gene expression changed substantially depending on the 3D environment, and on the duration of differentiation. The Venn-diagram (Fig. 3.7b) shows direct comparisons between groups, where each circle is a comparison with the NP3 condition. The NP14 samples had the fewest differentially expressed genes while the MP14 group had the most differentially expressed genes compared with the NP3 group, indicating the 3D environment played a central role in the differential gene expression. Genes commonly related to osteogenic differentiation (Fig. 3.7c-f) show a trend that osteogenic differentiation was increased in the MP hydrogel, and increased over incubation time. IBSP expression (Fig. 3.7d) is notable as a late stage marker of osteogenesis. These results indicate that encapsulated MSCs have distinct gene expression depending on the length of culture and the 3D environmental conditions, and confirm the increase in osteogenesis for cells encapsulated in the MP condition.

Expression data for selected genes related to osteogenesis, cell adhesions, cytoskeletal organization, cell-cell connections, ECM remodeling and deposition are shown in Fig. 3.8.

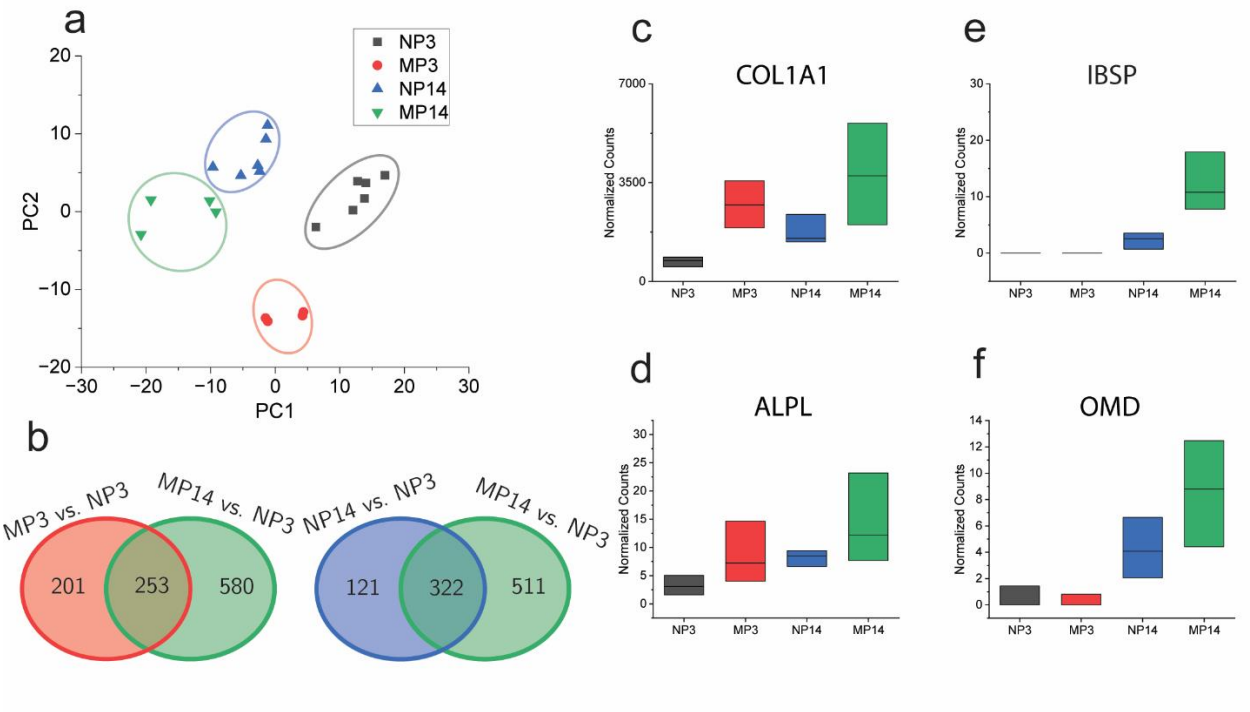

Figure 3.7: Differential gene expression identified by RNA-Seq. (a) PCA of sample set. (b) Differential gene expression between groups, comparing culture condition and time. (c-e) Gene expression of genes directly related to osteogenesis, collagen I alpha chain 1 (COL1A1), integrin binding sialoprotein (IBSP), alkaline phosphatase, biomineralization related (ALPL), and osteomodulin (OMD). Abbreviations: NP3 (Nonporous day 3), MP3 (Microporous day 3), NP14 (Nonporous day 14), MP14 (Porous, day 14). Data shown are median, bounded by the interquartile range.

Osteogenesis genes: Osteonectin (SPARC) is another protein involved in calcium mineral deposition, which had increased expression in the MP condition, providing further evidence of the increase in osteogenesis for these cells.

Cell adhesion, focal adhesion genes: Increase in integrin $\alpha_5\beta_1$, one of the primary integrins involved in binding to gelatin, in MP gels is consistent with an increase in cell spreading as visualized in confocal images[37]. However, expression of proteins related to focal adhesions and focal adhesion-mediated signaling overall did not show a clear trend (PXN, RUNX2, YAP1), though vinculin (VCL) expression was upregulated in the

MP gels, and with increasing culture length. In similar 3D matrices, it was previously reported that differences in gene expression of mechanotransduction-related genes was diminished as length of culture increased[38], which could explain this trend. Additionally, while cell spreading is higher for cells in MP gels, substrate stiffness is similar between MP and NP gels, which may have resulted in insignificant differences of these genes.

Cytoskeletal organization genes: Gene expression related to cytoskeletal organization (MFAP5, ENAH, ACTB, NEXN) shows a general trend of increased expression for cells encapsulated in MP gel, and an increase in expression over culture period, likely as a product of increased cell spreading.

Cell-cell connection genes: Among the genes related to cell connections, an increase in CDH11 expression in MP gel was noted. On 2D surfaces, higher CDH11 expression was correlated with higher osteogenesis of MSCs. CDH11 expression was constant for cells encapsulated in NP condition, though expression at day 3 was higher than in MP gel. Among gap-junction proteins, which have been previously implicated to regulate MSC differentiation[39], GJD3 was highly expressed, and had increased expression for cells in MP conditions.

Wnt/Notch signaling genes: CTNNB1, NOTCH1, FZD4 are involved in cell signaling pathways (Wnt/Notch). We hypothesize that over the culture period, cells encapsulated in the MP condition increased the number of cell-cell connections as cell density in the hydrogel increased, leading to increased expression of cell-cell connection-related genes, and potentially associated pathways, such as the Notch pathway. However, gene expression for cells encapsulated in the NP condition were generally prevented from making these connections, and expression of cell-cell connection related genes

remained constant as a result. Additionally, CTNNB1 and FZD4 participate in Wnt signaling, which mediates mechanical stretching-induced osteogenesis[40], which may have been promoted or inhibited by the differing microenvironments, and has been previously implicated to mediate osteogenesis for MSC aggregates on differing biomaterial substrates[41].

ECM remodeling genes: Lysyl hydroxylase 1 (PLOD1) and lysyl oxidase (LOX) are involved with collagen production, indicating ECM deposition was increased in MP gels in comparison to NP gels. We hypothesize that the open pore space may enable more rapid production of ECM, as cells in this condition do not need to degrade the surrounding matrix. MMP2 and MMP9 are gelatinases, some of the primary means for cells to degrade gelatin. Cells encapsulated in NP gel may need to degrade the surrounding polymer mesh for division, spreading, and new ECM production, likely leading to increased production of MMP2. MMP9 expression was not detected in any sample groups by RNA-seq.

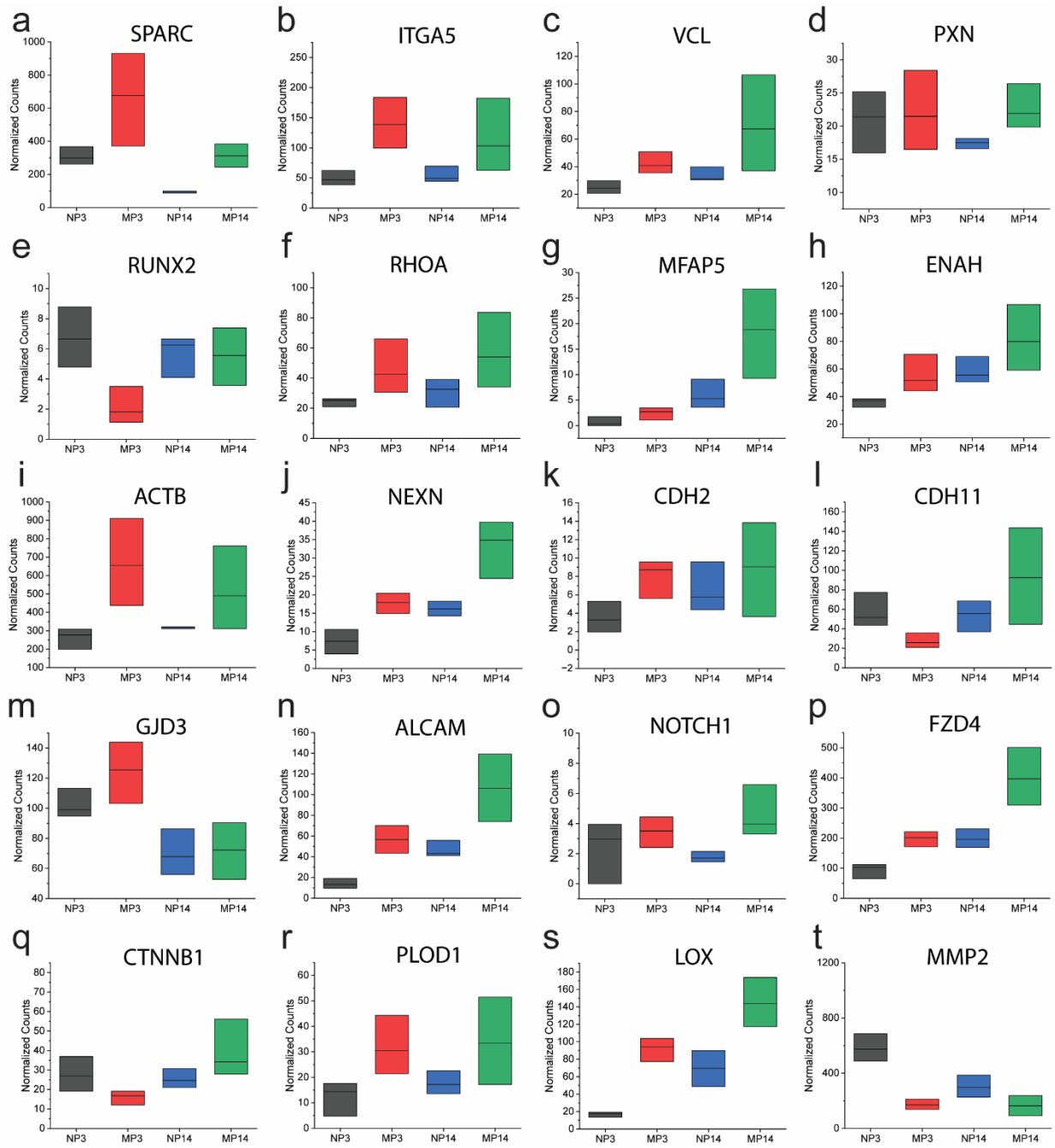

Figure 3.8: Gene expression for genes of interest in different 3D environments and time points, for genes related to osteogenesis (a), mechanotransduction (b, c, d, e, f), cystoskeleton production and organization (g, h, I, j), cell-cell connections (k, l, m, n, o, p, q), extracellular matrix production and matrix remodeling (r, s, t). Data is separated between culture condition and time point (NP3 = nonporous day 3, MP3 = porous day 3, NP14 = nonporous day 14, MP14 = porous day 14). (a) Secreted Protein Acidic and Cysteine Rich (SPARC), (b) Integrin Subunit Alpha 5 (ITGA5), (c) Vinculin (VCL), (d) Paxillin (PXN), (e) Runt-related Transcription Factor 2 (RUNX2), (f) Ras Homolog Family Member A (RHOA), (g) Microfibril Associated Protein 5 (MFAP5), (h) ENAH Actin Regulator (ENAH), (i) Actin Beta (ACTB), (j) Nexilin F-Actin Binding Protein

(NEXN), (k) Cadherin 2 (CDH2), (l) Cadherin 11 (CDH11), (m) Gap Junction Protein Delta 3 (GJD3), (n) Activated Leukocyte Cell Adhesion Molecule (ALCAM), (o) Notch Receptor 1 (NOTCH1), (p) Frizzled Class Receptor 4 (FZD4), (q) catenin beta 1 (CTNNB1), (r) Procollagen-Lysine, 2-Oxoglutarate 5-Dioxygenase 1 (PLOD1), (s) Lysyl Oxidase (LOX), (t) Matrix Metalloproteinase 2 (MMP2).

3.4 Conclusion

In this work we examined the use of a microporous injectable hydrogel to promote MSC osteogenic differentiation in comparison to a traditional injectable hydrogel. MP gels promoted cell spreading, and cell-cell connections of the encapsulated MSCs because of the interconnected pore network, and induced more efficient osteogenic differentiation than NP gels. RNA-seq identified genes differentially expressed as a result of encapsulation in the contrasted encapsulation conditions. Additionally, this work demonstrates a functional injectable system which can provide a stiff 3D environment to MSCs, yet facilitates cell spreading, elongation, and cell-cell connections, in contrast with contemporary injectable systems. This research demonstrates the potential use of the microgel-based injectable hydrogel systems for bone repair.

References

(1) Xue, X.; Hu, Y.; Deng, Y.; Su, J. Recent Advances in Design of Functional Biocompatible Hydrogels for Bone Tissue Engineering. *Adv. Funct. Mater.* **2021**, *31* (19), 2009432. https://doi.org/10.1002/ADFM.202009432.

(2) Agarwal, R.; García, A. J. Biomaterial Strategies for Engineering Implants for Enhanced Osseointegration and Bone Repair. *Adv. Drug Deliv. Rev.* **2015**, *94*, 53–62. https://doi.org/10.1016/J.ADDR.2015.03.013.

(3) Shang, F.; Yu, Y.; Liu, S.; Ming, L.; Zhang, Y.; Zhou, Z.; Zhao, J.; Jin, Y. Advancing Application of Mesenchymal Stem Cell-Based Bone Tissue Regeneration. *Bioact. Mater.* **2020**, *6* (3), 666–683. https://doi.org/10.1016/J.BIOACTMAT.2020.08.014.

(4) Kangari, P.; Talaei-Khozani, T.; Razeghian-Jahromi, I.; Razmkhah, M. Mesenchymal Stem Cells: Amazing Remedies for Bone and Cartilage Defects. *Stem Cell Res. Ther.* **2020**, *11* (1), 1–21. https://doi.org/10.1186/S13287-020-02001-1.

(5) Foster, A. A.; Marquardt, L. M.; Heilshorn, S. C. The Diverse Roles of Hydrogel Mechanics in Injectable Stem Cell Transplantation. *Curr. Opin. Chem. Eng.* **2017**, *15*, 15–23. https://doi.org/10.1016/J.COCHE.2016.11.003.

(6) Discher, D. E.; Janmey, P.; Wang, Y. L. Tissue Cells Feel and Respond to the Stiffness of Their Substrate. *Science* **2005**, *310* (5751), 1139–1143. https://doi.org/10.1126/SCIENCE.1116995.

(7) Bettinger, C. J.; Langer, R.; Borenstein, J. T. Engineering Substrate Topography at the Micro- and Nanoscale to Control Cell Function. *Angew. Chem. Int. Ed. Engl.* **2009**, *48* (30), 5406–5415. https://doi.org/10.1002/ANIE.200805179.

(8) Engler, A. J.; Sen, S.; Sweeney, H. L.; Discher, D. E. Matrix Elasticity Directs Stem Cell Lineage Specification. *Cell* **2006**, *126* (4), 677–689. https://doi.org/10.1016/J.CELL.2006.06.044.

(9) Chaudhuri, O.; Gu, L.; Klumpers, D.; Darnell, M.; Bencherif, S. A.; Weaver, J. C.; Huebsch, N.; Lee, H. P.; Lippens, E.; Duda, G. N.; Mooney, D. J. Hydrogels with Tunable Stress Relaxation Regulate Stem Cell Fate and Activity. *Nat. Mater.* **2015**, *15* (3), 326–334. https://doi.org/10.1038/nmat4489.

(10) Khetan, S.; Guvendiren, M.; Legant, W. R.; Cohen, D. M.; Chen, C. S.; Burdick, J. A. Degradation-Mediated Cellular Traction Directs Stem Cell Fate in Covalently Crosslinked Three-Dimensional Hydrogels. *Nat. Mater.* **2013**, *12* (5), 458–465. https://doi.org/10.1038/nmat3586.

(11) Ugarte, F.; Ryser, M.; Thieme, S.; Fierro, F. A.; Navratiel, K.; Bornhäuser, M.; Brenner, S. Notch Signaling Enhances Osteogenic Differentiation While Inhibiting Adipogenesis in Primary Human Bone Marrow Stromal Cells. *Exp. Hematol.* **2009**, *37* (7). https://doi.org/10.1016/J.EXPHEM.2009.03.007.

(12) Xu, Y.; Shu, B.; Tian, Y.; Chelly, M.; Morandi, M. M.; Barton, S.; Shang, X.; Dong, Y. Notch Activation Promotes Osteoblast Mineralization by Inhibition of Apoptosis. *J. Cell. Physiol.* **2018**, *233* (10), 6921–6928. https://doi.org/10.1002/JCP.26592.

(13) Hilton, M. J.; Tu, X.; Wu, X.; Bai, S.; Zhao, H.; Kobayashi, T.; Kronenberg, H. M.;

Teitelbaum, S. L.; Ross, F. P.; Kopan, R.; Long, F. Notch Signaling Maintains Bone Marrow Mesenchymal Progenitors by Suppressing Osteoblast Differentiation. *Nat. Med. 2008 143* **2008**, *14* (3), 306–314. https://doi.org/10.1038/nm1716.

(14) Marie, P. J.; Haÿ, E.; Saidak, Z. Integrin and Cadherin Signaling in Bone: Role and Potential Therapeutic Targets. *Trends Endocrinol. Metab.* **2014**, *25* (11), 567–575. https://doi.org/10.1016/J.TEM.2014.06.009.

(15) Zhu, M.; Lin, S.; Sun, Y.; Feng, Q.; Li, G.; Bian, L. Hydrogels Functionalized with N-Cadherin Mimetic Peptide Enhance Osteogenesis of HMSCs by Emulating the Osteogenic Niche. *Biomaterials* **2016**, *77*, 44–52. https://doi.org/10.1016/J.BIOMATERIALS.2015.10.072.

(16) Passanha, F. R.; Geuens, T.; Konig, S.; van Blitterswijk, C. A.; LaPointe, V. L. Cell Culture Dimensionality Influences Mesenchymal Stem Cell Fate through Cadherin-2 and Cadherin-11. *Biomaterials* **2020**, *254*. https://doi.org/10.1016/J.BIOMATERIALS.2020.120127.

(17) Tan, S. J.; Fang, J. Y.; Yang, Z.; Nimni, M. E.; Han, B. The Synergetic Effect of Hydrogel Stiffness and Growth Factor on Osteogenic Differentiation. *Biomaterials* **2014**, *35* (20), 5294–5306. https://doi.org/10.1016/J.BIOMATERIALS.2014.02.040.

(18) Hou, S.; Niu, X.; Li, L.; Zhou, J.; Qian, Z.; Yao, D.; Yang, F.; Ma, P. X.; Fan, Y. Simultaneous Nano- and Microscale Structural Control of Injectable Hydrogels via the Assembly of Nanofibrous Protein Microparticles for Tissue Regeneration.

Biomaterials **2019**, *223*, 119458. https://doi.org/10.1016/J.BIOMATERIALS.2019.119458.

(19) Even-Ram, S.; Yamada, K. M. Cell Migration in 3D Matrix. *Curr. Opin. Cell Biol.* **2005**, *17* (5), 524–532. https://doi.org/10.1016/J.CEB.2005.08.015.

(20) Caliari, S. R.; Vega, S. L.; Kwon, M.; Soulas, E. M.; Burdick, J. A. Dimensionality and Spreading Influence MSC YAP/TAZ Signaling in Hydrogel Environments. *Biomaterials* **2016**, *103*, 314–323. https://doi.org/10.1016/J.BIOMATERIALS.2016.06.061.

(21) Mabry, K. M.; Lawrence, R. L.; Anseth, K. S. Dynamic Stiffening of Poly(Ethylene Glycol)-Based Hydrogels to Direct Valvular Interstitial Cell Phenotype in a Three-Dimensional Environment. *Biomaterials* **2015**, *49*, 47–56. https://doi.org/10.1016/J.BIOMATERIALS.2015.01.047.

(22) Truong, N. F.; Kurt, E.; Tahmizyan, N.; Lesher-Pérez, S. C.; Chen, M.; Darling, N. J.; Xi, W.; Segura, T. Microporous Annealed Particle Hydrogel Stiffness, Void Space Size, and Adhesion Properties Impact Cell Proliferation, Cell Spreading, and Gene Transfer. *Acta Biomater.* **2019**, *94*, 160–172. https://doi.org/10.1016/J.ACTBIO.2019.02.054.

(23) Koh, J.; Griffin, D. R.; Archang, M. M.; Feng, A. C.; Horn, T.; Margolis, M.; Zalazar, D.; Segura, T.; Scumpia, P. O.; Di Carlo, D. Enhanced In Vivo Delivery of Stem Cells Using Microporous Annealed Particle Scaffolds. *Small* **2019**, *15* (39), 1903147. https://doi.org/10.1002/SMLL.201903147.

(24) Griffin, D. R.; Weaver, W. M.; Scumpia, P. O.; Di Carlo, D.; Segura, T.

Accelerated Wound Healing by Injectable Microporous Gel Scaffolds Assembled from Annealed Building Blocks. *Nat. Mater. 2014 147* **2015**, *14* (7), 737–744. https://doi.org/10.1038/nmat4294.

(25) Highley, C. B.; Hoon Song, K.; Daly, A. C.; Burdick, J. A.; Highley, C. B.; Song, K. H.; Daly, A. C.; Burdick, J. A. Jammed Microgel Inks for 3D Printing Applications. *Adv. Sci.* **2019**, *6* (1), 1801076. https://doi.org/10.1002/ADVS.201801076.

(26) Bazzoni, G.; Dejana, E. Endothelial Cell-to-Cell Junctions: Molecular Organization and Role in Vascular Homeostasis. *Physiol. Rev.* **2004**, *84* (3), 869–901. https://doi.org/10.1152/PHYSREV.00035.2003.

(27) Jiao, Q.; Li, X.; An, J.; Zhang, Z.; Chen, X.; Tan, J.; Zhang, P.; Lu, H.; Liu, Y. Cell-Cell Connection Enhances Proliferation and Neuronal Differentiation of Rat Embryonic Neural Stem/Progenitor Cells. *Front. Cell. Neurosci.* **2017**, *11*. https://doi.org/10.3389/FNCEL.2017.00200/FULL.

(28) Hou, S.; Lake, R.; Park, S.; Edwards, S.; Jones, C.; Jeong, K. J. Injectable Macroporous Hydrogel Formed by Enzymatic Cross-Linking of Gelatin Microgels. *ACS Appl. Bio Mater.* **2018**, *1* (5), 1430–1439. https://doi.org/10.1021/ACSABM.8B00380.

(29) Bolger, A. M.; Lohse, M.; Usadel, B. Trimmomatic: A Flexible Trimmer for Illumina Sequence Data. *Bioinformatics* **2014**, *30* (15), 2114–2120. https://doi.org/10.1093/BIOINFORMATICS/BTU170.

(30) Dobin, A.; Davis, C. A.; Schlesinger, F.; Drenkow, J.; Zaleski, C.; Jha, S.; Batut, P.; Chaisson, M.; Gingeras, T. R. STAR: Ultrafast Universal RNA-Seq Aligner.

Bioinformatics **2013**, *29* (1), 15–21. https://doi.org/10.1093/BIOINFORMATICS/BTS635.

(31) Anders, S.; Pyl, P. T.; Huber, W. HTSeq—a Python Framework to Work with High-Throughput Sequencing Data. *Bioinformatics* **2015**, *31* (2), 166–169. https://doi.org/10.1093/BIOINFORMATICS/BTU638.

(32) Love, M. I.; Huber, W.; Anders, S. Moderated Estimation of Fold Change and Dispersion for RNA-Seq Data with DESeq2. *Genome Biol.* **2014**, *15* (12), 1–21. https://doi.org/10.1186/S13059-014-0550-8.

(33) Subramanian, A.; Tamayo, P.; Mootha, V. K.; Mukherjee, S.; Ebert, B. L.; Gillette, M. A.; Paulovich, A.; Pomeroy, S. L.; Golub, T. R.; Lander, E. S.; Mesirov, J. P. Gene Set Enrichment Analysis: A Knowledge-Based Approach for Interpreting Genome-Wide Expression Profiles. *Proc. Natl. Acad. Sci. U. S. A.* **2005**, *102* (43), 15545–15550. https://doi.org/10.1073/PNAS.0506580102.

(34) Khan, A. U.; Qu, R.; Fan, T.; Ouyang, J.; Dai, J. A Glance on the Role of Actin in Osteogenic and Adipogenic Differentiation of Mesenchymal Stem Cells. *Stem Cell Res. Ther.* **2020**, *11* (1), 1–14. https://doi.org/10.1186/S13287-020-01789-2.

(35) Peng, R.; Yao, X.; Ding, J. Effect of Cell Anisotropy on Differentiation of Stem Cells on Micropatterned Surfaces through the Controlled Single Cell Adhesion. *Biomaterials* **2011**, *32* (32), 8048–8057. https://doi.org/10.1016/J.BIOMATERIALS.2011.07.035.

(36) Kilian, K. A.; Bugarija, B.; Lahn, B. T.; Mrksich, M. Geometric Cues for Directing the Differentiation of Mesenchymal Stem Cells. *Proc. Natl. Acad. Sci. U. S. A.*

2010, *107* (11), 4872–4877. https://doi.org/10.1073/PNAS.0903269107.

(37) Davidenko, N.; Schuster, C. F.; Bax, D. V.; Farndale, R. W.; Hamaia, S.; Best, S. M.; Cameron, R. E. Evaluation of Cell Binding to Collagen and Gelatin: A Study of the Effect of 2D and 3D Architecture and Surface Chemistry. *J. Mater. Sci. Mater. Med.* **2016**, *27* (10). https://doi.org/10.1007/S10856-016-5763-9.

(38) Lo, Y. P.; Liu, Y. S.; Rimando, M. G.; Ho, J. H. C.; Lin, K. H.; Lee, O. K. Three-Dimensional Spherical Spatial Boundary Conditions Differentially Regulate Osteogenic Differentiation of Mesenchymal Stromal Cells. *Sci. Reports* **2016**, *6* (1), 1–14. https://doi.org/10.1038/srep21253.

(39) Tang, J.; Peng, R.; Ding, J. The Regulation of Stem Cell Differentiation by Cell-Cell Contact on Micropatterned Material Surfaces. *Biomaterials* **2010**, *31* (9), 2470–2476. https://doi.org/10.1016/J.BIOMATERIALS.2009.12.006.

(40) Gu, Q.; Tian, H.; Zhang, K.; Chen, D.; Chen, D.; Wang, X.; Zhao, J. Wnt5a/FZD4 Mediates the Mechanical Stretch-Induced Osteogenic Differentiation of Bone Mesenchymal Stem Cells. *Cell. Physiol. Biochem.* **2018**, *48* (1), 215–226. https://doi.org/10.1159/000491721.

(41) Hsu, S. hui; Huang, G. S. Substrate-Dependent Wnt Signaling in MSC Differentiation within Biomaterial-Derived 3D Spheroids. *Biomaterials* **2013**, *34* (20), 4725–4738. https://doi.org/10.1016/J.BIOMATERIALS.2013.03.031.

Chapter 4

Encapsulation of Neural Progenitor Cells in Laminin Functionalized Gelatin Microporous Hydrogel for Cell Delivery

4.1 Introduction

Treatment of neurological damage such as spinal cord injury and traumatic brain injury are hampered due to the limited regenerative capacity of neural tissues.[1] In addition, there are many neurodegenerative diseases without effective treatment, such as Alzheimer's, Parkinsons, and Huntington's disease. Neural stem and progenitor cells (NSPCs) develop the central nervous system (CNS) during development, and some portion of NSPCs remain in the CNS throughout adulthood. Despite the seemingly minimal regenerative capacity of neurological tissues, adult NSPCs have been shown to respond and integrate into damaged tissues, indicating the significant regenerative potential of these cells.[2] Strategies for utilizing these cells for regenerative medicine involve recruiting endogenous NSPCs and homing of those cells to a damaged tissue site[3], or to isolate, expand, and deliver them to aid in the tissue regeneration[4,5]. Cell delivery is a promising approach[6], but clinical translation for applications in regenerative

medicine is challenged by limited cell survival and retention at the site of damage, and by lack of therapeutic efficacy of delivered cells. The utilization of injectable hydrogels as a depot for delivered cells is promising due to the distinct advantages over implantable systems, namely the circumvention of invasive surgical procedures, and conformation of the hydrogel to the defect site.[7] NSPC differentiation has been shown to be influenced by various environmental factors, such as substrate stiffness, topography, and ability to remodel the surrounding matrix.[8] Neuronal differentiation of NSPC is known to be facilitated by physical cell-cell connections.[9–11] Additionally, the development of mature synapses requires cell-cell communication[12], and as a result injectable hydrogels should be optimized to provide such environmental factors to the delivered cells.

The ability of hydrogels to improve encapsulated cell retention on injection is well documented, however traditional injectable hydrogels have design limitations due to the requirement of injectability.[13] Essentially, there is a tradeoff between hydrogel mechanical stiffness and strength, which govern stability after injection, and the ability of encapsulated cells to spread, migrate, proliferate, and make cell-cell connections, which are desirable for generation of functional neurons from NSPCs.[14] The use of microgel-based microporous injectable hydrogels, (MIHs) to encapsulate cells can be utilized to overcome this design consideration. Microgels - hydrogels with diameter on the micrometer scale - are injectable as a suspension, and can be annealed together at the site of injection to form a bulk scaffold.[15] Research on MIHs have utilized their unique porous structure to facilitate wound healing[16], for drug delivery[17], and to improve retention of injected cells[18]. However, there is limited research on utilizing the pore

space of MIHs to facilitate desired cellular responses, which holds considerable potential due to the improved capabilities to modulate microgel mechanical and surface chemical properties in comparison to contemporary injectable hydrogels.

In this report, we utilize a gelatin-based MIH for the encapsulation of an established neural progenitor cell line, ReNcell VM (ReNcells),[19] to assess the impact of the interconnected pore structure on NSPC growth and differentiation. To encapsulate cells, we use an enzymatic crosslinker, microbial transglutaminase (mTG), which forms covalent bonds between glutamine and lysine amino acid residues. This crosslinking also enabled the incorporation of laminin, an important adhesive protein for neural tissues, during the crosslinking process, which promoted cell attachment on the gelatin surface, and led to differences in cell organization in the 3D environment. In addition to cell growth and differentiation, mitochondrial activity, which is known to be regulated by cell differentiation, was observed by fluorescent imaging. **Fig. 4.1** is a visual description of our experimental approach to encapsulating ReNcells in this MIH.

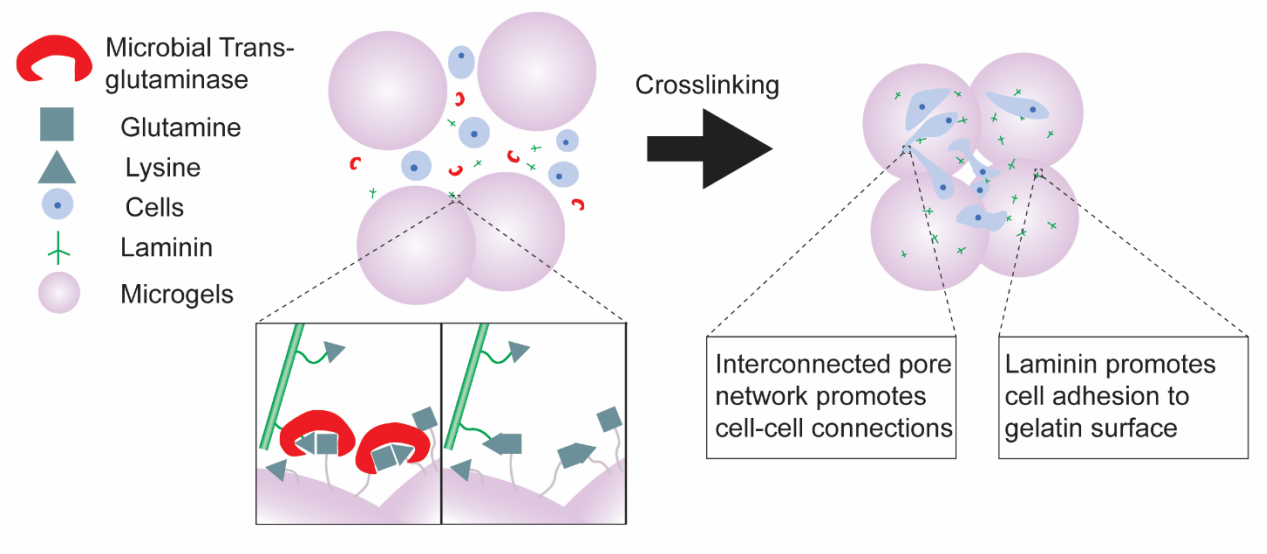

Figure 4.1. Schematic overview of encapsulation of ReNcells in gelatin MIH, and conjugation of the microgel surfaces with laminin through the enzymatic action of mTG.

4.2 Materials and Methods

4.2.1 Materials

Human neural progenitor cell line, ReNcell VM, and associated basal medium, growth factors EGF and bFGF, laminin, and 300 bloom gelatin type A were purchased from Sigma Aldrich. Penicillin/streptomycin (pen/strep, AlamarBlue assay, actin red 555, 4',6-Diamidino-2-Phenylindole Dihydrochloride (DAPI), Live/Dead assay, JC-1 assay, TRIzol, and all antibodies were purchased from Thermo Fisher Scientific. Reverse transcription kit, SYBR green master mix, and MAP2/GAPDH gene primer assays were obtained from Qiagen. Fluo-8 calcium flux assay was obtained from Abcam.

4.2.2 Microgel production

Gelatin microgel production was performed as previously described. A 20 mL 10% w/v solution of gelatin in DI H_2O was added to 200 mL olive oil at 55 °C and stirred for 1 hour. The emulsion was cooled by adding to an ice bath with continued stirring for 30 minutes, to physically crosslink gelatin microgels, followed by addition of 100 mL precooled acetone for 30 minutes. After separating microgels by vacuum filtration, they were sterilized in 70% ethanol, and freeze dried, before being used in cell experiments. As described previously, gelatin microgels have an average diameter of 253 µm in diameter after swelling.

4.2.3 Protein conjugation to gelatin microgel

Protein conjugation to microgel surface was investigated using fluorescein isothiocyanate labeled bovine serum albumin (FITC-BSA). 8% w/v gelatin MIH were either crosslinked in the presence of 200 µg/ml FITC-BSA, or crosslinked first, before submerging in a bath containing 200 µg/ml FITC-BSA for 24 hours. Both samples were washed 5x in PBS for 1 hour before imaging with confocal microscopy, to remove any unbound FITC-BSA. 3D sections containing both hydrogels were imaged to directly compare the fluorescence between hydrogels.

4.2.4 Cell encapsulation

ReNcells were cultured following manufacturer protocol on laminin coated flasks prior to cell encapsulation, in growth medium (GM), composed of ReNcell basal medium, 20 ng/ml EGF, and 20 ng/ml bFGF. To encapsulate cells, 20 mg of microgel was mixed with 150 µl GM in a 48 well plate well, followed by addition of 50 µl of cell suspension and 50 µl filter-sterilized mTG solution (**MP- gels**). The cell-encapsulated

scaffold contained 8% gelatin, $6x10^6$ cells/ml, and 4% mTG. The hydrogels were incubated at 37 °C for 1 hour for crosslinking. For nonporous hydrogels (**NP- gels**), 150 µl of 13.3% gelatin solution in GM was mixed with 50 µl of cell suspension and 50 µl mTG solution, before incubation at 37 °C for 1 hour. To generate laminin-conjugated hydrogels, laminin was added during rehydration of MP gels (**MP+ gels**), and to the NP gel solution (**NP+ gels**) to a final concentration of 20 µg/ml final concentration before crosslinking. After crosslinking, hydrogels were supplemented with 0.75 ml GM daily for 48 hours before being moved to 24 well plates. At this point, hydrogels were either supplemented with 2 ml GM for examining cell growth, or with 2 ml differentiation medium (DM), composed of ReNcell basal medium to induce differentiation.

4.2.5 Live/dead assay

Cell-encapsulated hydrogels 48 hours after encapsulation, and again on day 5 and 16 when cultured in GM or DM, were incubated with HBSS containing calcein-AM and ethidium homodimer to visualize living cell and dead cells respectively, for 1 hour before imaging (Nikon A1R HD). 3D confocal images of cell encapsulated hydrogels were taken and converted to Z projections using ImageJ.

4.2.6 Proliferation experiments

Cell proliferation of cell-encapsulated constructs was measured using alamarBlue assay at 24 hours and 7 days after encapsulation, where cells seeded on TCPS were used as a positive control. AlamarBlue reagent was added for 2 hours in GM to hydrogels, then removed and fluorescence was quantified at 560/590 excitation/emission.

4.2.7 Immunofluorescence staining

Cell-encapsulated hydrogels were fixed after 5 and 16 days of culture in both GM and DM with 4% paraformaldehyde in PBS for 1 hour. Cells were permeabilized with 0.1% Triton-X 100 for 1 hour, then washed 3x in PBS. Samples were blocked in blocking buffer, composed of 5% goat serum, 1% BSA, 0.1% Tween-20 in PBS overnight at 4 °C. Primary antibodies raised in rabbit against microtubule-associated protein 2 (MAP2), glial fibril acidic protein (GFAP), and Nestin were added to samples in blocking buffer following manufacture-specified dilutions, for 24 hours at 4 °C. Samples were washed 4x in PBS for 1 hour before addition of goat-anti-rabbit secondary antibody, at 1:500 dilution, along with DAPI and actin-red 555 dye, in PBS for 24 hours at 4 °C. Samples were washed 3x in PBS before fluorescence imaging.

4.2.8 Reverse transcription quantitative PCR (qPCR)

After 3 and 14 days of incubation in differentiation medium, RNA was extracted from encapsulated cells using TRIzol. RNA for cells cultured in GM or DM on 2D substrates was extracted as controls. RNA was converted to cDNA using Quantitect Reverse Transcription kit, and PCR was performed on Applied Biosystems Quantstudio3 system, for 45 cycles and cycle parameters according to manufacturer specifications. All samples were run in duplicate and values were averaged before analysis. Relative gene expression was obtained by comparing MAP2 expression with GAPDH, a housekeeping gene for each sample.

4.2.9 Calcium Flux Imaging

Cells encapsulated in MP+ and NP+ gels were incubated in differentiation medium for 26 days before calcium flux assay. Fluo-8 was supplied to samples in the provided assay buffer following the manufacturer protocol. After incubation at 37 °C for 1 hour, samples were washed with HBSS buffer before imaging. During imaging, samples were supplemented with 50 µM glutamate. Images were captured at 1 frame/second on a single Z axis via confocal microscopy. Fluorescence of isolated cells was graphed using ImageJ.

4.2.10 JC-1 Assay

Hydrogels containing proliferating and differentiating cells 5 and 16 days after initiation of culture were stained with JC-1 (2 µg/ml) in HBSS for 1 hour before imaging. Confocal microscope images were obtained by excitation wavelength at 488 nm for both forms, and emission wavelengths at 590 and 525 for aggregate and monomer form, respectively. 3D slices of mitochondrial activity were converted to Z-projection images using ImageJ.

4.3 Results and Discussion

4.3.1 Laminin Conjugation

Laminin is a major extracellular matrix (ECM) component of neuronal tissues, and has been utilized to promote NSPC attachment and differentiation in vitro[20]. As a result, there is considerable interest in conjugating laminin or laminin-derived short peptides to biomaterials for the culture of NSPCs[21]. Because mTG crosslinks glutamine and lysine amino acid residues, which both laminin and gelatin contain, we

hypothesized that laminin could be chemically coupled to gelatin microgel surfaces by simply mixing laminin with microgels during the mTG-crosslinking process. The feasibility of laminin protein conjugation to gelatin microgel surfaces during mTG-crosslinking was tested using a model protein, FITC-BSA (**Fig. 4.2)**. Gelatin MIH was crosslinked in the presence of FITC-BSA (Fig. 4.2a) before imaging. For comparison, gelatin MIH was first crosslinked by mTG, then incubated with FITC-BSA, in which case FITC-BSA has no mechanism to adhere to the microgels by covalent bonds (Fig. 4.2b). Both samples were washed thoroughly with PBS, then the fluorescence intensity from FITC-BSA was compared directly against each other by confocal imaging. Incorporation of FITC-BSA during mTG-crosslinking showed much stronger fluorescence than when physically adsorbed, indicating efficient chemical attachment of FITC-BSA to the surface of microgels. Because the samples are imaged at the same time, relative fluorescence intensity can be compared directly (Fig 4.2c), where average pixel intensity and standard deviation are shown. During Crosslinking refers to the condition shown by Fig. 4.2a, and After Crosslinking refers to the condition shown in Fig. 4.2b. Utilization of mTG demonstrates a simple method of incorporating functional ECM proteins (e.g. laminin) into the surface of gelatin-based biomaterials.

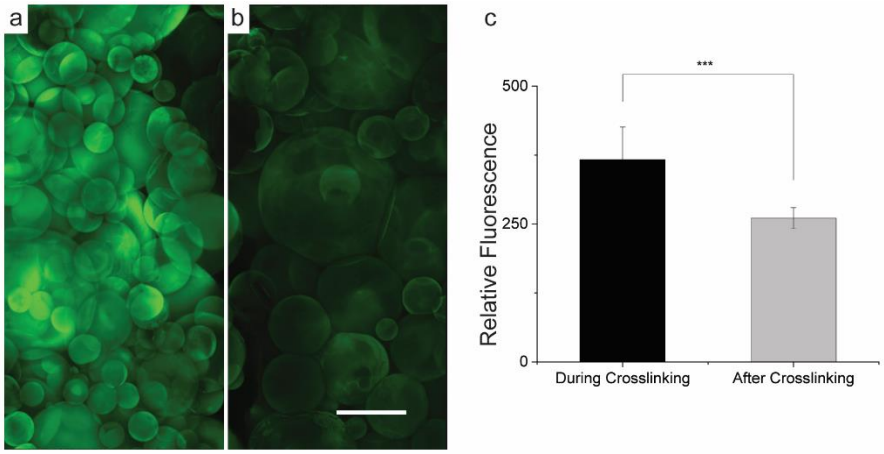

Figure 4.2. Conjugation of FITC-BSA to gelatin microporous hydrogel surface. FITC-BSA was added to gelatin microporous hydrogel either (a) during the crosslinking, or (b) after crosslinking. (c) Relative fluorescence intensity of the hydrogel.Scale = 200 µm. (***) $p < .001$

4.3.2 Cell Growth and Morphology

Cell attachment, morphology, and growth were examined using live/dead assay (**Fig. 4.3**), and alamarBlue assay (**Fig. 4.4**). After 48 hours of culture (Fig. 4.3a-d), cells of high viability were seen in all conditions. When encapsulated in the MIH without the presence of laminin (**MP-**) (Fig. 4.3a), cells were seen to aggregate into clusters, which continued after 5 days of culture (Fig. 4.3e). For cells encapsulated in the MIH with the addition of laminin (**MP+**), cells spread on the surface of microgels, and were able to make direct cell-cell connections, but did not form cell aggregates (Fig. 4.3b). In this condition, cells were observed to spread as early as 48 hours after encapsulation, and continued to grow on the surface of microgels throughout the culture period (Fig. 4.3f). Minimal cell spreading was observed for cells encapsulated in nonporous hydrogels

without or with incorporation of laminin (**NP-** and **NP+**, respectively) (Fig. 4.3c,d). After 5 days of culture (Fig. 4.3g,h), cell spreading continued to be low, likely because cells were entrapped by the polymer chains, and viability of encapsulated cells was greatly diminished, as demonstrated by the increase in red fluorescence. Cell proliferation assay confirmed the observed trend of high cell attachment and growth in the MIH, and low proliferation of cells in the NP condition. Cell proliferation is similar between all conditions on day 1 (Fig. 4.4a), and much lower for cells encapsulated in NP gels by day 7 (Fig 4.4b).

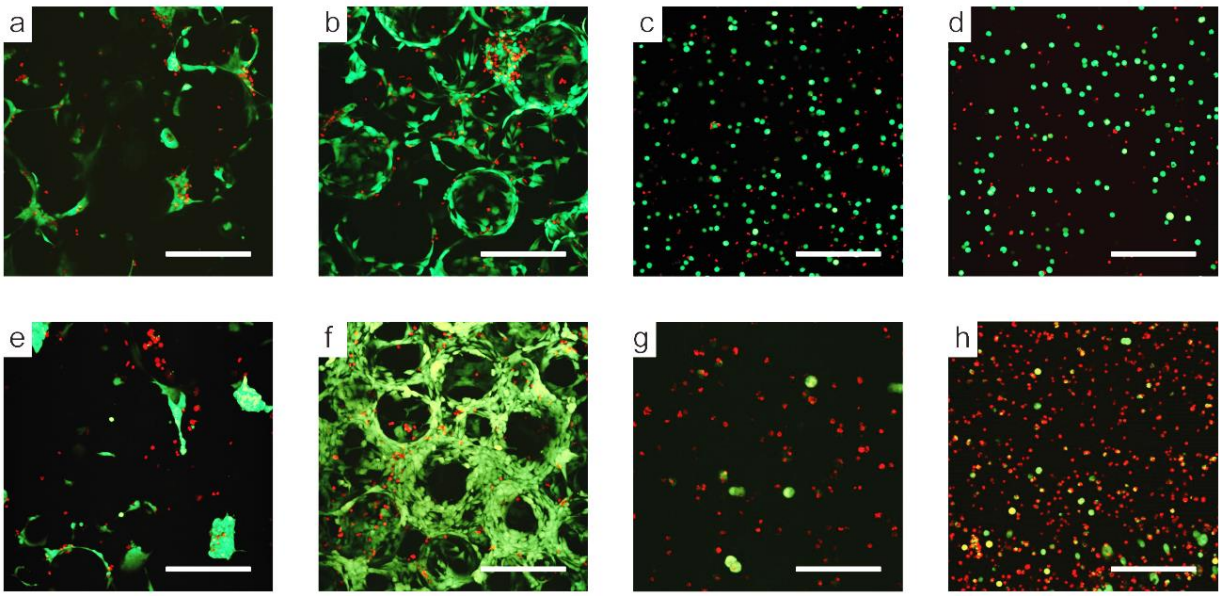

Figure 4.3. Comparison of growth of ReNcells encapsulated in the differing 3D environments. Z-projection images show live (green) and dead (red) ReNcells encapsulated in MP- (a, e), MP+ (b, f), NP- (c, g) and NP+ (d, h), on day 2 (a-d) and day 5 (e-h) in growth medium. Scale bar = 200 µm.

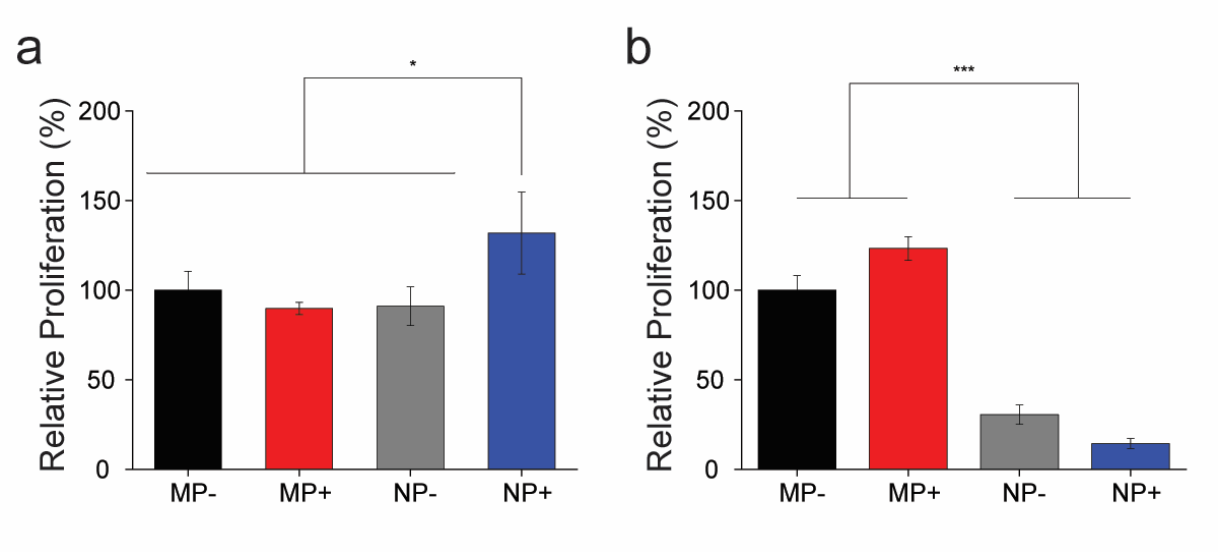

Figure 4.4. Proliferation of encapsulated ReNcells on day 1 (a) and day 7 (b) after encapsulation. Data shown are average and standard deviation. (*) $p < 0.05$, (***) $p < .001$.

4.3.3 Observations of Cell Morphology during ReNcell Differentiation

For differentiation studies, after 48 hours of incubation in GM, cell-encapsulated constructs were moved to the differentiation medium (DM). Cell morphological changes during differentiation were observed at 3 (Fig. 4.5 a-d) and 14 (Fig. 4.5 e-j) days after induction of differentiation using live/dead assay and confocal microscopy. Similar to culture in GM, cell organization in the porous condition was dependent on the presence of laminin (Fig. 4.5 a,b). Significant elongation of cells was observed in the MP conditions between 3 (Fig. 4.5 a,b) and 14 (Fig. 4.5 e,f) days of differentiation, with the appearance of cell connections forming with (**MP+**) or without (**MP-**) the presence of

laminin. Minimal changes in morphology were observed for cells encapsulated in the NP gels, and cell viability was observed to decrease between day 5 (Fig 4.5 c,d) and 16 (Fig 4.5g,h), in line with cell proliferation results. Autofluorescence of the microporous hydrogel in the blue channel further demonstrates the differences in organization of encapsulated cells in the microporous environment without (**MP-**, Fig. 4.5 i), or with laminin (**MP+**, Fig. 4.5 j).

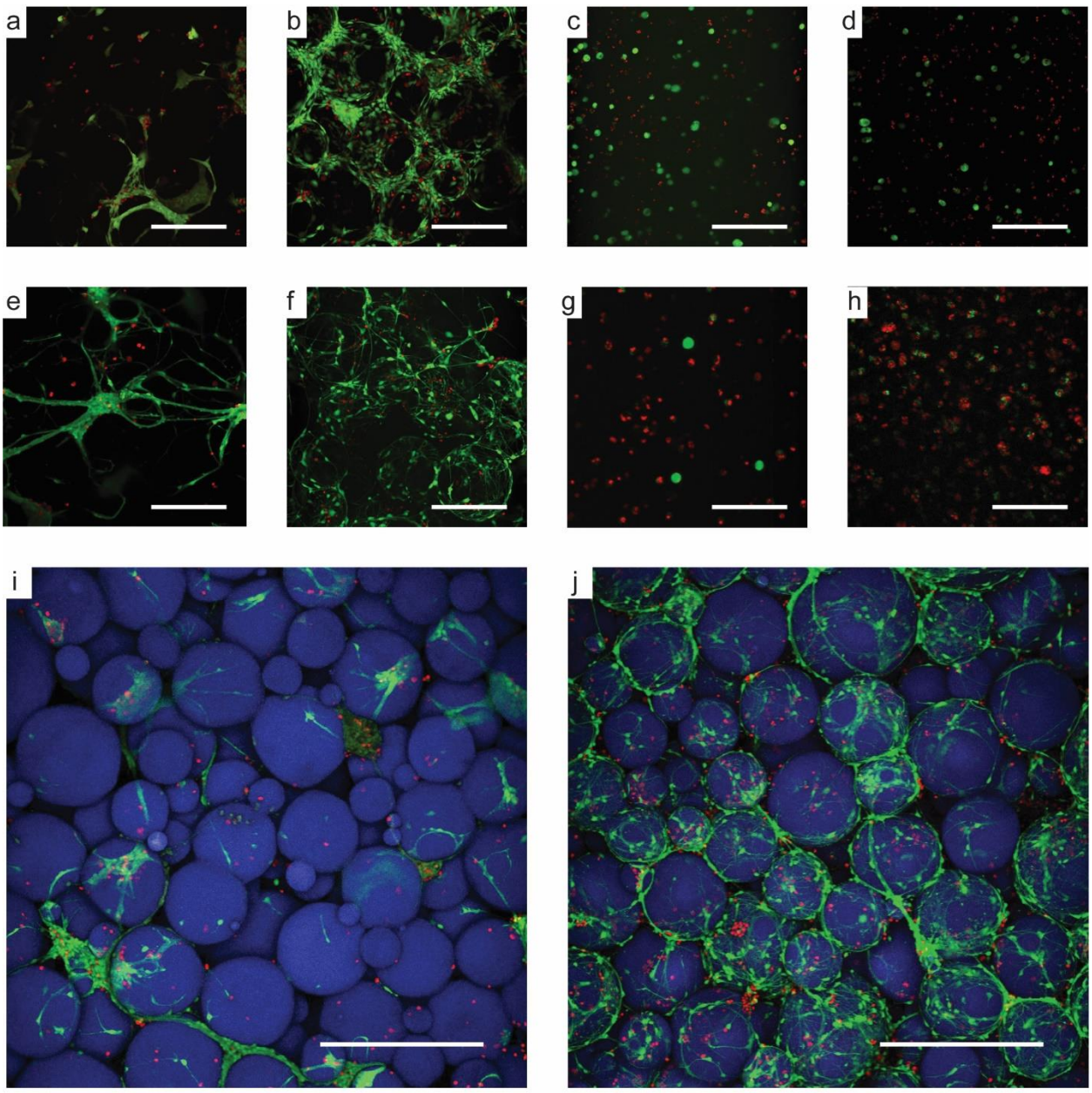

Figure 4.5. Cell morphology of differentiating ReNcells. Z-projections of living (green) and dead (red) cells on day 5 (a-d) or day 16 (e-j) after induction of differentiation on day 2. Cells are encapsulated either in microporous hydrogel without laminin (a, e, i), microporous hydrogel with laminin (b, f, j), nonporous hydrogel without laminin (c, g) or nonporous hydrogel with laminin (d, h). Autofluorescence of the microgels (blue) were included to show the 3D microenvironment provided to encapsulated cells in the microporous condition: MP- (i), MP+ (j). Scale = 200 µm.

4.3.4 Immunofluorescence imaging of differentiating ReNcells

Differentiation of encapsulated cells was further explored through immunofluorescence staining for MAP2 (**Fig. 4.6**, **Fig. 4.7**) and GFAP (**Fig. 4.8**, **Fig. 4.9**.), markers for mature neurons[22], and astrocytes[23], respectively. To generate functional neural tissues, NSPCs differentiation into both lineages is essential. In addition to differentiation markers (green) (Fig. 4.6 – Fig. 4.9 i-l), cell nuclei (blue) (Fig. 4.6 – 4.9 e-h) and actin cytoskeleton (red) (Fig. 4.6 – Fig. 4.9 a-d) were also imaged. After 3 days of induction of differentiation, MAP2 was sporadically stained in MP conditions (Fig. 4.6 i, j), but cells encapsulated in NP gel showed minimal expression (Fig. 4.6 k, l). After 14 days of differentiation, cells encapsulated in the MP gel had increased expression of MAP2 (Fig. 4.7 i, j), but low expression in NP gels was observed, potentially due to diminished cell viability and growth in comparison to cells in the MP gel. A similar trend is seen for astrocyte differentiation. In MP gels, GFAP was highly expressed at both 3 days (Fig. 4.8 i, j), and 14 days (Fig. 4.9 i, j), and though a higher percentage of cells encapsulated in NP gel are stained positively for GFAP at the later timepoint (Fig. 4.8k, l), it remained a small population. We observed that cell elongations are highly stained for MAP2 and GFAP, which coincides with the in vivo phenotype of these cells, which are characterized by microtubule protrusions[24,25]. The formation of microtubule structures was markedly increased between time points for cells encapsulated in MP gels, but absent from NP gels.

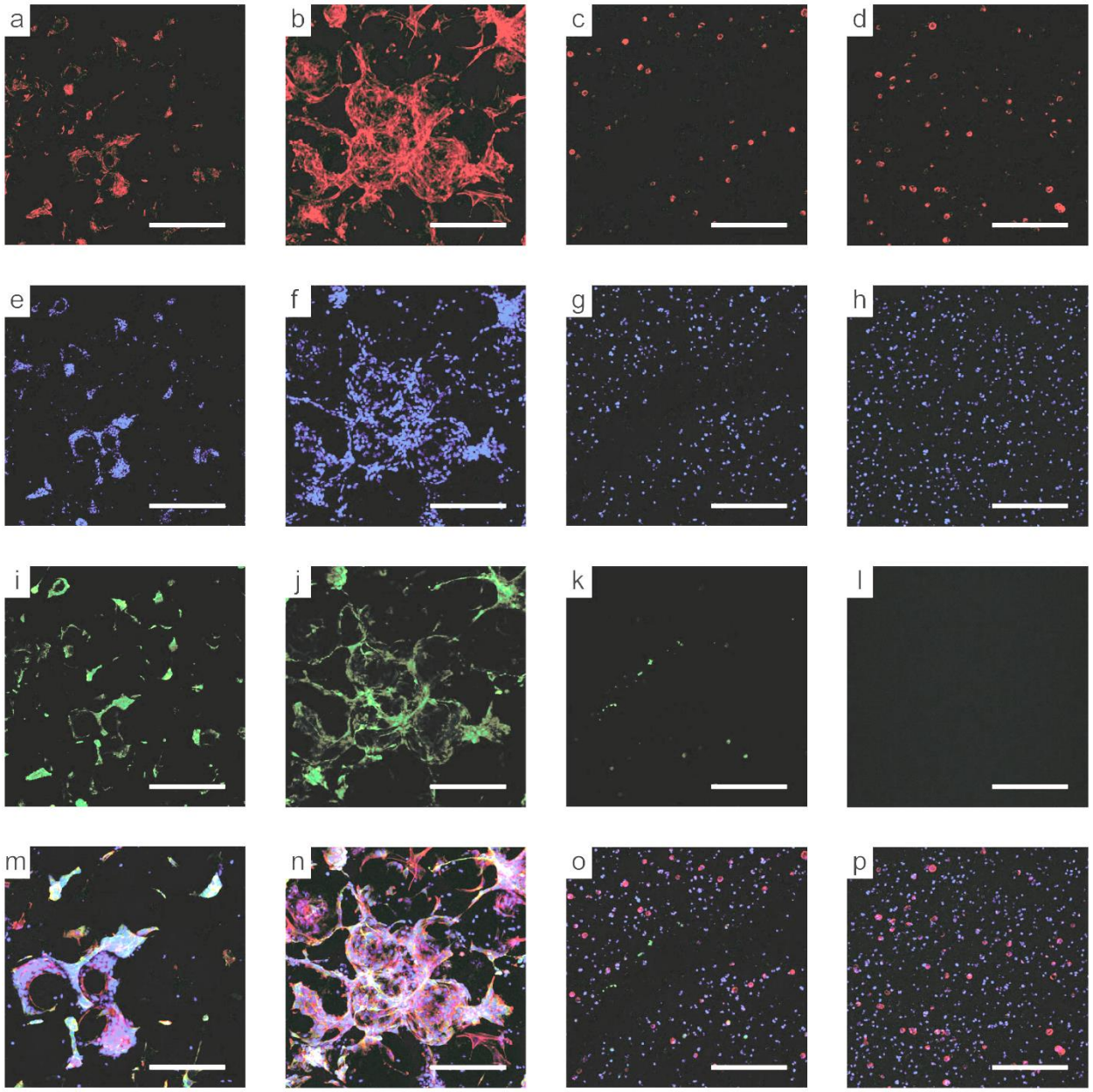

Figure 4.6. MAP2 immunofluorescence of encapsulated cells 3 days after induction of differentiation. Z-projection images of cell-encapsulated hydrogels labeled with phalloidin for actin cytoskeleton (red) (a-d), DAPI for cell nuclei (blue) (e-h), fluorescent antibody against MAP2 (a-h) (green), and composite images, for cells encapsulated in MP- (a, e, i, m), MP+ (b, f, j, n), NP- (c, g, k, o), and NP+ (d, h, l, p) conditions. Scale = 200 µm.

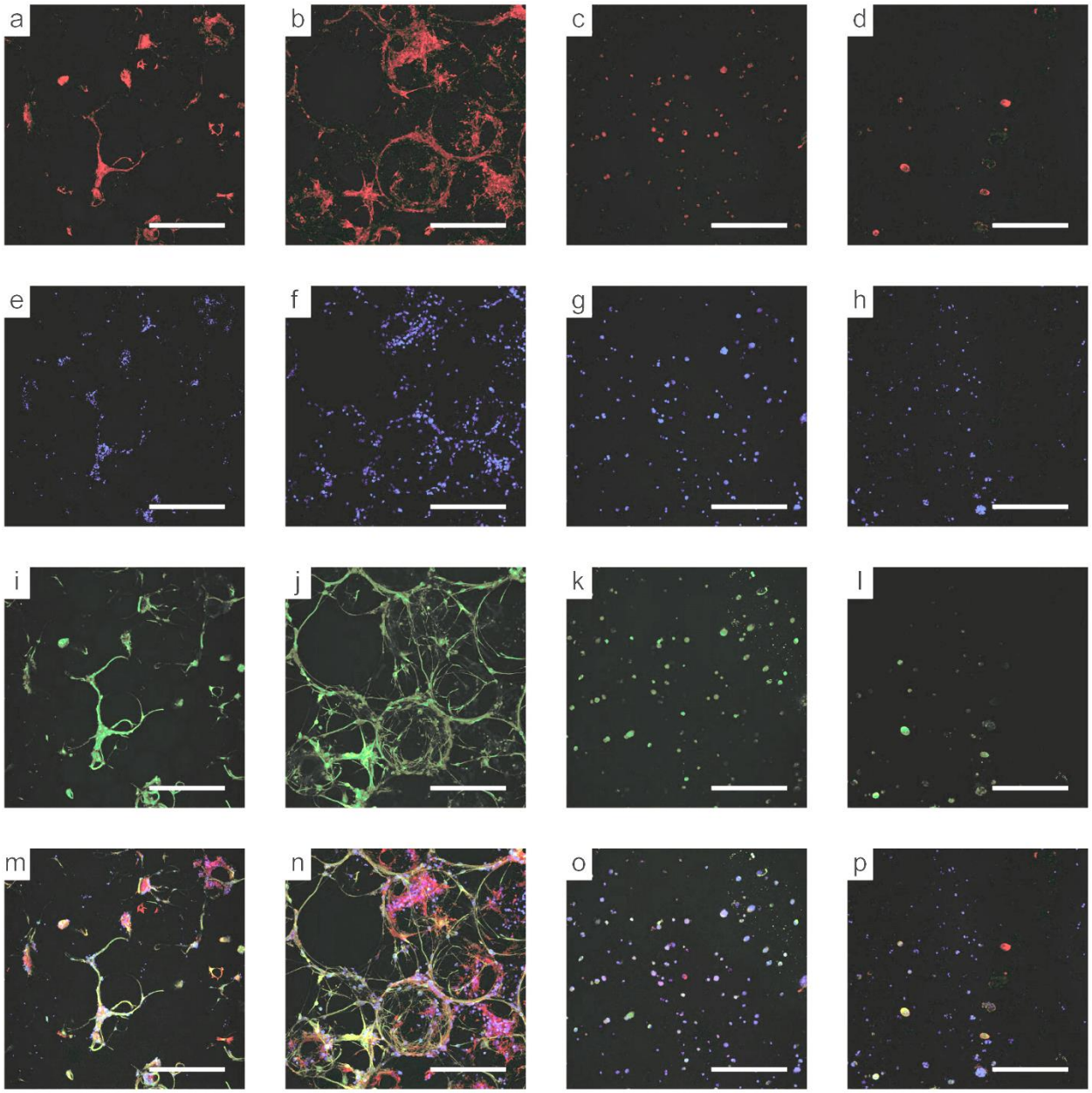

Figure 4.7. MAP2 immunofluorescence of encapsulated cells 14 days after induction of differentiation. Z-projection images of cell-encapsulated hydrogels labeled with phalloidin for actin cytoskeleton (red) (a-d), DAPI for cell nuclei (blue) (e-h), fluorescent antibody against MAP2 (a-h) (green), and composite images, for cells encapsulated in MP- (a, e, i, m), MP+ (b, f, j, n), NP- (c, g, k, o), and NP+ (d, h, l, p) conditions. Scale = 200 µm.

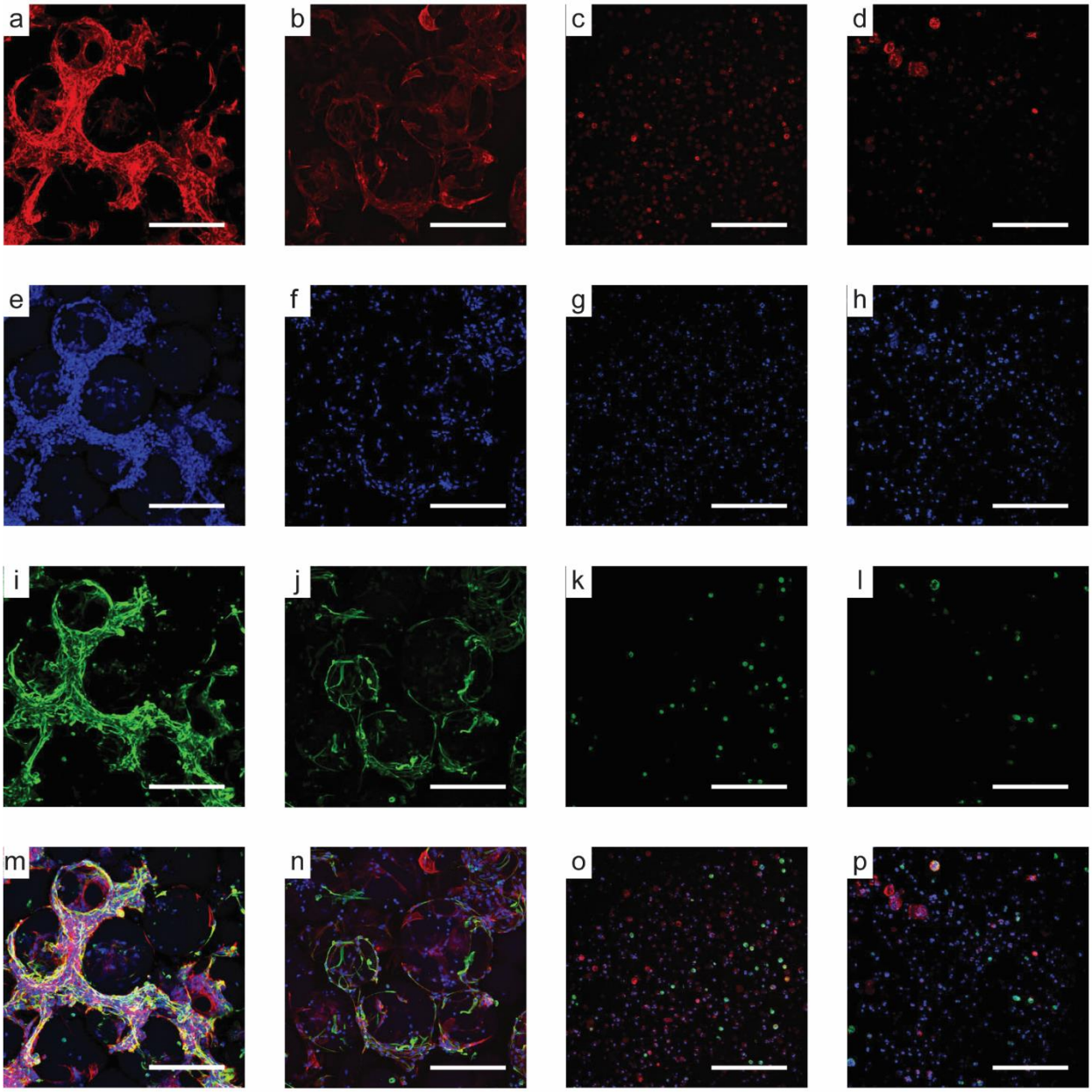

Figure 4.8. GFAP immunofluorescence of encapsulated cells 3 days after induction of differentiation. Z-projection images of cell-encapsulated hydrogels labeled with phalloidin for actin cytoskeleton (red) (a-d), DAPI for cell nuclei (blue) (e-h), fluorescent antibody against MAP2 (a-h) (green), and composite images, for cells encapsulated in MP- (a, e, i, m), MP+ (b, f, j, n), NP- (c, g, k, o), and NP+ (d, h, l, p) conditions. Scale = 200 µm.

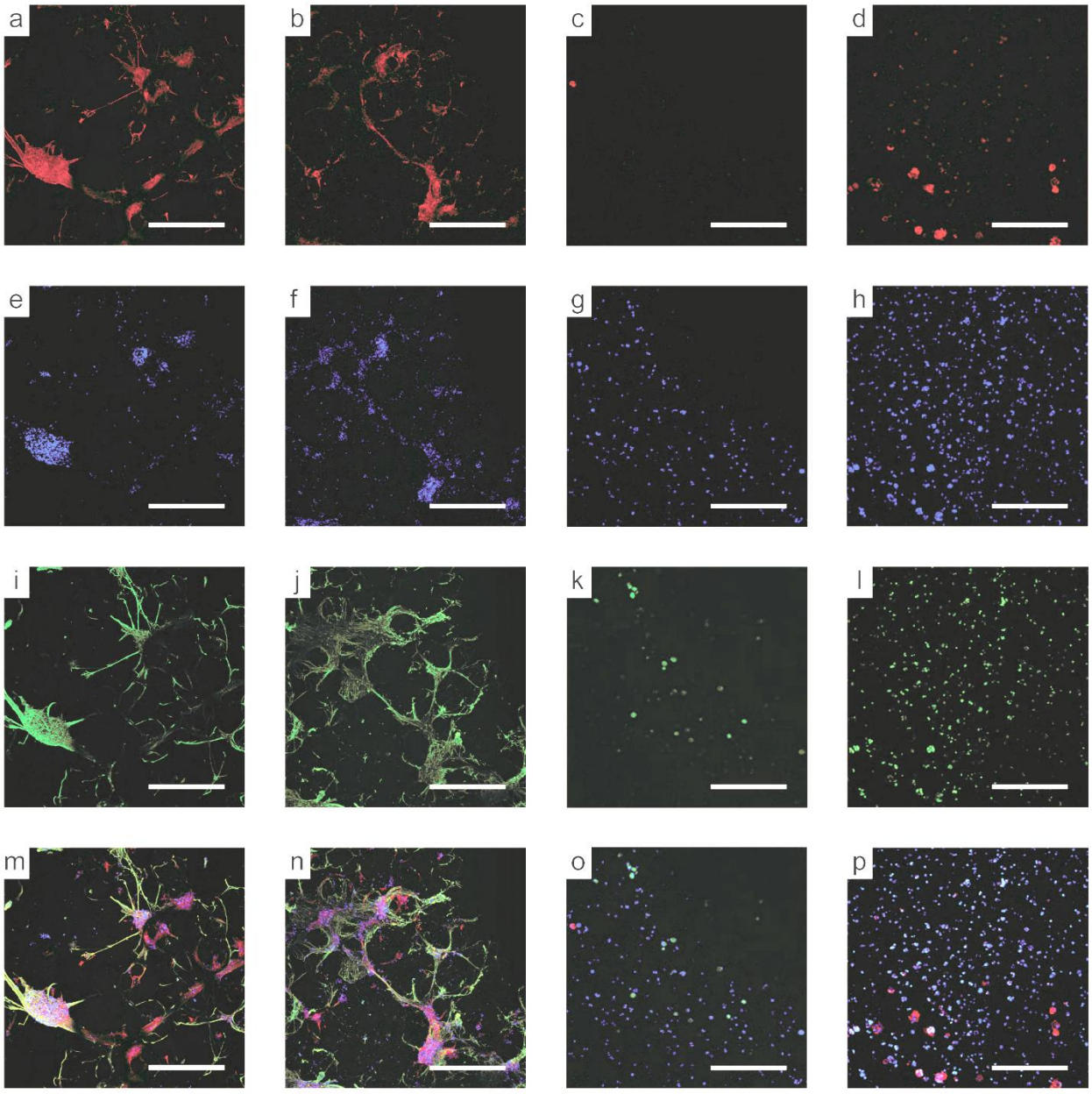

Figure 4.9. GFAP immunofluorescence of encapsulated cells 14 days after induction of differentiation. Z-projection images of cell-encapsulated hydrogels labeled with phalloidin for actin cytoskeleton (red) (a-d), DAPI for cell nuclei (blue) (e-h), fluorescent antibody against MAP2 (a-h) (green), and composite images, for cells encapsulated in MP- (a, e, i, m), MP+ (b, f, j, n), NP- (c, g, k, o), and NP+ (d, h, l, p) conditions. Scale = 200 µm.

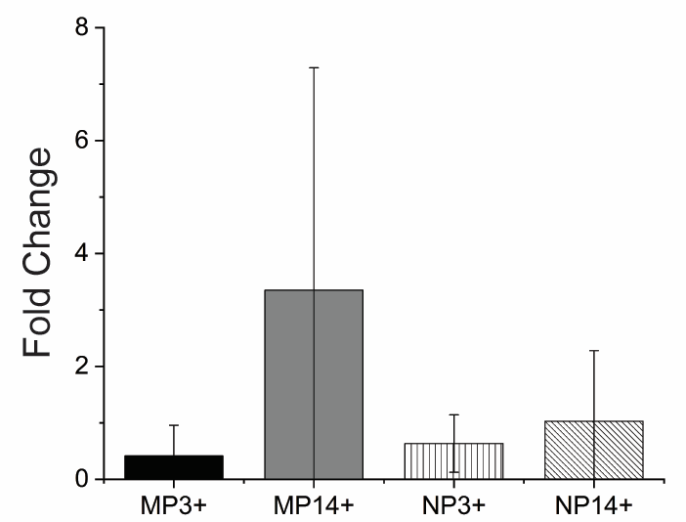

Figure 4.10. MAP2 gene expression. Fold change refers to normalized MAP2 gene expression in comparison to cells seeded on 2D plates incubated in growth medium. Abbreviations: microporous day 3 including laminin (MP3+), microporous day 14 including laminin (MP14+), nonporous day 3 including laminin (NP3+), and nonporous day 14 including laminin (NP14+). Data is presented as average and standard deviation.

4.3.5 Results of qPCR

qPCR of MAP2 gene expression was performed to assess the differentiation of encapsulated ReNcells (**Fig. 4.10**). It appears that by day 14, a much higher percent of ReNcells differentiated into neurons when cultured in the MP+ condition, in comparison to the NP+ condition. Despite large variences in the obtained data (due to the low amounts of extracted mRNA), these results are encouraging for future studies.

4.3.6 Calcium Flux Imaging

The overall goal of this project is to generate functional neuronal tissue, which includes differentiation into electrically active neurons. The function of differentiated NPCs was assessed by examining calcium flux, where Fluo-8 fluorescence is

proportional to the intracellular calcium concentration. The generation of action potential by neurons induces rapid changes in the intracellular Ca^{+2} concentration, and these firing events were examined over time after stimulation with glutamate, a neurotransmitter (**Fig. 4.11**). Single cells in the MP+ (Fig 4.11a, b) and NP+ (Fig 4.11c, d) were identifed by a region of interest, and fluorecence in these regions were graphed over the course of the experiment. It can be seen that overall, fluorescence decreases over time due to eventual photobleaching of the sample. However, throughout the imaging period, there are clear fluctuations in the fluorescence for cells in the MP+ condition, indicating the successful differentiation of encapsulated NSPCs into functioning neurons. In comparison, fluctuations in fluorescence due to cell firing was not observed in the NP+ condition, indicating that complete differentiation was inhibited in these samples.

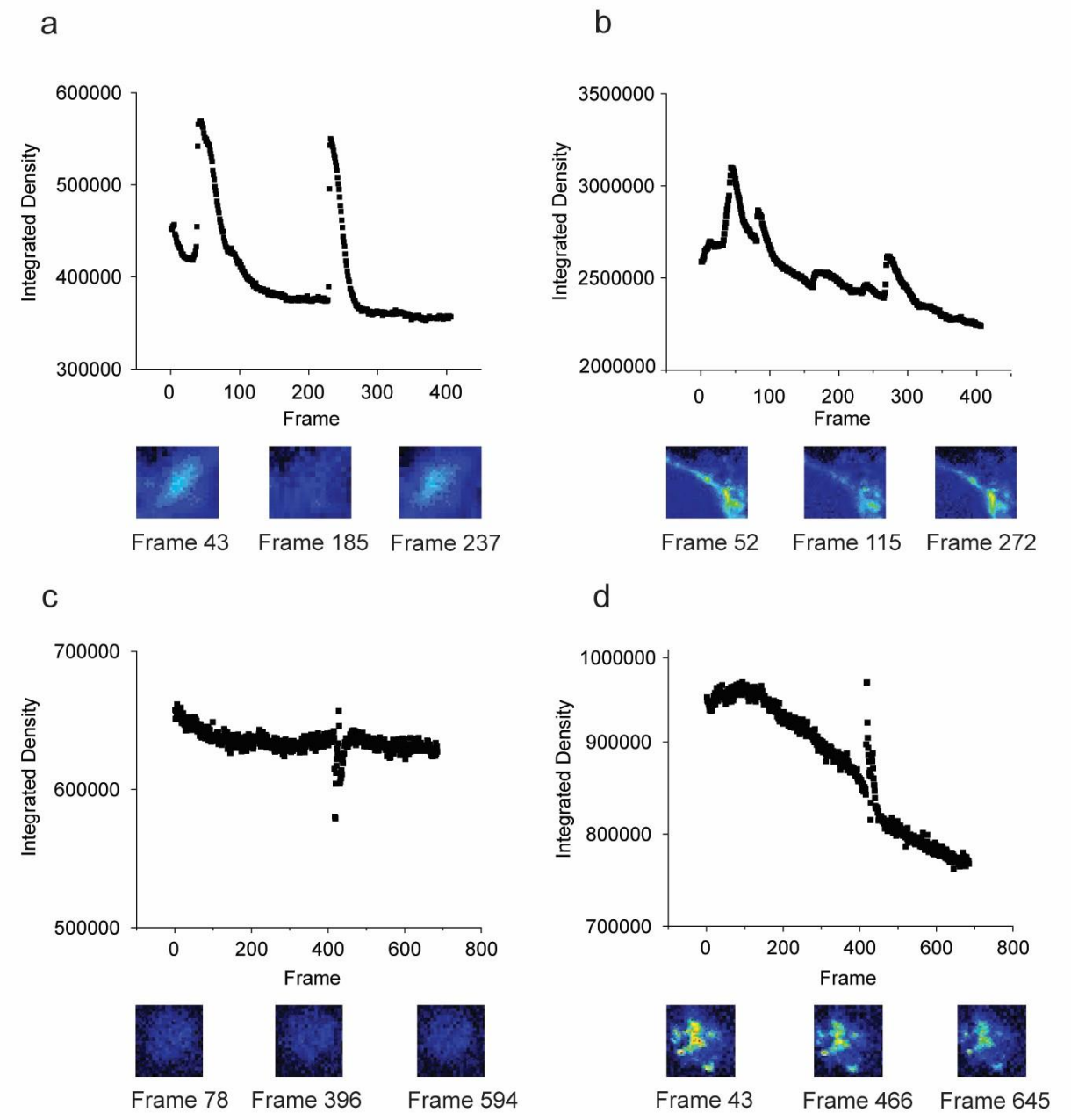

Figure 4.11. Calcium flux of differentiating ReNcells. Integrated fluorescence density for encapsulated cells in the MP+ (a, b) and NP+ (c, d) conditions after 26 days of differentiation. Graphs show the integrated density, which is proportional to the fluorescence intensity in the provided regions of interest, shown by imaged highlights of single cells. Fluorescence was imaged on a color spectrum, where blue = low intensity, and red = high intensity.

4.3.7 Mitochondrial Activity

The role of mitochondria in stem cell differentiation has just begun to be appreciated in the literature. In general, mitochondrial biogenesis (i.e. increase in the number of mitochondria) and increase in mitochondrial metabolic activities are known to accompany the differentiation process of stem cells. [26–28] Therefore, it is expected that the neural differentiation of NPSCs in MIH will be associated with increased mitochondria both in number and activities. Mitochondrial activity can be assessed by mitochondrial membrane potential. Mitochondria utilize proton pumps to generate an electrostatic potential across their inner membrane, which is used for generation of ATP to drive cellular processes.

JC-1 is a cationic dye that aggregates (red) in polarized mitochondria, and dissociates into monomers (green) in depolarized mitochondria. JC-1 assay was used to examine mitochondria polarity of NSPCs encapsulated in contrasting 3D environments (**Fig**. **4.12**, **Fig**. **4.13**, **Fig**. **4.14**, **Fig**. **4.15**, **Fig**. **4.16**). Cells cultured with GM (Fig 4.12, Fig. 4.14) had minimal changes in membrane polarization, likely due to continued proliferation. By comparison, cells undergoing differentiation in all conditions (Fig. 4.13, 4.15) appear to show increased membrane polarization. Furthermore, membrane polarization was observed to increase for differentiating cells between day 5 (Fig. 4.13) and day 16 (Fig. 4.15), indicating a higher percentage of differentiating cells. Larger images of cells encapsulated in the MP+ condition for 16 days are shown for easier direct comparison (Fig. 4.16). To the best of our knowledge, this is the first demonstration that NSPCs increase their mitochondrial density and activities during the differentiation process in 3D hydrogels. Our results are consistent with the current

understanding that increased mitochondrial activities of stem cells are associated with the cellular differentiation.

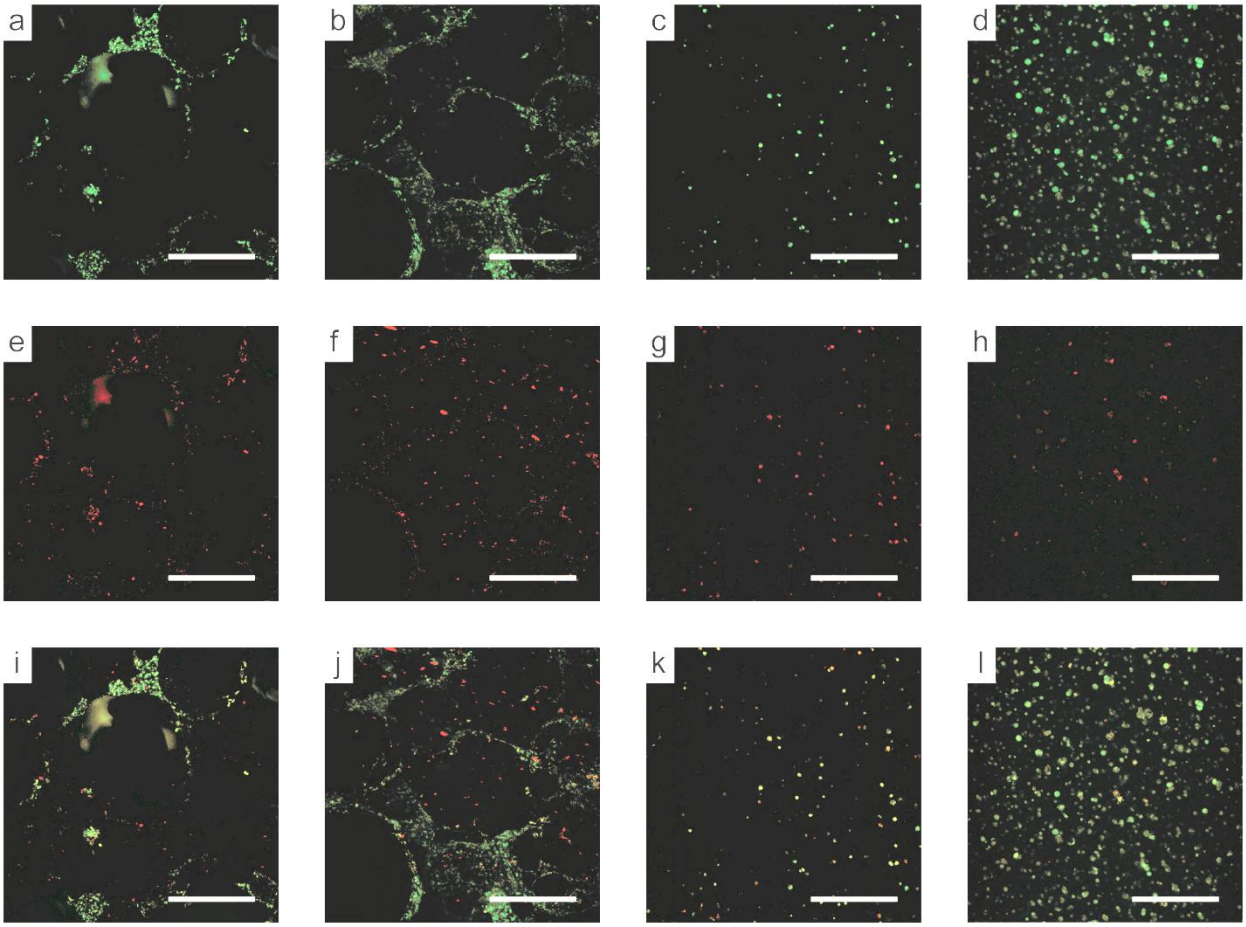

Figure 4.12. Mitochondrial activity of ReNcells in different 3D microenvironments after 5 days of culture in growth medium. Z-projection images of mitochondria with low membrane potential (green) (a-d) or high membrane potential (red) (e-h), along with composite images (i-l). Cells were encapsulated in MP- (a, e, i), MP+ (b, f, j), NP- (c, g, k), and NP+ (d, h, l) hydrogels. Scale = 200 µm.

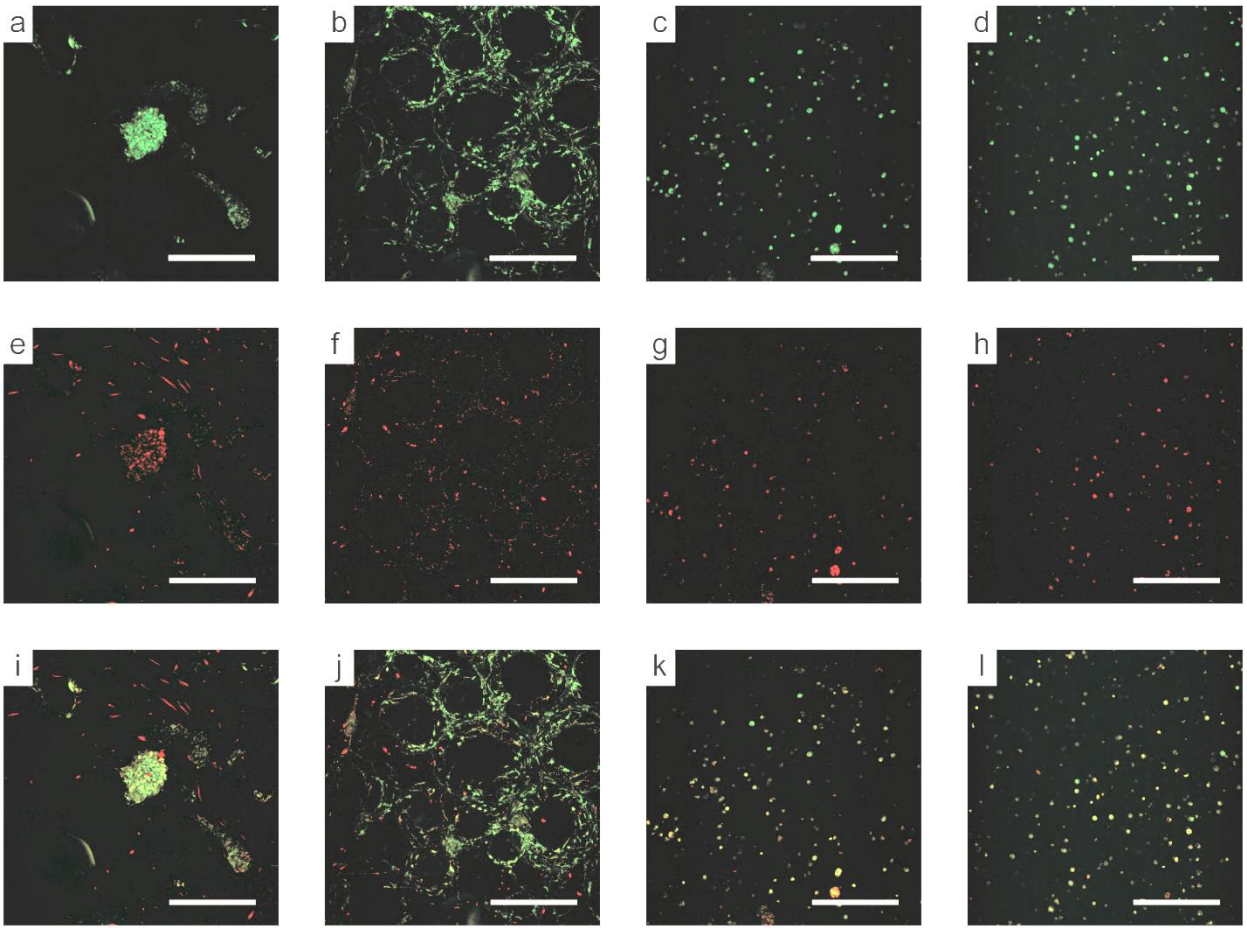

Figure 4.13. Mitochondrial activity of ReNcells in different 3D microenvironments after 5 days of culture in the differentiation condition. Z-projection images of mitochondria with low membrane potential (green) (a-d) or high membrane potential (red) (e-h), along with composite images (i-l). Cells were encapsulated in MP- (a, e, i), MP+ (b, f, j), NP- (c, g, k), and NP+ (d, h, l) hydrogels. Scale = 200 µm.

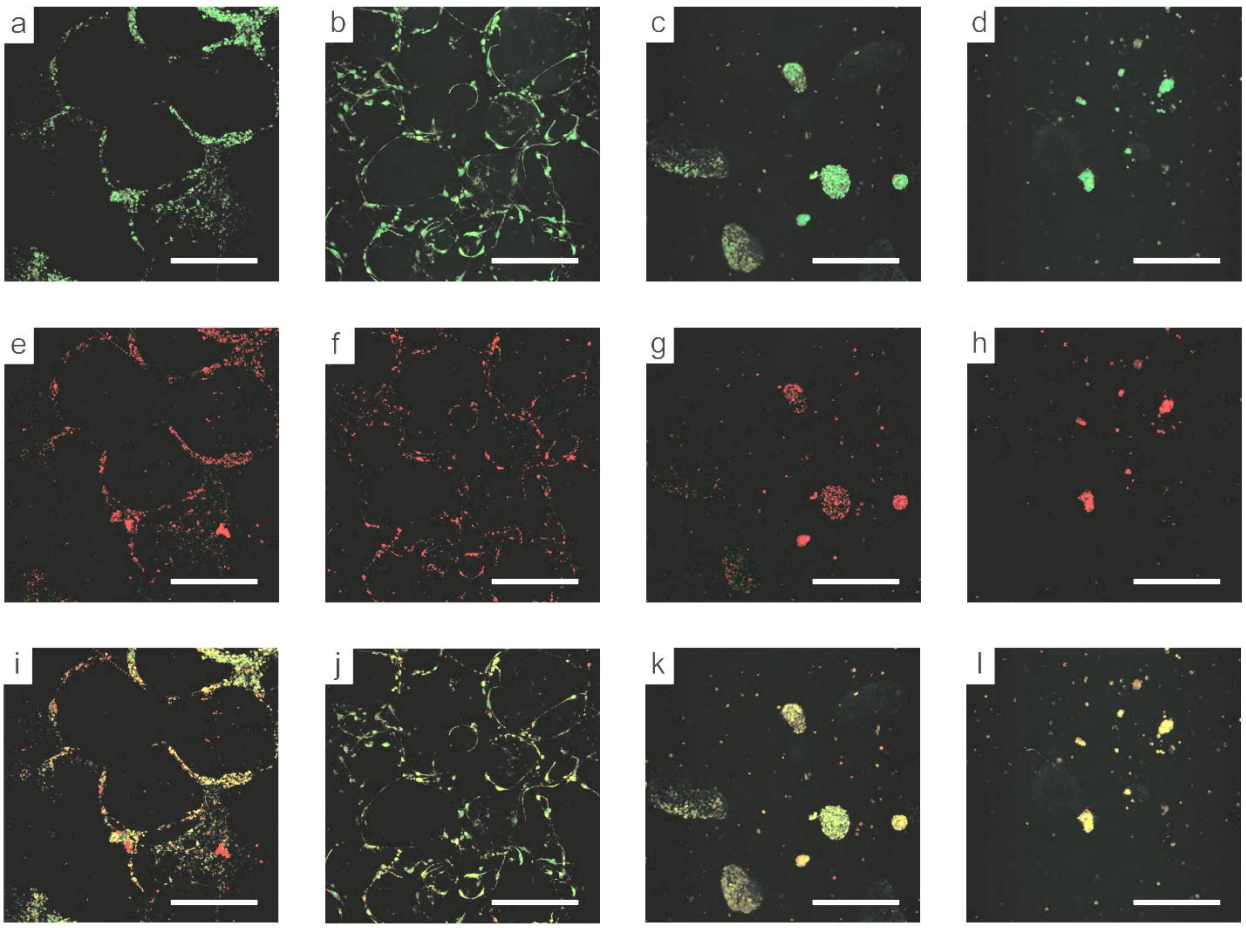

Figure 4.14. Mitochondrial activity of ReNcells in different 3D microenvironments after 16 days of culture in growth medium. Z-projection images of mitochondria with low membrane potential (green) (a-d) or high membrane potential (red) (e-h), along with composite images (i-l). Cells were encapsulated in MP- (a, e, i), MP+ (b, f, j), NP- (c, g, k), and NP+ (d, h, l) hydrogels. Scale = 200 µm.

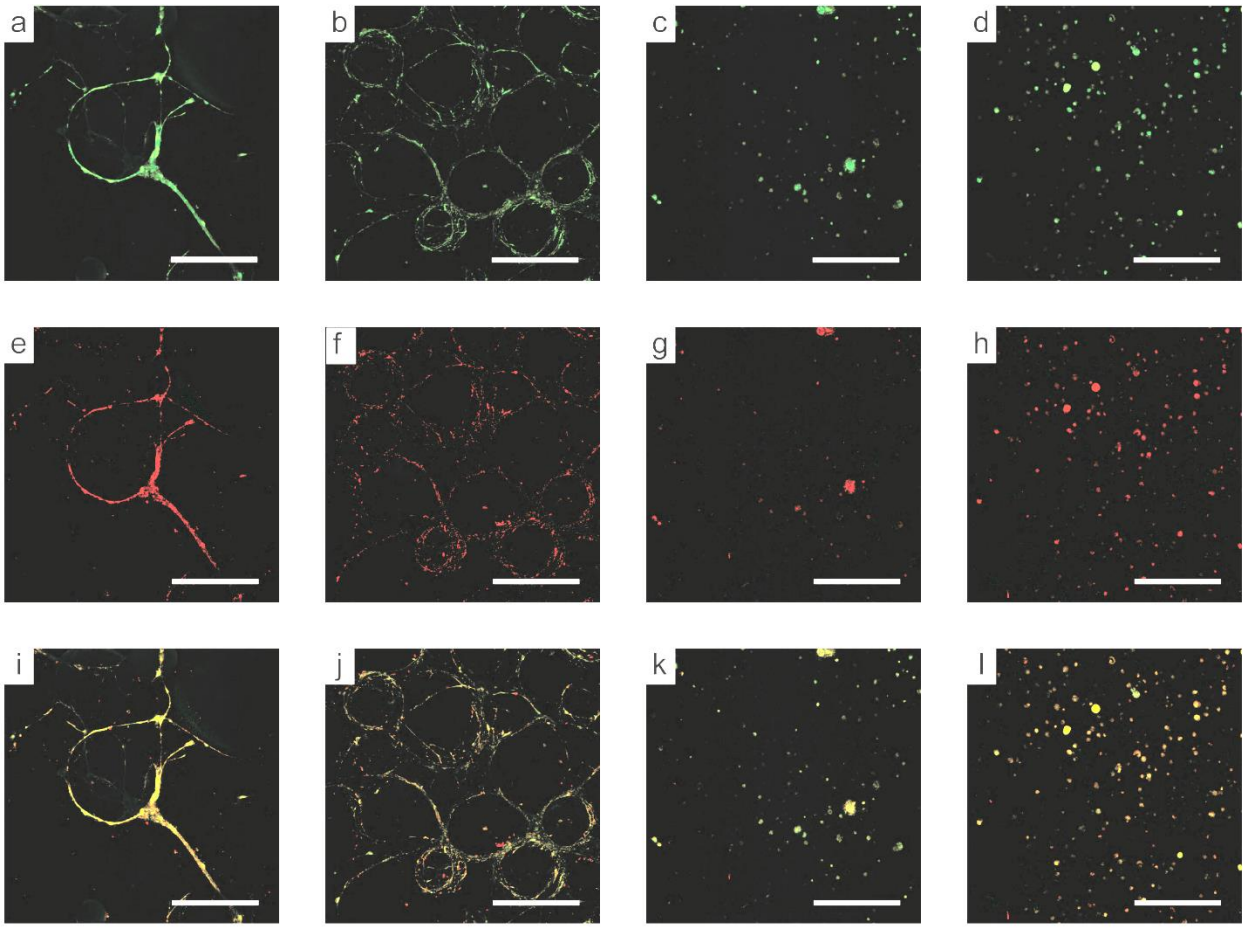

Figure 4.15. Mitochondrial activity of ReNcells in different 3D microenvironments after 16 days of culture in the differentiation condition. Z-projection images of mitochondria with low membrane potential (green) (a-d) or high membrane potential (red) (e-h), along with composite images (i-l). Cells were encapsulated in MP- (a, e, i), MP+ (b, f, j), NP- (c, g, k), and NP+ (d, h, l) hydrogels. Scale = 200 µm.

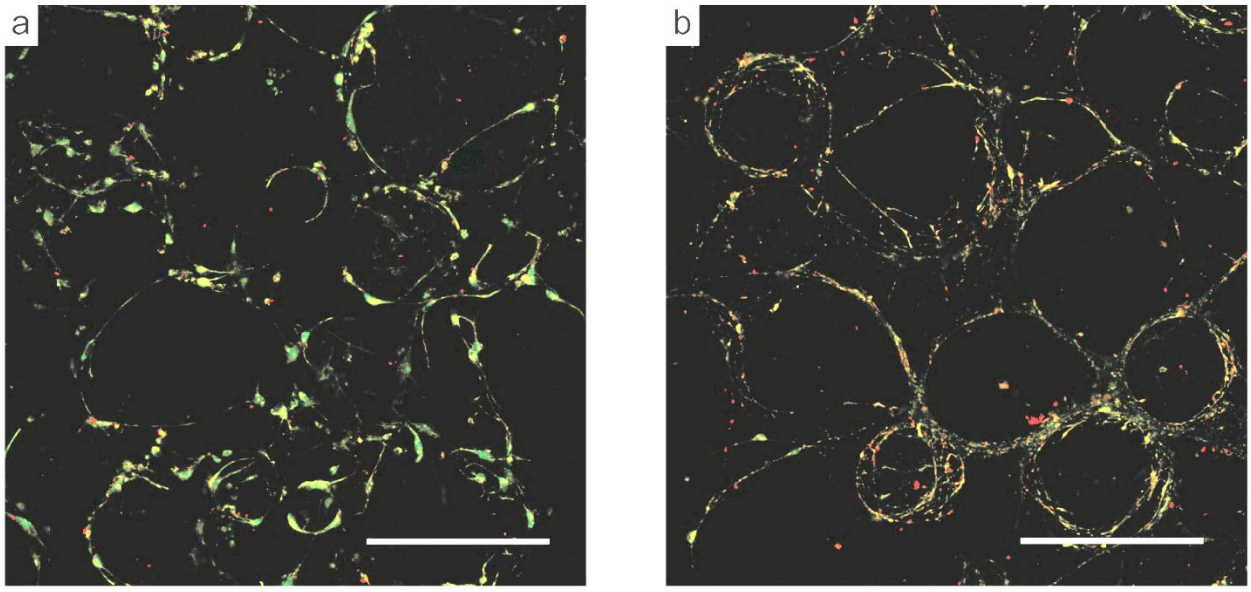

Figure 4.16. Direct comparison of mitochondrial polarization between cells cultured in MP+ condition for 16 days either in (a) growth medium or (b) differentiation medium. Scale = 200 µm.

4.4 Conclusion

The results presented here investigated the growth and differentiation of ReNcells encapsulated in differing 3D microenvironments using microgel-based hydrogels. mTG which was used for enzymatic crosslinking of microgels also allowed facile covalent conjugation of laminin to the microgel surfaces, which significantly enhanced cell adhesion and proliferation. However, the ability of these cells to undergo differentiation was independent of laminin conjugation. When encapsulated in traditional injectable nonporous gelatin hydrogel with an equal polymer concentration, ReNcells were observed to decrease in viability over culture period, indicating the environment was not conducive for cell proliferation and differentiation. Generation of functional

neurons was demonstrated by imaging of neuronal firing events in the MP condition, but these events were not observed in the MP condition. Mitochondrial membrane potential was shown to increase for differentiating ReNcells. In summary, this work demonstrates the potential for MIHs to encapsulate NSPCs to treat damaged neuronal tissues.

References

(1) Huebner, E. A.; Strittmatter, S. M. Axon Regeneration in the Peripheral and Central Nervous Systems. *Results Probl. Cell Differ.* **2009**, *48*, 339. https://doi.org/10.1007/400_2009_19.

(2) Garzón-Muvdi, T.; Quiñones-Hinojosa, A. Neural Stem Cell Niches and Homing: Recruitment and Integration into Functional Tissues. *ILAR J.* **2009**, *51* (1), 3–23. https://doi.org/10.1093/ILAR.51.1.3.

(3) Liu, W.; Xu, B.; Xue, W.; Yang, B.; Fan, Y.; Chen, B.; Xiao, Z.; Xue, X.; Sun, Z.; Shu, M.; Zhang, Q.; Shi, Y.; Zhao, Y.; Dai, J. A Functional Scaffold to Promote the Migration and Neuronal Differentiation of Neural Stem/Progenitor Cells for Spinal Cord Injury Repair. *Biomaterials* **2020**, *243*. https://doi.org/10.1016/J.BIOMATERIALS.2020.119941.

(4) Comella-Bolla, A.; Orlandi, J. G.; Miguez, A.; Straccia, M.; García-Bravo, M.; Bombau, G.; Galofré, M.; Sanders, P.; Carrere, J.; Segovia, J. C.; Blasi, J.; Allen, N. D.; Alberch, J.; Soriano, J.; Canals, J. M. Human Pluripotent Stem Cell-Derived Neurons Are Functionally Mature In Vitro and Integrate into the Mouse Striatum Following Transplantation. *Mol. Neurobiol.* **2020**, *57* (6), 2766–2798. https://doi.org/10.1007/S12035-020-01907-4.

(5) Sukhinich, K. K.; Kosykh, A. V.; Aleksandrova, M. A. Differentiation and Cell-Cell Interactions of Neural Progenitor Cells Transplanted into Intact Adult Brain. *Bull. Exp. Biol. Med.* **2015**, *160* (1), 115–122. https://doi.org/10.1007/S10517-015-3111-6.

(6) Fan, L.; Liu, C.; Chen, X.; Zou, Y.; Zhou, Z.; Lin, C.; Tan, G.; Zhou, L.; Ning, C.; Wang, Q. Directing Induced Pluripotent Stem Cell Derived Neural Stem Cell Fate with a Three-Dimensional Biomimetic Hydrogel for Spinal Cord Injury Repair. *ACS Appl. Mater. Interfaces* **2018**, *10* (21), 17742–17755. https://doi.org/10.1021/ACSAMI.8B05293.

(7) Tong, X.; Yang, F. Recent Progress in Developing Injectable Matrices for Enhancing Cell Delivery and Tissue Regeneration. *Adv. Healthc. Mater.* **2018**, *7* (7), 1701065. https://doi.org/10.1002/ADHM.201701065.

(8) Chighizola, M.; Dini, T.; Lenardi, C.; Milani, P.; Podestà, A.; Schulte, C. Mechanotransduction in Neuronal Cell Development and Functioning. *Biophys. Rev.* **2019**, *11* (5), 701–720. https://doi.org/10.1007/S12551-019-00587-2.

(9) McIntyre, W. B.; Karimzadeh, M.; Riazalhosseini, Y.; Khazaei, M.; Fehlings, M. G. Cell-Cell Contact Mediates Gene Expression and Fate Choice of Human Neural Stem/Progenitor Cells. *Cells* **2022**, *11* (11). https://doi.org/10.3390/CELLS11111741.

(10) Jiao, Q.; Li, X.; An, J.; Zhang, Z.; Chen, X.; Tan, J.; Zhang, P.; Lu, H.; Liu, Y. Cell-Cell Connection Enhances Proliferation and Neuronal Differentiation of Rat Embryonic Neural Stem/Progenitor Cells. *Front. Cell. Neurosci.* **2017**, *11*. https://doi.org/10.3389/FNCEL.2017.00200.

(11) Cherry, J. F.; Bennett, N. K.; Schachner, M.; Moghe, P. V. Engineered N-Cadherin and L1 Biomimetic Substrates Concertedly Promote Neuronal Differentiation, Neurite Extension and Neuroprotection of Human Neural Stem

Cells. *Acta Biomater.* **2014**, *10* (10), 4113–4126. https://doi.org/10.1016/J.ACTBIO.2014.06.001.

(12) Liebau, S.; Vaida, B.; Storch, A.; Boeckers, T. M. Maturation of Synaptic Contacts in Differentiating Neural Stem Cells. *Stem Cells* **2007**, *25* (7), 1720–1729. https://doi.org/10.1634/STEMCELLS.2006-0823.

(13) Bertsch, P.; Diba, M.; Mooney, D. J.; Leeuwenburgh, S. C. G. Self-Healing Injectable Hydrogels for Tissue Regeneration. *Chem. Rev.* **2023**, *123* (2), 834–873. https://doi.org/10.1021/ACS.CHEMREV.2C00179.

(14) Griveau, L.; Lafont, M.; le Goff, H.; Drouglazet, C.; Robbiani, B.; Berthier, A.; Sigaudo-Roussel, D.; Latif, N.; Visage, C. Le; Gache, V.; Debret, R.; Weiss, P.; Sohier, J. Design and Characterization of an in Vivo Injectable Hydrogel with Effervescently Generated Porosity for Regenerative Medicine Applications. *Acta Biomater.* **2022**, *140*, 324–337. https://doi.org/10.1016/J.ACTBIO.2021.11.036.

(15) Daly, A. C.; Riley, L.; Segura, T.; Burdick, J. A. Hydrogel Microparticles for Biomedical Applications. *Nat. Rev. Mater. 2019 51* **2019**, *5* (1), 20–43. https://doi.org/10.1038/s41578-019-0148-6.

(16) Griffin, D. R.; Weaver, W. M.; Scumpia, P. O.; Di Carlo, D.; Segura, T. Accelerated Wound Healing by Injectable Microporous Gel Scaffolds Assembled from Annealed Building Blocks. *Nat. Mater.* **2015**, *14* (7), 737–744. https://doi.org/10.1038/nmat4294.

(17) Fang, J.; Koh, J.; Fang, Q.; Qiu, H.; Archang, M. M.; Hasani-Sadrabadi, M. M.; Miwa, H.; Zhong, X.; Sievers, R.; Gao, D. W.; Lee, R.; Di Carlo, D.; Li, S.

Injectable Drug-Releasing Microporous Annealed Particle Scaffolds for Treating Myocardial Infarction. *Adv. Funct. Mater.* **2020**, *30* (43), 2004307. https://doi.org/10.1002/ADFM.202004307.

(18) Koh, J.; Griffin, D. R.; Archang, M. M.; Feng, A. C.; Horn, T.; Margolis, M.; Zalazar, D.; Segura, T.; Scumpia, P. O.; Di Carlo, D. Enhanced In Vivo Delivery of Stem Cells Using Microporous Annealed Particle Scaffolds. *Small* **2019**, *15* (39), 1903147. https://doi.org/10.1002/SMLL.201903147.

(19) Song, Y.; Subramanian, K.; Berberich, M. J.; Rodriguez, S.; Latorre, I. J.; Luria, C. M.; Everley, R.; Albers, M. W.; Mitchison, T. J.; Sorger, P. K. A Dynamic View of the Proteomic Landscape during Differentiation of ReNcell VM Cells, an Immortalized Human Neural Progenitor Line. *Sci. data* **2019**, *6*. https://doi.org/10.1038/SDATA.2019.16.

(20) Hyysalo, A.; Ristola, M.; Mäkinen, M. E. L.; Häyrynen, S.; Nykter, M.; Narkilahti, S. Laminin A5 Substrates Promote Survival, Network Formation and Functional Development of Human Pluripotent Stem Cell-Derived Neurons in Vitro. *Stem Cell Res.* **2017**, *24*, 118–127. https://doi.org/10.1016/J.SCR.2017.09.002.

(21) Barros, D.; Conde-Sousa, E.; Gonçalves, A. M.; Han, W. M.; García, A. J.; Amaral, I. F.; Pêgo, A. P. Engineering Hydrogels with Affinity-Bound Laminin as 3D Neural Stem Cell Culture Systems. *Biomater. Sci.* **2019**, *7* (12), 5338. https://doi.org/10.1039/C9BM00348G.

(22) Lepski, G.; Jannes, C. E.; Nikkhah, G.; Bischofberger, J. CAMP Promotes the Differentiation of Neural Progenitor Cells in Vitro via Modulation of Voltage-Gated

Calcium Channels. *Front. Cell. Neurosci.* **2013**, *7*, 155. https://doi.org/10.3389/FNCEL.2013.00155.

(23) Zhang, S.; Wu, M.; Peng, C.; Zhao, G.; Gu, R. GFAP Expression in Injured Astrocytes in Rats. *Exp. Ther. Med.* **2017**, *14* (3), 1905. https://doi.org/10.3892/ETM.2017.4760.

(24) Weigel, M.; Wang, L.; Fu, M. meng. Microtubule Organization and Dynamics in Oligodendrocytes, Astrocytes, and Microglia. *Dev. Neurobiol.* **2021**, *81* (3), 310–320. https://doi.org/10.1002/DNEU.22753.

(25) Dent, E. W.; Baas, P. W. Microtubules in Neurons as Information Carriers. *J. Neurochem.* **2014**, *129* (2), 235. https://doi.org/10.1111/JNC.12621.

(26) Sundelacruz, S.; Levin, M.; Kaplan, D. L. Membrane Potential Controls Adipogenic and Osteogenic Differentiation of Mesenchymal Stem Cells. *PLoS One* **2008**, *3* (11), e3737. https://doi.org/10.1371/JOURNAL.PONE.0003737.

(27) Yasuda, T.; Bartlett, P. F.; Adams, D. J. Kir and Kv Channels Regulate Electrical Properties and Proliferation of Adult Neural Precursor Cells. *Mol. Cell. Neurosci.* **2008**, *37* (2), 284–297. https://doi.org/10.1016/J.MCN.2007.10.003.

(28) Gottlieb, E.; Armour, S. M.; Harris, M. H.; Thompson, C. B. Mitochondrial Membrane Potential Regulates Matrix Configuration and Cytochrome c Release during Apoptosis. *Cell Death Differ. 2003 106* **2003**, *10* (6), 709–717. https://doi.org/10.1038/sj.cdd.4401231.

Chapter 5

Future Work

5.1 Future Research Directions of Gelatin Microporous Injectable Hydrogels

The hydrogels discussed in this dissertation have the potential to expand in the following directions: 1) use gelatin MIH systems for other biomedical applications, 2) introduce additional complexity to the material properties of MIHs, and 3) apply MIH in additive biomanufacturing.

5.2 Other Medical Applications

One of the core ideas presented in this thesis is that MIHs provide a highly interconnected pore space that enhances cell spreading and cell-cell connections. These cell behaviors are important for many tissues, and gelatin MIH is broadly applicable to provide a network that promote these cellular responses. For example, we have interest in applying MIHs to applications in liver tissue engineering, and for enabling rapid scaffold vascularization.

The liver is important from a tissue engineering perspective, because 1) liver disease (e.g. diabetes, nonalcoholic fatty liver disease (NAFLD)) is a major cause of numerous chronic metabolic diseases[1] and death worldwide, 2) despite the high success rate of liver transplantation, the need for liver transplant is greater than the

available donor tissue, and 3) engineered liver tissue can serve as a model system to study liver diseases and drug interactions.[2] However, development of engineered liver tissue is challenged due to the rapid reduction of cell function when cultured in vitro. While hepatocytes, the primary cell constituent of the liver, have been shown to de-differentiate to regenerate liver tissue in the body, they rapidly lose function when cultured in vitro.[3] Although advances have been made, describing the positive effect of aggregation on maintenance of cell function[4], more innovations are needed to prolong tissue function. Other cell sources, such as hepatocyte-like cell lines are frequently used to model aspects of liver function. Induced pluripotent stem cell (iPSC) derived hepatocytes (iHEPs) have a path to clinical translation, but differentiated iHEPs resemble immature hepatocytes rather than adult cells.[5] Since MIHs promote direct cell-cell connection, which has been shown to improve maintenance of hepatocyte function[6], they represent an ideal system for generating mature hepatocytes from iHEP.

Scaffold vascularization remains a major challenge to the generation of functional 3D tissues. For large tissues, diffusion limits the availability of required nutrients, and as a result, scaffolds that are either pre-vascularized, or that promote rapid vascularization are needed to create transplantation-ready tissues.[7] Vascular endothelial cells form blood vessel walls, and their organization into tube-like structures is driven by cell-cell connections. We tested the potential for creating vasculature using the interstitial space as a template for endothelial vascular assembly, by encapsulating human umbilical vein endothelial cells (HUVECs) with human dermal fibroblasts (HDFs) as a support cell, or HUVECs alone and examining the cell assembly in the 3D matrix (**Fig. 5.1**).

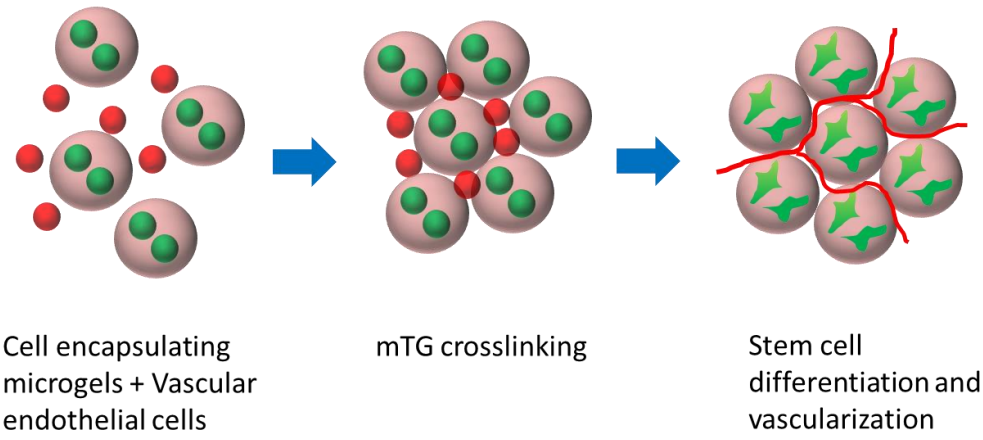

Figure 5.1. Vascularized engineered tissues using the interstitial space of MIH as templates for vasculature.

Cell organization was examined by confocal microscopy, by staining for CD31 (green), a HUVEC marker, actin cytoskeleton (pink), and cell nuclei (blue) (**Fig. 5.2**). Without inclusion of HDFs (Fig 5.2 a, c, e, g), HUVECs grew on the surface of microgels, and made cell-cell connections, but did not appear to assemble into blood vessel-like structures. In contrast, When co-encapsulated with HDFs (Fig. 5.2 b, d, f, h), HUVECs aggregate and form what appear to be the beginning of tubular structures. We intend to continue exploring MIHs for driving organization of endothelial cells into vessel-like structures.

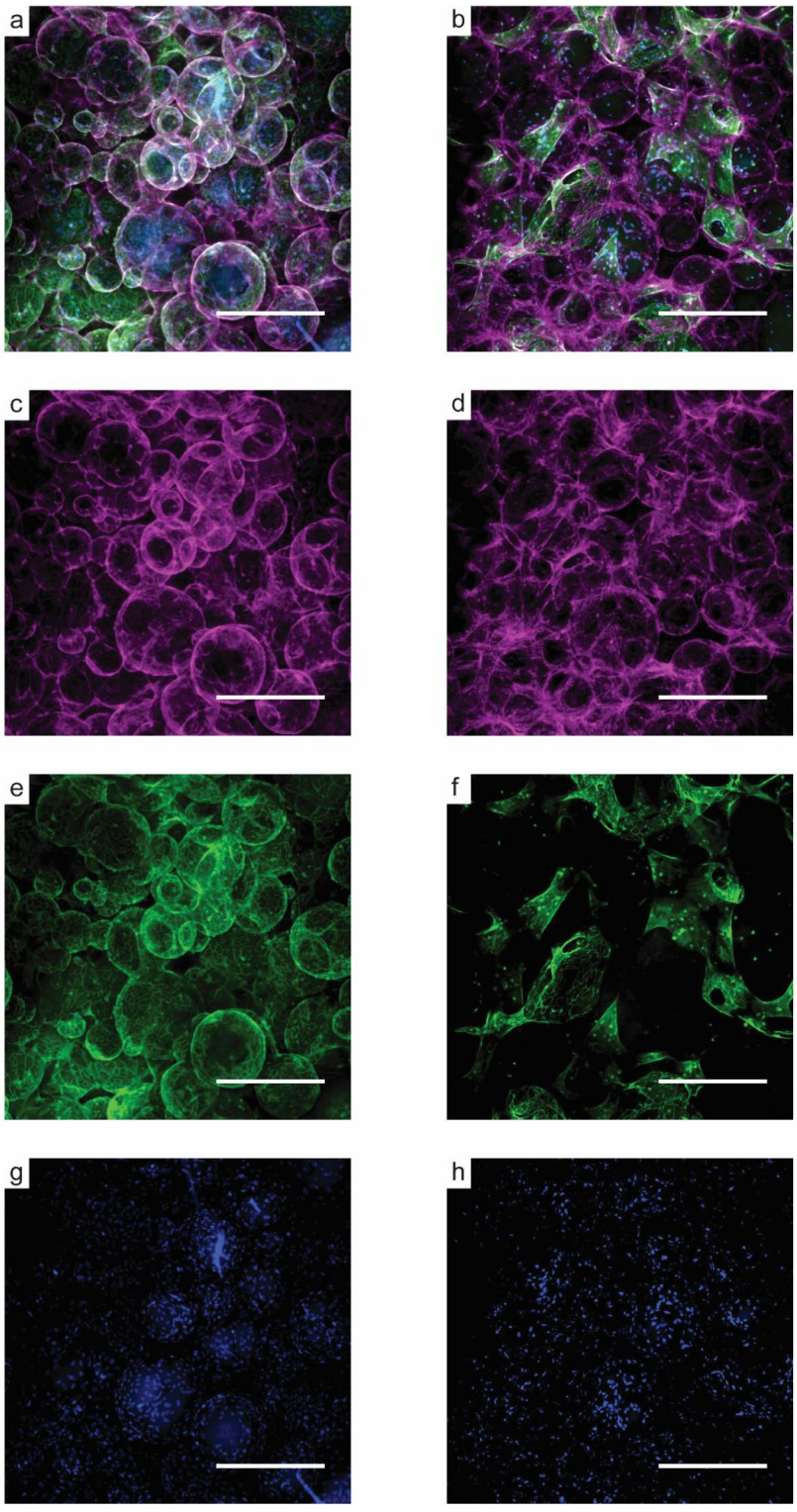

Figure 5.2. HUVEC Encapsulation. HUVEC cells were encapsulated in the microporous hydrogel either without (a, c, d, g) or with (b, d, f, h) inclusion of supporting cells (HDFs). Composite images (a, b), and each separate channel; actin cytoskeleton (pink) (c, d), CD31 (green) (e, f) and cell nuclei (blue) (g, h) were imaged. Scale = 400 µm.

5.3 Addition of Mechanical Complexity

One of the advantages of using microgels to create injectable hydrogels is that they can be further functionalized after microgel formation but before injection. To take advantage of this, we have begun functionalizing gelatin microgels with hydroxyapatite and magnetic nanoparticles. Hydroxyapatite, a calcium phosphate mineral, is a major component of bone.[8] Incorporation of hydroxyapatite into our injectable hydrogel could have several distinct advantages. 1) The presence of hydroxyapatite has been previously shown to promote MSC osteogenic differentiation, and therefore could modulate the osteogenic differentiation of encapsulated MSCs.[9] And 2) there are many examples of the introduction of inorganic nanomaterials improving hydrogel strength, therefore inclusion of hydroxyapatite could improve hydrogel mechanical properties.[10] **Fig. 5.3** shows evidence of calcium and phosphate deposition on gelatin microgel surface, along with a representative SEM sample.

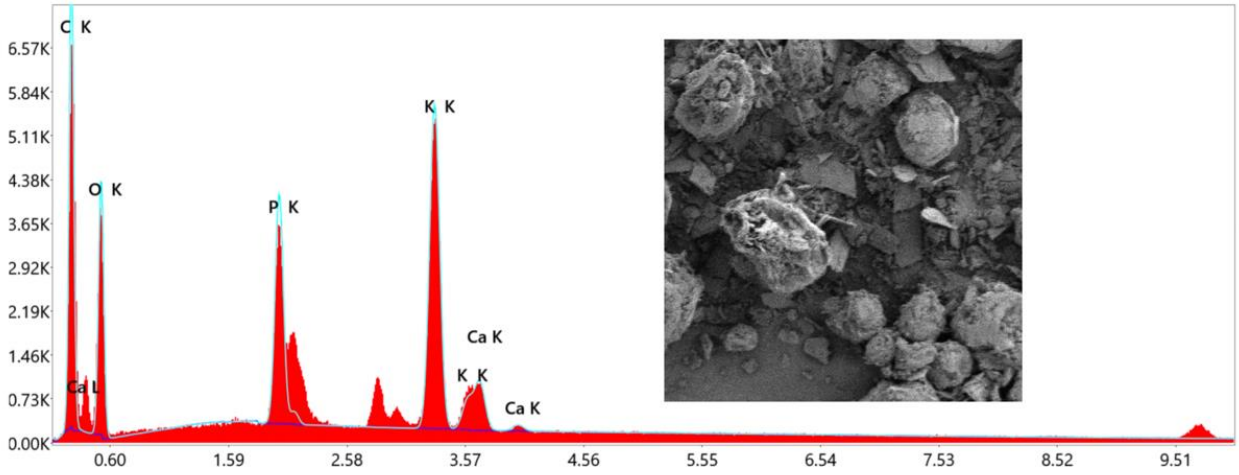

Figure 5.3. SEM/EDS of hydroxyapatite-gelatin microgels. EDS spectrum and representative SEM image of gelatin microgel functionalized with hydroxyapatite, showing the presence of calcium and phosphate.

Microgels functionalized with magnetic nanoparticles could be manipulated by introduction of an external magnetic field, and as a result mechanical stimulations could be applied to encapsulated cells. Cyclical perturbations have been shown to induce stem cell differentiation into specific lineages.[11,12] Gelatin microgels functionalized with Fe_3O_4 nanoparticles formed in situ were produced by submerging the microgels in Fe^{3+} and Fe^{2+} aqueous solutions, then triggering mineral formation by increasing solution pH. When placed in an external magnetic field, the hydrogel moved accordingly (**Fig. 5.4**). This is our first evidence that functionalized hydrogel (black) moves in response to the placement of a magnet.

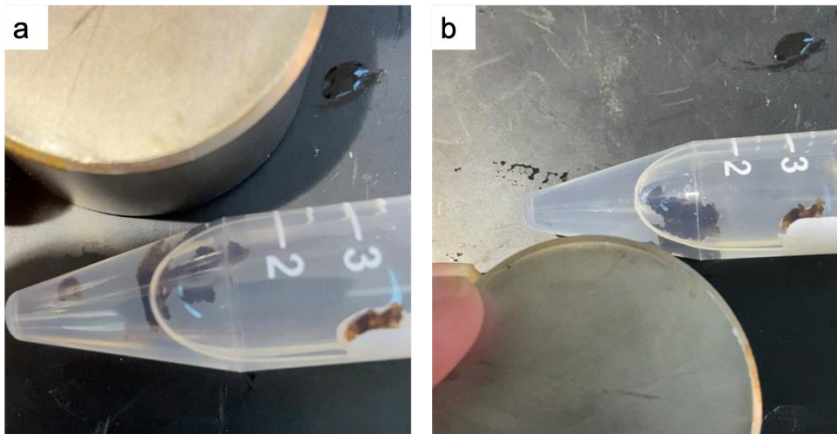

Figure 5.4. Magnetic nanoparticle-functionalized gelatin hydrogel (black) can be controlled with the application of a magnetic field (a, b).

In addition to the incorporation of functional nanoparticles, our lab has been exploring creating highly porous microgels by post-processing methods after microgel formation through methods such as freeze-drying, which can create large pores in the space occupied by ice crystals.[13] Highly porous microgels, provide additional surface area for the growth of cells, or improve diffusion of nutrient and waste products through the hydrogel (**Fig. 5.5**). These new avenues of research on MIHs can dramatically improve the physical properties of the hydrogel and are promising means to increase their functionality.

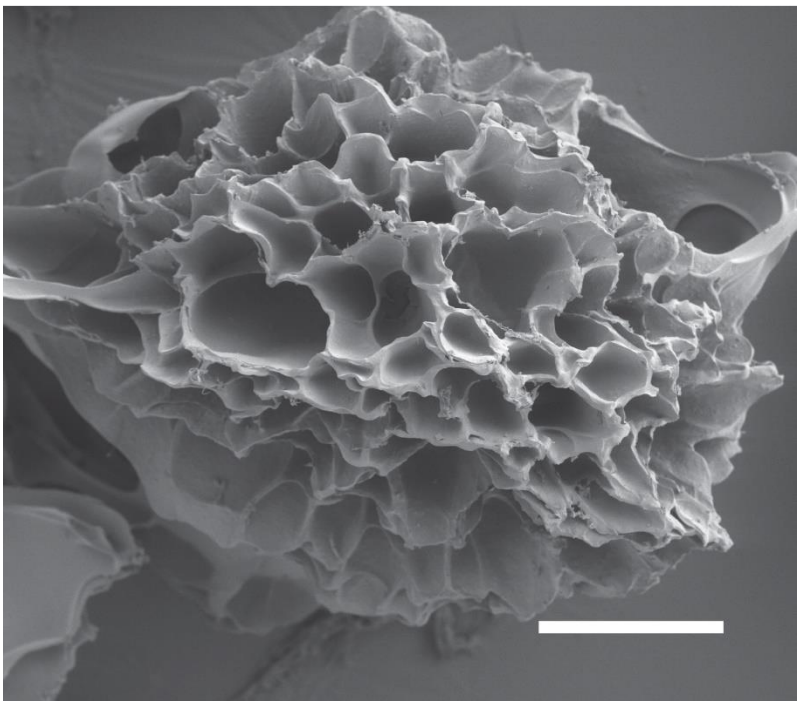

Figure 5.5. SEM Image of porous gelatin microgels. Scale = 100 µm.

5.4 Additive biomanufacturing – 3D bioprinting

Lastly, we are making strides in the utilization of microgels for biofabrication. Our lab intends to move to a microfluidic system for the generation of monodisperse microgels. Up until now, we have used batch emulsion for microgel production, which produces polydisperse particles. Monodisperse microgels produced by microfluidic system allows for more direct control over the microgel size and cellular responses. Additionally, we are exploring the application of microgels for 3D bioprinting. Our lab has been working on using 3D bioprinting to create mechanically strong hydrogel scaffolds with high printing resolution (**Fig. 5.6**), and will be also be working on utilizing microgel suspensions as bioink. The key advantages of these advanced manufacturing

techniques for microgel generation and 3D scaffold production are that 1) they enable control over the microscopic features of the scaffold, as microgel diameter controls pore size within the annealed scaffold, the surface curvature that encapsulated cells experience, and printability, and 2) utilization of 3D printing enables control over macroscopic scaffold features, such as generation of tissue-mimetic structures and macroscopic pores.[14]

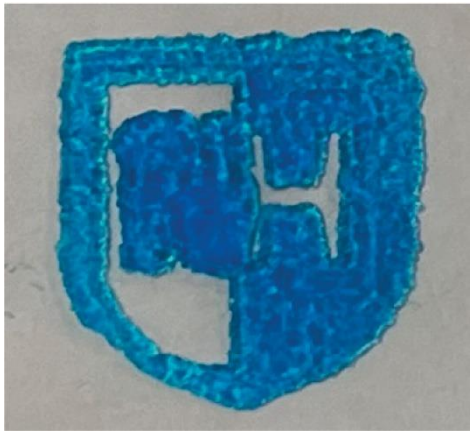

Figure 5.6. 3D bioprinted UNH logo using a composite bioink which generates a mechanically strong hydrogel.

5.5 Conclusion

In summary, the future of research on gelatin MIHs has many potential paths forward that were established in part as a result of the work completed in this dissertation. Promising strategies for innovating on this technology include application to

new biological systems, functional manipulation of the hydrogel through physical or chemical means, and by applications in additive manufacturing.

References

(1) Mikolasevic, I.; Milic, S.; Wensveen, T. T.; Grgic, I.; Jakopcic, I.; Stimac, D.; Wensveen, F.; Orlic, L. Nonalcoholic Fatty Liver Disease - A Multisystem Disease? *World J. Gastroenterol.* **2016**, *22* (43), 9488. https://doi.org/10.3748/WJG.V22.I43.9488.

(2) Mirdamadi, E. S.; Kalhori, D.; Zakeri, N.; Azarpira, N.; Solati-Hashjin, M. Liver Tissue Engineering as an Emerging Alternative for Liver Disease Treatment. *Tissue Eng. - Part B Rev.* **2020**, *26* (2), 145–163. https://doi.org/10.1089/TEN.TEB.2019.0233.

(3) Bram, Y.; Nguyen, D. H. T.; Gupta, V.; Park, J.; Richardson, C.; Chandar, V.; Schwartz, R. E. Cell and Tissue Therapy for the Treatment of Chronic Liver Disease. *Annu. Rev. Biomed. Eng.* **2021**, *23*, 517–546. https://doi.org/10.1146/ANNUREV-BIOENG-112619-044026.

(4) Bell, C. C.; Hendriks, D. F. G.; Moro, S. M. L.; Ellis, E.; Walsh, J.; Renblom, A.; Fredriksson Puigvert, L.; Dankers, A. C. A.; Jacobs, F.; Snoeys, J.; Sison-Young, R. L.; Jenkins, R. E.; Nordling, Å.; Mkrtchian, S.; Park, B. K.; Kitteringham, N. R.; Goldring, C. E. P.; Lauschke, V. M.; Ingelman-Sundberg, M. Characterization of Primary Human Hepatocyte Spheroids as a Model System for Drug-Induced Liver Injury, Liver Function and Disease. *Sci. Reports 2016 61* **2016**, *6* (1), 1–13. https://doi.org/10.1038/srep25187.

(5) Baxter, M.; Withey, S.; Harrison, S.; Segeritz, C. P.; Zhang, F.; Atkinson-Dell, R.; Rowe, C.; Gerrard, D. T.; Sison-Young, R.; Jenkins, R.; Henry, J.; Berry, A. A.;

Mohamet, L.; Best, M.; Fenwick, S. W.; Malik, H.; Kitteringham, N. R.; Goldring, C. E.; Piper Hanley, K.; Vallier, L.; Hanley, N. A. Phenotypic and Functional Analyses Show Stem Cell-Derived Hepatocyte-like Cells Better Mimic Fetal Rather than Adult Hepatocytes. *J. Hepatol.* **2015**, *62* (3), 581–589. https://doi.org/10.1016/J.JHEP.2014.10.016.

(6) Bhatia, S. N.; Balis, U. J.; Yarmush, M. L.; Toner, M. Effect of Cell–Cell Interactions in Preservation of Cellular Phenotype: Cocultivation of Hepatocytes and Nonparenchymal Cells. *FASEB J.* **1999**, *13* (14), 1883–1900. https://doi.org/10.1096/FASEBJ.13.14.1883.

(7) Masson-Meyers, D. S.; Tayebi, L. Vascularization Strategies in Tissue Engineering Approaches for Soft Tissue Repair. *J. Tissue Eng. Regen. Med.* **2021**, *15* (9), 747. https://doi.org/10.1002/TERM.3225.

(8) Hart, N. H.; Nimphius, S.; Rantalainen, T.; Ireland, A.; Siafarikas, A.; Newton, R. U. Mechanical Basis of Bone Strength: Influence of Bone Material, Bone Structure and Muscle Action. *J. Musculoskelet. Neuronal Interact.* **2017**, *17* (3), 114.

(9) Lin, L.; Chow, K. L.; Leng, Y. Study of Hydroxyapatite Osteoinductivity with an Osteogenic Differentiation of Mesenchymal Stem Cells. *J. Biomed. Mater. Res. Part A* **2009**, *89A* (2), 326–335. https://doi.org/10.1002/JBM.A.31994.

(10) Thoniyot, P.; Jin Tan, M.; Abdul Karim, A.; James Young, D.; Jun Loh, X.; Thoniyot, P.; Tan, M. J.; Karim, A. A.; Young, D. J.; Loh, X. J. Nanoparticle–Hydrogel Composites: Concept, Design, and Applications of These Promising, Multi-Functional Materials. *Adv. Sci.* **2015**, *2* (1–2), 1400010.

https://doi.org/10.1002/ADVS.201400010.

(11) Subramony, S. D.; Dargis, B. R.; Castillo, M.; Azeloglu, E. U.; Tracey, M. S.; Su, A.; Lu, H. H. The Guidance of Stem Cell Differentiation by Substrate Alignment and Mechanical Stimulation. *Biomaterials* **2013**, *34* (8), 1942–1953. https://doi.org/10.1016/J.BIOMATERIALS.2012.11.012.

(12) Schätti, O.; Grad, S.; Goldhahn, J.; Salzmann, G.; Li, Z.; Alini, M.; Stoddart, M. J. A Combination of Shear and Dynamic Compression Leads to Mechanically Induced Chondrogenesis of Human Mesenchymal Stem Cells. *Eur. Cell. Mater.* **2011**, *22*, 214–225. https://doi.org/10.22203/ECM.V022A17.

(13) Koshy, S. T.; Ferrante, T. C.; Lewin, S. A.; Mooney, D. J. Injectable, Porous, and Cell-Responsive Gelatin Cryogels. *Biomaterials* **2014**, *35* (8), 2477–2487. https://doi.org/10.1016/J.BIOMATERIALS.2013.11.044.

(14) Seymour, A. J.; Shin, S.; Heilshorn, S. C. 3D Printing of Microgel Scaffolds with Tunable Void Fraction to Promote Cell Infiltration. *Adv. Healthc. Mater.* **2021**, *10* (18), 2100644. https://doi.org/10.1002/ADHM.202100644.

Chapter 6

Summary

6.1 Summary of Presented Work

The work presented in this dissertation focused on the use of gelatin microgel-based microporous injectable hydrogels (MIHs) for applications in cell delivery, and demonstrates the utility of these systems for the successful encapsulation of cells. In addition, this work serves as evidence for the utilization of MIHs to influence cell behavior, as a consequence of the unique interconnected pore environment provided to cells. This interstitial pore space promoted cell spreading and cell-cell communication, which modulated behavior of encapsulated stem cells. The secretion of immunomodulatory factors from mesenchymal stem cells (MSCs), generation of bone-forming cells from MSCs, and the differentiation of neural progenitor cells was found to be dependent on the provided 3D hydrogel environment. This work has examined the influence of environmental factors on the phenotype of therapeutically relevant cells in 3D, and as a result of the improvement of cell activity in comparison to traditional injectable hydrogels, MIHs have major potential to change the material landscape of tissue engineering in the years to come.